UC Berkeley
UC Berkeley Electronic Theses and Dissertations

Title

Numerical methods for the Landau-Lifshitz equation in micromagnetics : the mimetic finite difference method and the mass-lumped finite element method

Permalink

Author

Kim, Eugenia Hail

Publication Date

2017

Peer reviewed|Thesis/dissertation

Numerical methods for the Landau-Lifshitz equation in micromagnetics : the mimetic finite difference method and the mass-lumped finite element method

by

Eugenia Hail Kim

A dissertation submitted in partial satisfaction of the

requirements for the degree of

Doctor of Philosophy

in

Mathematics

in the

Graduate Division

of the

University of California, Berkeley

Committee in charge:

Professor Jon Wilkening, Chair
Professor Per-Olof Persson
Professor Daniel Tataru
Professor David Bogy

Spring 2017

Numerical methods for the Landau-Lifshitz equation in micromagnetics : the mimetic finite difference method and the mass-lumped finite element method

Abstract

Numerical methods for the Landau-Lifshitz equation in micromagnetics : the mimetic finite difference method and the mass-lumped finite element method

by

Eugenia Hail Kim

Doctor of Philosophy in Mathematics

University of California, Berkeley

Professor Jon Wilkening, Chair

Micromagnetics is a continuum theory describing magnetization patterns inside ferromagnetic media. The dynamics of a ferromagnetic material are governed by the Landau-Lifshitz equation. This equation is highly nonlinear, has a non-convex constraint, has several equivalent forms, and involves solving an auxiliary problem in the infinite domain, which pose interesting challenges in developing numerical methods. In this thesis, we first present a low order mimetic finite difference method for the Landau-Lifshitz equation, that works on general polytopal meshes on general geometries, preserves non-convex constraint, is energy (exchange) decreasing, requires only a linear solver at each time step and is easily applicable to the limiting cases. Secondly, we present a high order mimetic finite difference method for the Landau-Lifshitz equation which is third order in space and second order in time. In fact, it can be arbitrarily high order in space. This method works on general polytopal meshes, and preserves the non-convex constraint in a certain sense. Lastly, we present a new class of convergent mass-lumped finite element methods to solve a weak formulation of the Landau-Lifshitz equation. The scheme preserves a non-convex constraint, requires only a linear solver at each time step and is easily applicable to the limiting cases. We provide a rigorous convergence proof that the numerical solution of our finite element method for the Landau-Lifshitz equation converges weakly to a weak solution of the Landau-Lifshitz-Gilbert equation.

To Mom and Dad

Contents

List of Figures

List of Tables

Acknowledgments

I would first like to thank my advisor Jon Wilkening for introducing the topic of numerical micromagnetics, and serving as a dissertation committee chair. I feel grateful for his tremendous support, guidance, patience during my Ph.D. and for becoming a great friend. I'd like to give greatest appreciation to the dissertation committee, Professor Per-Olof Persson, Professor Daniel Tataru, and Professor David Bogy.

It was a great experience to work at Los Alamos National Laboratory as a DOE SCGSR fellow during 2015-2016 academic year. I feel grateful to work with my mentor Dr. Konstantin Lipnikov, and thank him for his insightful discussions, guidance and support. I'd like to appreciate Dr. Pieter Swart at T-5, Applied Mathematics and Plasma Physics group for his kind support and guidance. I'd like to thank condensed matter physicists Avadh Saxena, Charles Reichardt and Cynthia Reichardt who introduced me the topic of skyrmions.

I'd like to acknowledge many professors at UC Berkeley, Daniel Tataru, James Sethian, Per-Olof Persson, John Strain, James Demmel for their inspiring lectures, insightful discussions and support. I'd like to thank many colleagues and friends academically and personally in the Department of Mathematics at UC Berkeley, Jae-young Park, Robert Saye, Jeff Donatelli, Anna Lieb, Catherine Cannizzo, Luming Wang, Meire Fortunato, Woo-hyun Cook, Minjae Lee, Chanwoo Oh, and Changyeon Cho. I'd like to thank my friends in KGSA Tennis Club. It was really awesome to meet my best friend Jeaneun Park at Berkeley and share good memories. I'd like to give greatest appreciation from professors at KAIST, Yong-Jung Kim, Chang-Ock Lee, Do-young Kwak and Sujin Shin for their support and guidance. I express my greatest gratitude to my family, mom, dad and my sister Nayeon for their solid support and encouragement.

Chapter 1

Introduction

1.1 Micromagnetics

Micromagnetics is a continuum theory describing magnetization patterns in ferromagnetic media. It can be used to explain the magnetization process of ferromagnetic materials between magnetic domains at submicrometer length scales. These scale are large enough to use continuum physics, neglecting the description of the atomic structure of the material, but are small enough to resolve complex magnetic structures such as domain walls, magnetic vortices and skyrmions [83, 65, 95, 94, 56, 66, 57, 50, 19].

In micromagnetics, the quantity of interest is the magnetization $\mathbf{M}$. Mathematically, it is a vector field from the domain Ω to $\mathbb{R}^3$. Magnetization is defined as the magnetic dipole moment per unit volume [44]. It is a property of materials that describes to what extent they are affected by magnetic fields, and also determines the magnetic field that the material itself creates [29]. In ferromagnetic materials, far below the *Curie temperature*, the length of the magnetization stays constant throughout the domain, i.e.

$$|\mathbf{M}| = M_s. \tag{1.1}$$

where M_s is the saturation magnetization. For convenience, we normalize the magnetization and set $\mathbf{m} := \frac{\mathbf{M}}{M_s}$ so that the magnetization is a vector field of unit length.

Micromagnetics can handle both static equilibria and dynamic behavior inside ferromagnetic materials. For the static case, the magnetization patterns or domain structures inside ferromagnetic materials are local or global minima of the total energy called the *Landau-Lifshitz energy*, or *free energy* [29, 40].

1.2 The Landau-Lifshitz energy

The Landau-Lifshitz energy has four contributions : exchange energy, anisotropy energy, stray field energy and the external field energy. It is given by

$$E(\mathbf{m}) = \frac{\eta}{2} \int_{\Omega} |\nabla \mathbf{m}|^2 \, \mathrm{d}x + \frac{Q}{2} \int_{\Omega} (m_2^2 + m_3^2) \, \mathrm{d}x - \frac{1}{2} \int_{\Omega} \mathbf{h_s} \cdot \mathbf{m} \, \mathrm{d}x - \int_{\Omega} \mathbf{h_e} \cdot \mathbf{m} \, \mathrm{d}x, \qquad (1.2)$$

where each term will be described in more detail below.

1.2.1 Exchange energy

The exchange energy prefers the alignment of the magnetization along a common direction and penalizes spatial change in magnetization $\mathbf{m}$. It is minimized when the magnetization is uniform. The exchange energy can be written as

$$E_{\mathrm{ex}}(\mathbf{m}) = \frac{\eta}{2} \int_{\Omega} |\nabla \mathbf{m}|^2 \, \mathrm{d}x$$

where η is the exchange constant.

1.2.2 Anisotropy energy

The anisotropy energy prefers certain orientation of the spins due to the crystallographic properties of the ferromagnetic material. In the crystal lattice, it tries to align in one or more specific directions, called *easy axes*. The anisotropy energy is given by

$$E_{\mathrm{ani}}(\mathbf{m}) = \frac{Q}{2} \int_{\Omega} \psi(\mathbf{m}) \, \mathrm{d}x.$$

where Q is an anisotropy constant and $\psi : \mathbb{S}^2 \to \mathbb{R}^+$. For the material with uniaxial anisotropy with easy axis along the x-axis, the anisotropy energy is given by

$$E_{\mathrm{ani}}(\mathbf{m}) = \frac{Q}{2} \int_{\Omega} (m_2^2 + m_3^2) \, \mathrm{d}x.$$

This energy is minimized when the magnetization aligns along the easy axis.

1.2.3 Stray field energy

The magnetic material itself creates a magnetic field known as the *stray field*, or *magneto-static field*. The stray field is given by

$$E_{\mathrm{stray}}(\mathbf{m}) = -\frac{1}{2} \int_{\Omega} \mathbf{h_s} \cdot \mathbf{m} \, \mathrm{d}x$$

In the absence of the electric currents and charges, Maxwell's equations reduce to [40, 44]

$$\mathbf{div\ B} = 0,$$
$$\nabla \times \mathbf{H}_s = 0,$$

$$(1.3)$$

where $\mathbf{B}$ is the magnetic induction and $\mathbf{H}_s$ is the stray field (magnetic field). The relation of $\mathbf{B}$, $\mathbf{H}_s$ and $\mathbf{M}$ is

$$\mathbf{B} = \mu_0(\mathbf{H}_s + \mathbf{M}).$$

$$(1.4)$$

where μ_0 is magnetic permeability of vacuum.

Normalizing the stray field by $\mathbf{h_s} := \frac{\mathbf{H}_s}{M_s}$, we have $\nabla \times \mathbf{h_s} = 0$ from (1.3). Then, the stray field is given by $\mathbf{h_s} = -\nabla\phi$ for some potential ϕ. We have

$$\mathbf{div}\ (-\nabla\phi + \mathbf{m}) = 0 \quad \text{in } \Omega$$

$$(1.5)$$

from (1.3) and (1.4). Let Ω^c denote the complement of Ω. Then, the potential ϕ satisfies

$$\triangle\phi = \begin{cases} \mathbf{div\ m} & \text{in } \Omega, \\ 0 & \text{on } \Omega^c, \end{cases}$$
$$[\phi]_{\partial\Omega} = 0,$$
$$[\nabla\phi \cdot \boldsymbol{n}]_{\partial\Omega} = -\mathbf{m} \cdot \mathbf{n},$$

$$(1.6)$$

where $[v]_{\partial\Omega}$ denotes the jump of the function v across the domain boundary, and $\boldsymbol{n}$ is the outward unit normal vector. Hence, the stray field $\mathbf{h_s}$ is given by $\mathbf{h_s} = -\nabla\phi$, where

$$\phi(x) = \frac{1}{4\pi}\int_\Omega \nabla\left(\frac{1}{|x-y|}\right) \cdot \mathbf{m}(y)\ \mathrm{d}y$$
$$= -\frac{1}{4\pi}\left(\int_\Omega \frac{\nabla \cdot \mathbf{m}(y)}{|x-y|}\mathrm{d}y - \int_{\partial\Omega} \frac{\mathbf{m}(y) \cdot \mathbf{n}}{|x-y|}\mathrm{d}S(y)\right).$$

$$(1.7)$$

1.2.4   External energy

The *external energy* tries to align the magnetization with an external field. It is also called *Zeeman's energy* or the *applied field energy*. The energy is given by

$$E_{\text{ext}}(\mathbf{m}) = -\int_\Omega \mathbf{h_e} \cdot \mathbf{m}\ \mathrm{d}x.$$

This energy is minimized when the magnetization aligns with the external field.

1.3   The Landau-Lifshitz equation

The dynamics of the magnetic distribution in a ferromagnetic material occupying a region $\Omega \subset \mathbb{R}^d$ where $d = 2$, or 3, are governed by the Landau-Lifshitz (LL) equation. The magnetization $\mathbf{m} : \Omega \times [0, T] \to \mathbb{R}^3$ satisfies

$$\frac{\partial \mathbf{m}}{\partial t} = -\mathbf{m} \times \mathbf{h} - \alpha \mathbf{m} \times (\mathbf{m} \times \mathbf{h}), \tag{1.8}$$

where α is a dimensionless damping parameter and $\mathbf{h}$ is the effective field. The first term on the right-hand side of (1.8) is called the *gyromagnetic term*. Gyromagnetic precession is a conservative motion that describes the rotation of the magnetization $\mathbf{m}$ around the effective field $\mathbf{h}$. The second term on the right-hand side of (1.8) is called the *damping term*, which leads to dissipative precession. Dissipative precession is the mechanism through which the magnetization $\mathbf{m}$ relaxes to align parallel with the effective field $\mathbf{h}$ as the system proceeds to equilibrium.

The effective field is defined as the functional derivative of the Landau-Lifshitz energy (1.2)

$$\mathbf{h}(\mathbf{m}) := -\frac{\delta E(\mathbf{m})}{\delta \mathbf{m}} = \eta \triangle \mathbf{m} - Q(m_2 e_2 + m_3 e_3) + \mathbf{h_s}(\mathbf{m}) + \mathbf{h_e}, \tag{1.9}$$

where η is the exchange constant, Q is an anisotropy constant, $\mathbf{h}_s$ is the stray field, and $\mathbf{h}_e$ is the external field.

Remark 1. *The terms corresponding to the exchange, anisotropic and external energy are local terms in that local change in the magnetization affects them locally. But the stray field energy term is nonlocal in that local change in the magnetization has a global effect.*

We define the *low order terms* $\bar{\mathbf{h}}(\mathbf{m})$ in (1.9) as

$$\bar{\mathbf{h}}(\mathbf{m}) := -Q(m_2 e_2 + m_3 e_3) + \mathbf{h_s}(\mathbf{m}) + \mathbf{h_e}. \tag{1.10}$$

These terms can be regarded as low-order (relative to $\Delta \mathbf{m}$) when considering mathematical properties such as existence and regularity of the solution [6]. Also, they have few derivatives than $\Delta \mathbf{m}$.

The problem is closed with initial condition

$$\mathbf{m}(x, 0) = \mathbf{m}_0(x),$$

and Neumann or Dirichlet boundary conditions. In most of the literature [40], the problem is imposed with homogeneous Neumann boundary condition, i.e.

$$\frac{\partial \mathbf{m}}{\partial \mathbf{n}} = 0.$$

Remark 2. *From* (1.8)*, we can immediately derive the nonconvex constraint* $|\mathbf{m}| = 1$. *Taking a dot product with* $\mathbf{m}$ *in both sides of* (1.8) *we have*

$$\mathbf{m} \cdot \frac{\partial \mathbf{m}}{\partial t} = 0.$$

Thus, we have

$$\frac{1}{2} \frac{\partial |\mathbf{m}|^2}{\partial t} = \mathbf{m} \cdot \frac{\partial \mathbf{m}}{\partial t} = 0. \tag{1.11}$$

From this equation, we get that the length of $\mathbf{m}$*,* $|\mathbf{m}|$ *is constant in time.*

1.3.1 The Landau-Lifshitz-Gilbert equation

There are several equivalent forms of the Landau-Lifshitz equation (1.8) which lead to a large family of numerical schemes for the Landau-Lifshitz equation. The *Landau-Lifshitz-Gilbert equation* was proposed by Gilbert [43] with the damping term,

$$\frac{\partial \mathbf{m}}{\partial t} - \alpha \mathbf{m} \times \frac{\partial \mathbf{m}}{\partial t} = -(1 + \alpha^2)(\mathbf{m} \times \mathbf{h}). \tag{1.12}$$

Another equivalent form is the *modified Landau-Lifshitz-Gilbert equation*

$$\alpha \frac{\partial \mathbf{m}}{\partial t} + \mathbf{m} \times \frac{\partial \mathbf{m}}{\partial t} = (1 + \alpha^2)(\mathbf{h} - (\mathbf{h} \cdot \mathbf{m})\mathbf{m}). \tag{1.13}$$

which is used in [6] to develop a numerical scheme. The equations (1.8), (1.12) and (1.13) are equivalent, and can be derived from each other using the vector identity

$$\mathbf{a} \times (\mathbf{b} \times \mathbf{c}) = (\mathbf{a} \cdot \mathbf{c})\mathbf{b} - (\mathbf{a} \cdot \mathbf{b})\mathbf{c}. \tag{1.14}$$

In the special case of $\mathbf{h} = \triangle \mathbf{m}$, that is $\bar{\mathbf{h}} = 0$, we have more equivalent forms:

$$\begin{aligned}
\frac{\partial \mathbf{m}}{\partial t} = & -\mathbf{m} \times \Delta \mathbf{m} - \alpha \mathbf{m} \times (\mathbf{m} \times \Delta \mathbf{m}) \\
= & -\mathbf{m} \times \Delta \mathbf{m} + \alpha \Delta \mathbf{m} - \alpha(\mathbf{m} \cdot \Delta \mathbf{m})\mathbf{m} \\
= & -\mathbf{m} \times \Delta \mathbf{m} + \alpha \Delta \mathbf{m} + \alpha |\nabla \mathbf{m}|^2 \mathbf{m}.
\end{aligned} \tag{1.15}$$

We used the vector identity (1.14) in the second equality and the nonconvex constraint $|\mathbf{m}| = 1$, and in turn

$$\mathbf{m} \cdot \frac{\partial \mathbf{m}}{\partial u} = 0, \quad u \in \{x, y, z\}$$

in the last equality.

1.3.2 Harmonic map heat flow into $\mathbb{S}^2$ and the Schrödinger map

Taking only the damping term on the right-hand side of (1.15), we have the *harmonic map heat flow into* $\mathbb{S}^2$ [46],

$$\frac{\partial \mathbf{m}}{\partial t} = \alpha \Delta \mathbf{m} + \alpha |\nabla \mathbf{m}|^2 \mathbf{m}.$$

This is a geometric generalization of the linear heat equation. Taking only the gyromagnetic term on the right-hand side of (1.15), we have the *Schrödinger map* [46],

$$\frac{\partial \mathbf{m}}{\partial t} = -\mathbf{m} \times \triangle \mathbf{m}.$$

This is a geometric generalization of the linear Schrödinger equation.

By designing a numerical scheme based on the Landau-Lifshitz equation (1.8), instead of the Landau-Lifshitz-Gilbert equation (1.12) or other form (1.13), we can easily apply the method to the harmonic map heat flow into $\mathbb{S}^2$ and the Schrödinger map.

1.4 Properties of the Landau-Lifshitz equation

1.4.1 Nonconvex constraint

One of the important properties of the Landau-Lifshitz equation is the nonconvex constraint that the length of the magnetization is conserved in time; See (1.11). There are a wide variety of numerical methods that preserve the nonconvex constraint in various ways [29]:

- direct conservation of the nonconvex constraint can be built into the time stepping schemes : see section 1.7.1 below.

- nonlinear projection step : this is also a direct conservation of the nonconvex constraint, employing a projection back to the sphere in a nonlinear fashion.

- asymptotic conservation of the nonconvex constraint.

1.4.2 Lyapunov structure

In the case of constant applied field and $\alpha \neq 0$, we see that the Landau-Lifshitz energy decreases in time due to the *Lyapunov structure*. Formally, we have

$$\frac{dE}{dt} = -\int_\Omega \mathbf{h} \cdot \frac{\partial \mathbf{m}}{\partial t} \, \mathrm{d}x = -\alpha \int_\Omega |\mathbf{m} \times \mathbf{h}|^2 \, \mathrm{d}x = -\frac{\alpha}{1+\alpha^2} \int_\Omega \left|\frac{\partial \mathbf{m}}{\partial t}\right|^2 \, \mathrm{d}x$$

Since the right-hand side of the equation is less than or equal to 0, the energy does not increase.

1.4.3 Hamiltonian structure

In the case of constant applied field, we have the conservation of the Landau-Lifshitz energy in time, if there is no damping ($\alpha = 0$). Formally, we have

$$\frac{dE}{dt} = -\int_\Omega \mathbf{h} \cdot \frac{\partial \mathbf{m}}{\partial t} \, \mathrm{d}x = 0.$$

This is called the *Hamiltonian structure*.

1.5 Stray field computation

The most time consuming part of micromagnetic simulation is the computation of the stray field $\mathbf{h}_s$, which involves solving an infinite domain exterior field problems (1.6).

The numerical methods for the stray field calculation can be divided into two groups [2]. The first group are methods that solve a PDE posed in $\mathbb{R}^d$ for the potential field (1.6), where hybrid numerical methods are typically used. In [37, 42], the finite element and boundary element methods are used and in [22], the finite element method and the shell transformation are employed. The computational costs are reduced by using multigrid preconditioners [84] and $\mathcal{H}$-matrix approximation [70].

The second group includes methods based on direct evaluation of the integral with a nonlocal kernel (1.7), using the fast Fourier transform [61, 1, 96, 41], the fast multipole method [17], the nonuniform grid method [60], and the tensor grid method [34].

The computational costs are between $O(N)$ and $O(N \log N)$, where N is the number of unknowns.

1.6 Previous mathematical results

Local existence and uniqueness, and global existence and uniqueness with small-energy initial data for strong solutions of the Landau-Lifshitz equation in $\mathbb{R}^3$ was shown in [23]. Local existence and uniqueness of strong solutions of the Landau-Lifshitz equation on a bounded domain Ω was shown in [24]. Global existence and uniqueness of strong solutions of the Landau-Lifshitz equation for small-energy initial data on bounded domain $\Omega \subset \mathbb{R}^2$ was shown in [24].

The existence of weak solutions was shown in the following papers : In [8, 45], global existence of weak solutions of the Landau-Lifshitz equation with $\mathbf{h} = \triangle \mathbf{m}$ was proved for $\Omega \subset \mathbb{R}^3$. Moreover, the nonuniqueness of weak solutions of the Landau-Lifshitz equation with $\mathbf{h} = \triangle \mathbf{m}$ and $\alpha \neq 0$ was proved in [8].

1.7 Previous numerical methods

1.7.1 Time-stepping schemes

Several time-stepping schemes have been developed that preserve the unit length constraint, but without rigorous convergence analysis. To the best of our knowledge, these methods have only been tested on finite difference schemes, although they could also be used for finite element discretization.

1.7.1.1 The Gauss-Seidel projection method

The Gauss-Seidel projection method [87, 88, 39] uses another formulation of the Landau-Lifshitz equation, the last equation in (1.15). It treats the gyromagnetic and damping terms separately to overcome the difficulties associated with the stiffness and nonlinearity. It regards $|\nabla \boldsymbol{m}|^2$ as the Lagrange multiplier for the pointwise constraint $|\mathbf{m}| = 1$. This method is first-order accurate in time and unconditionally stable. It was further improved to be second-order accurate but without unconditional stability.

1.7.1.2 Geometric integration method

In [49], Jiang, Kaper, and Leaf develop the semi-analytic integration method. It uses the fact that $\mathbf{m}$ is determined by $(\mathbf{m} \cdot \mathbf{h})$ and $\mathbf{m} \times \mathbf{h}$ and analytically integrates the system of ODEs for $(\mathbf{m} \cdot \mathbf{h})\mathbf{h}$ and $\mathbf{h} \times (\mathbf{m} \times \mathbf{h})$. This method is first-order accurate and explicit, so it is subject to a CFL time step constraint.

The geometric integrators were used in [51] and, in a more general setting, in [54]. They are more amenable for building high order scheme than previous methods. The methods use the Cayley transform to lift the Landau-Lifshitz-Gilbert equation to the Lie algebra of the three dimensional rotation group. In [51], the scheme, which is second-order accurate, is studied numerically, and yields the same scheme as the mid-point method. In [54], the schemes that are first, second and fourth-order accurate, are examined.

1.7.1.3 Mid-point method

In [15, 32], the mid-point method is studied. It is second-order accurate, unconditionally stable, and preserves the Lyapunov and Hamiltonian structures of the Landau-Lifshitz equation. This method can also be regarded as a geometric integration method.

1.7.2 Semi-implicit schemes in [72] and [31] for 2D and 3D formulations, respectively, of the Landau-Lifshitz equation

Semi-implicit schemes are introduced in [72] for 2D, and in [31] for 3D formulation of the Landau-Lifshitz equation and error estimates are derived under the assumption that there

exists a strong solution. These schemes are linear and preserve the nonconvex constraint asymptotically.

1.7.3 Finite element methods

The finite element methods for the Landau-Lifshitz equation deal with weak solutions, and, in some cases, also include a rigorous convergence analysis.

1.7.3.1 Alouges et al's scheme

The finite element method for the Landau-Lifshitz equation with rigorous convergence proof was first presented by Alouges and his collaborators in a series of paper [6, 5, 7]. It is developed based on the modified Landau-Lifshitz-Gilbert equation (1.13), which only requires a linear solver for each time step. It is first order accurate in time and second order accurate in space (in L^2 norm). The method was further developed to reach almost second order accuracy in time [52, 9].

1.7.3.2 Bartels and Prohl's scheme

In [13], Bartels and Prohl presented an implicit time integration method based on the Landau-Lifshitz-Gilbert equation. It is second order accurate in both space and time, and unconditionally stable, but a nonlinear solver is needed for each time step. However, there is a step size constraint $\frac{k}{h^2} \leq C$ to guarantee the existence of the solution for the fixed point iteration.

1.7.3.3 Cimrák's scheme

In [30], Cimrák developed a scheme which is based on the Landau-Lifshitz equation. It is second order accurate in both space and time, but a nonlinear solver is necessary for each time step. It also had the step size constraint $\frac{k}{h^2} \leq C$ to guarantee the existence of the solution for the fixed point iteration.

1.8 Applications

Application areas of micromagnetics include the following areas and magnetic materials :

- magnetic sensor technology [73, 81, 53, 80, 85].

- magnetic recording [78, 74, 33, 69, 93].

- magnetic storage devices such as hard drives and magnetic memory (MRAM) [18, 75, 97, 92, 16, 26, 55].

- permanent composite magnets [36, 71, 35, 79, 77, 67] : Permanent composite magnets are used in electric cars, computers, and wind turbine generators. These materials consist of hard and soft magnetic grains or crystals in which have different properties.

- magnetoelastic materials [48, 76, 25, 11, 3, 27, 64, 90, 91] : Magnetoelastic materials change their shape in response to an applied magnetic field with volume conservation. They play important roles in actuation and sensing applications.

1.9 Outline

The remainder of this thesis is organized into three additional chapters. In chapter 2, the mimetic finite difference method for the Landau-Lifshitz equation is presented. Chapter 2 has been adapted from the paper

- E. Kim and K. Lipnikov, The mimetic finite difference method for the Landau-Lifshitz equation, *Journal of Computational Physics*, **328**:109–130, 2017.

In chapter 3, high order mimetic finite difference method for the Landau-Lifshitz equation is presented. I anticipate adapting the material of this chapter into a journal manuscript entitled

- E. Kim and K. Lipnikov, High order mimetic finite difference method for the Landau-Lifshitz equation.

In chapter 4, numerical analysis of the mass-lumped finite element method for the Landau-Lifshitz equation that deals with weak solutions is given. Chapter 4 has been adapted from the paper

- E. Kim and J. Wilkening, Convergence of a mass-lumped finite element method for the Landau-Lifshitz equation, 2016, arXiv:1608.07312.

Chapter 2

The mimetic finite difference method for the Landau-Lifshitz equation

2.1 The mimetic finite difference method

The mimetic finite difference (MFD) method mimics fundamental properties of the differential equations such as conservation laws, symmetry, positivity of solution, duality and self-adjointness of the operators, and exact mathematical identities of the vector and tensor calculus. The MFD method constructs a discrete approximation on general polygonal or polyhedral meshes that mimics or preserves the properties of the underlying continuum equations. The MFD has been successfully applied in diffusion, electromagnetic, fluid flow and Lagrangian hydrodynamics, which has a fifty-year successful history [58].

For the mimetic discretization, the first step is to specify *degrees of freedom* and build *grid functions* for the discrete representation of scalar, vector and tensor fields on a computational mesh. The grid functions are the collections of degrees of freedom associated with mesh objects. The MFD uses discrete fields centered at various mesh objects such as nodes $(\mathcal{N})$, edges $(\mathcal{E})$, faces $(\mathcal{F})$ and elements $(\mathcal{Q})$. The choice of the discrete fields is problem dependent. The next step is to design the *primary operators* to represent first order operators **grad**, **curl**, **div**, which are

$$\nabla^h : \mathcal{N} \to \mathcal{E}, \qquad \nabla^h \times : \mathcal{E} \to \mathcal{F}, \qquad \text{div}^h : \mathcal{F} \to \mathcal{Q}.$$

The *derived operators*

$$\widetilde{\text{div}}^h : \mathcal{E} \to \mathcal{N}, \qquad \widetilde{\nabla}^h \times : \mathcal{F} \to \mathcal{E}, \qquad \widetilde{\nabla}^h : \mathcal{Q} \to \mathcal{F},$$

are constructed to preserve the duality of discrete operators from the duality principle of the underlying differential operators. For instance, **grad** and **div** are negatively adjoint under homogeneous boundary condition in continuum setting, and the MFD mimics this property to construct the discrete operators. In the MFD method, the primary and derived operators

are constructed to satisfy *discrete vector and tensor calclus* (DVTC) such as

$$\text{div}^{\,h}\ \nabla^h \times = 0, \qquad \nabla^h \times \nabla^h = 0.$$

2.2 Advantages of the mimetic finite difference method for the Landau-Lifshitz equation

In the following sections, we discuss explicit and implicit mimetic finite difference method (MFD) for the Landau-Lifshitz equation. Previous numerical methods for the Landau-Lifshitz equation use various time stepping strategies with conventional spatial discretization discussed in section 1.7.1. By contrast, our method incorporates new spatial discretization with a number of advantages and improvements from the previous numerical methods :

- The MFD method works on arbitrary polytopal meshes including locally refined meshes with degenerate cells. For the same mesh resolution, a polytopal mesh needs fewer cells to cover the domain than simplicial meshes, which leads to fewer unknowns and results in a more efficient method.

- The MFD method uses a mixed formulation of the Landau-Lifshitz equation. This simplifies the numerical control of nonconvex constraint, $|\mathbf{m}| = 1$. To the best of our knowledge, this method is the first scheme based on the mixed formulation of the Landau-Lifshitz equation.

- The MFD method could be applied to problems posed on general domains like the finite element method, which is a key advantage compared to traditional finite difference methods.

- The MFD method is based on the Landau-Lifshitz equation, which makes it more suitable to apply to limiting cases (See section 1.3.2).

- The exchange energy decreases on polygonal meshes under certain conditions.

- For our implicit scheme, we only need to solve a linear system for each time step, although the Landau-Lifshitz equation is highly nonlinear.

2.3 The mimetic finite difference method for the Landau-Lifshitz equation

In this section, we introduce the mimetic discretization for the Landau-Lifshitz equation (1.8). We consider the Landau-Lifshitz equation written as a system of two equations :

$$
\begin{aligned}
\mathbf{p} &= -\nabla \mathbf{m}, \\
\frac{\partial \mathbf{m}}{\partial t} &= \mathbf{m} \times \mathbf{div}\ \mathbf{p} + \alpha \mathbf{m} \times (\mathbf{m} \times \mathbf{div}\ \mathbf{p}) + \mathbf{f}(\mathbf{m}).
\end{aligned}
\tag{2.1}
$$

where

$$\mathbf{f}(\mathbf{m}) = -\mathbf{m} \times \bar{\mathbf{h}}(\mathbf{m}) - \alpha \mathbf{m} \times (\mathbf{m} \times \bar{\mathbf{h}}(\mathbf{m})) \qquad (2.2)$$

corresponds to the low-order terms (1.10). We refer to $\mathbf{p}$ as the magnetic flux tensor.

We assume that the magnetization $\mathbf{m}$ and the magnetic flux $\mathbf{p}$ are in appropriate spaces

$$\mathbf{m} \in \mathcal{Q} = (L^2(\Omega))^3$$

and

$$\mathbf{p} \in \mathcal{F} = \{\mathbf{p} \mid \mathbf{p} \in (L^s(\Omega))^{d \times 3}, \ s > 2, \ \mathbf{div} \, \mathbf{p} \in (L^2(\Omega))^3\}$$

to define the degrees of freedom for the mimetic discretization. The MFD method solves for $\mathbf{m}$ and $\mathbf{p}$ at the same time.

Let the computational domain Ω be decomposed into N_E non-overlapping polygonal or polyhedral elements E with the maximum diameter h. Let N_F denote the total number of mesh edges (faces in 3D). We use $|E|$ to denote the area (volume in 3D) of E. Similarly, $|f|$ denotes the length of mesh edge f (area of mesh face f in 3D). Let $\boldsymbol{n}_E$ be the unit vector normal to ∂E.

2.3.1 Global mimetic formulation

The first step of the MFD method is to specify the degrees of freedom for the primary variables $\mathbf{m}$ and $\mathbf{p}$.

Let the magnetization vector $\mathbf{m}$ be written $(m_x, \, m_y, \, m_z)$. The degrees of freedom for each component of the magnetization are associated with elements E and denoted as $m_{x,E}$, $m_{y,E}$, and $m_{z,E}$. We define

$$m_{u,E} = \frac{1}{|E|} \int_E m_u \, \mathrm{d}x, \quad u \in \{x, \, y, \, z\}.$$

They represent the mean values of m_u.

We define the vector space

$$\mathcal{Q}^h = \left\{ m_u^h \mid \ m_u^h = (m_{u,E_1}, \cdots, m_{u,E_{N_E}})^T \right\}. \qquad (2.3)$$

Thus, each component of the discrete magnetization m_u^h belongs to $\mathcal{Q}^h$ for $u \in \{x, y, z\}$ and we have the discrete magnetization $\mathbf{m}^h = (m_x^h, m_y^h, m_z^h)$. The dimension of the space $\mathcal{Q}^h$ is equal to N_E, the number of mesh elements. We can simply control the length of $\mathbf{m}_E$ to preserve the nonconvex constraint i.e. $|\mathbf{m}_E| = 1$.

Let the magnetic flux tensor be written $\mathbf{p}$ be written $(\mathbf{p}_x, \, \mathbf{p}_y, \, \mathbf{p}_z)$. The degrees of freedom for each component of the magnetic flux are associated with mesh edges f and denoted as $p_{x,E,f}$, $p_{y,E,f}$ and $p_{z,E,f}$. We define

$$p_{u,E,f} = \frac{1}{|f|} \int_f \mathbf{p}_u \cdot \boldsymbol{n}_E \, \mathrm{d}x, \quad u \in \{x, \, y, \, z\}. \qquad (2.4)$$

They represent the mean normal flux of edge f, with $f \in \partial E$.

We use additional notations for local degrees of freedom. Let $p_{u,E} = (p_{u,E,f_1}, \ldots, p_{u,E,f_m})^T$ be the vector of degrees of freedom associated with element E, where $f_1, \ldots, f_m \in \partial E$ and $\mathbf{p}_E = (p_{x,E},\, p_{y,E},\, p_{z,E})^T$. We define the vector space

$$\mathcal{F}^h = \left\{ p_u^h \mid p_u^h = (p_{u,E_1}, \cdots, p_{u,E_{N_E}})^T \right\}. \tag{2.5}$$

Thus, each component of the discrete magnetic flux p_u^h belongs to $\mathcal{F}^h$ for $u \in \{x, y, z\}$, and we have the discrete magnetic flux $\mathbf{p}^h = (p_x^h,\, p_y^h,\, p_z^h)$. The dimension of the space $\mathcal{F}^h$ is equal to the number of boundary edges plus twice the number of internal edges (faces in 3D).

By defining magnetic flux as in (2.4), we clearly have the flux continuity constraint

$$p_{u,E_1,f} + p_{u,E_2,f} = 0 \tag{2.6}$$

where f is an internal edge shared by two elements E_1 and E_2.

The second step of the MFD method is to define appropriate inner products in the discrete spaces. In the space of discrete magnetizations, we define the discrete inner product by

$$\langle \mathbf{m}^h,\, \mathbf{w}^h \rangle_{\mathcal{Q}} := \sum_{u \in \{x,y,z\}} \langle m_u^h,\, w_u^h \rangle_{\mathcal{Q}}, \quad \langle m_u^h,\, w_u^h \rangle_{\mathcal{Q}} := \sum_{E \in \Omega_h} \langle m_{u,E}^h,\, w_{u,E}^h \rangle_{\mathcal{Q},E}. \tag{2.7}$$

Note that $\langle m_{u,E}^h,\, w_{u,E}^h \rangle_{\mathcal{Q},E} = |E|\, m_{u,E}\, w_{u,E}$, because we have only one degree of freedom per mesh element for each component of the magnetization.

In the space of discrete flux tensors, we define the following inner product by

$$\langle \mathbf{p}^h,\, \mathbf{q}^h \rangle_{\mathcal{F}} := \sum_{u \in \{x,y,z\}} \langle p_u^h,\, q_u^h \rangle_{\mathcal{F}}, \quad \langle p_u^h,\, q_u^h \rangle_{\mathcal{F}} := \sum_{E \in \Omega_h} \langle p_{u,E},\, q_{u,E} \rangle_{\mathcal{F},E}. \tag{2.8}$$

Here $\langle \cdot,\, \cdot \rangle_{\mathcal{F},E}$ is an element-based inner product that is constructed to satisfy consistency and stability conditions discussed in section 2.4.

The third step of the MFD method is to discretize the divergence operator. For each component of the magnetic flux, we discretize the divergence theorem for element E and get the discrete divergence operator.

$$\mathcal{DIV}_E\, p_{u,E} = \frac{1}{|E|} \sum_{f \in \partial E} |f|\, p_{u,E,f}. \tag{2.9}$$

The degrees of freedom associated with the magnetic flux tensor were chosen to define the discrete divergence operator easily. We further define

$$\mathbf{DIV}_E\, \mathbf{p}_E = \begin{pmatrix} \mathcal{DIV}_E\, p_{x,E}, \\ \mathcal{DIV}_E\, p_{y,E}, \\ \mathcal{DIV}_E\, p_{z,E} \end{pmatrix}$$

The fourth step of the MFD method is to define the discrete gradient operator. In the continuum setting, the Green formula states that the gradient operator is negatively adjoint to the divergence operator with respect to the L^2-inner product, under the homogeneous boundary conditions:

$$\int_\Omega \mathbf{m} \cdot \mathbf{div}\,\mathbf{p}\;\mathrm{d}x = -\int_\Omega \nabla\mathbf{m}\colon \mathbf{p}\;\mathrm{d}x.$$

The discrete gradient operator is defined implicitly and uniquely from the discrete duality principle :

$$\langle \mathbf{m}^h,\, \mathbf{DIV}\,\mathbf{p}^h \rangle_\mathcal{Q} = -\langle \mathbf{GRAD}\,\mathbf{m}^h,\, \mathbf{p}^h \rangle_\mathcal{F} \qquad \forall \mathbf{m}^h, \mathbf{p}^h. \tag{2.10}$$

Using the above four-step mimetic discretization, we have a semi-discretization for (3.1). The semi-discrete mimetic formulation for the Landau-Lifshitz equation (1.8) is to find $\mathbf{m}^h$ and $\mathbf{p}^h$ such that

$$\mathbf{p}^h = -\mathbf{GRAD}\,\mathbf{m}^h,$$
$$\tfrac{\partial \mathbf{m}^h}{\partial t} = \mathbf{m}^h \times \mathbf{DIV}\mathbf{p}^h + \alpha\,(\mathbf{m}^h \cdot \mathbf{DIV}\,\mathbf{p}^h)\,\mathbf{m}^h - \alpha\,\mathbf{DIV}\,\mathbf{p}^h + \mathbf{f}^h(\mathbf{m}^h)$$

where $\mathbf{f}^h(\mathbf{m}^h)$ is a discretization of low-order terms (3.2).

2.3.2 Local mimetic formulation

For the local mimetic formulation, we define a local discrete gradient operator. We first discretize Green formula on each element E:

$$\int_E \mathbf{m} \cdot \mathbf{div}\,\mathbf{p}\;\mathrm{d}x = -\int_E \nabla\mathbf{m}\colon \mathbf{p}\;\mathrm{d}x + \int_{\partial E} (\mathbf{p}\cdot\mathbf{n})\cdot\mathbf{m}\;\mathrm{d}x \tag{2.11}$$

We need additional degrees of freedom for magnetization $\mathbf{m}$ associated with mesh edge f $\mathbf{m}_f = (m_{x,f}, m_{y,f}, m_{z,f})$ to discretize the last term in (2.11). The degrees of freedom for each component of the magnetization are associated with edges f, given by

$$m_{u,f} = \frac{1}{|f|} \int_f m_u \;\mathrm{d}x, \quad u \in \{x, y, z\}.$$

They represent mean value of m_u on each edge f. The number of these degrees of freedom is equal to the number of edges N_F. Let $\widetilde{\mathbf{m}}_E = (\widetilde{m}_{x,E}, \widetilde{m}_{y,E}, \widetilde{m}_{z,E})^T$ be the vector of these additional degrees of freedom associated with each element E, where $\widetilde{m}_{u,E} = (m_{u,f}, m_{u,f}, m_{u,f})^T_{f\in\partial E}$ for $u \in \{x, y, z\}$.

The local discrete gradient operator is defined implicitly by

$$\langle \mathbf{m}_E,\, \mathbf{DIV}_E\,\mathbf{p}_E \rangle_{\mathcal{Q},E} = -\langle \mathbf{GRAD}_E \begin{pmatrix} \mathbf{m}_E \\ \widetilde{\mathbf{m}}_E \end{pmatrix},\, \mathbf{p}_E \rangle_{\mathcal{F},E} + \sum_{f\in\partial E} |f|\,\mathbf{p}_f \cdot \mathbf{m}_f \tag{2.12}$$

for all $\mathbf{m}_E$, $\widetilde{\mathbf{m}}_E$, and $\mathbf{p}_E$. This follows from the discrete duality principle. Moreover, the local discrete gradient operator is defined uniquely, since these are bone a fide inner products.

Since the inner products defined in (3.18) and (2.8) are sums of inner products for vector components, we can also define a component-wise discrete gradient operator

$$\langle m_{u,E}, \, \mathcal{DIV}_E \, p_{u,E} \rangle_{\mathcal{Q},E} = -\langle \mathcal{GRAD}_E \begin{pmatrix} m_{u,E} \\ \widetilde{m}_{u,E} \end{pmatrix}, \, p_{u,E} \rangle_{\mathcal{F},E} + \sum_{f \in \partial E} |f| \, p_{u,E,f} \cdot m_{u,f}.$$

We introduce inner product matrices $\mathbb{M}_{\mathcal{Q},E}$ and $\mathbb{M}_{\mathcal{F},E}$ to simplify the above formulae:

$$\langle m_{u,E}, \, w_{u,E} \rangle_{\mathcal{Q},E} = m_{u,E} \, \mathbb{M}_{\mathcal{Q},E} \, w_{u,E}, \qquad \langle p_{u,E}, \, q_{u,E} \rangle_{\mathcal{F},E} = p_{u,E} \, \mathbb{M}_{\mathcal{F},E} \, q_{u,E}. \tag{2.13}$$

The matrix $\mathbb{M}_{\mathcal{Q},E}$ has entries $|E|$ on its diagonal. The construction of the second matrix $\mathbb{M}_{\mathcal{F},E}$ needs special attention; see section 2.3.4 below. We get the explicit formula for the discrete gradient operator

$$\mathcal{GRAD}_E \begin{pmatrix} m_{u,E} \\ \widetilde{m}_{u,E} \end{pmatrix} = \mathbb{M}_{\mathcal{F},E}^{-1} \begin{pmatrix} |f_1| \, (m_{u,f_1} - m_{u,E}) \\ |f_2| \, (m_{u,f_2} - m_{u,E}) \\ \vdots \\ |f_n| \, (m_{u,f_n} - m_{u,E}) \end{pmatrix}, \tag{2.14}$$

where n is the total number of edges (faces in 3D) of element E.

In summary, the semi-discrete mimetic formulation is to find $\mathbf{m}_E$, $\widetilde{\mathbf{m}}_E$, and $\mathbf{p}_E$, for $E \in \Omega^h$, such that

$$\begin{aligned} \mathbf{p}_E &= -\mathbf{GRAD}_E \begin{pmatrix} \mathbf{m}_E \\ \widetilde{\mathbf{m}}_E \end{pmatrix}, \\ \frac{\partial \mathbf{m}_E}{\partial t} &= \mathbf{m}_E \times \mathbf{DIV}_E \mathbf{p}_E + \alpha \, (\mathbf{m}_E \cdot \mathbf{DIV}_E \, \mathbf{p}_E) \, \mathbf{m}_E - \alpha \, \mathbf{DIV}_E \, \mathbf{p}_E + \mathbf{f}_E(\mathbf{m}_E), \end{aligned} \tag{2.15}$$

together with the flux continuity constraint (2.6), initial conditions and boundary conditions. If Dirichlet boundary conditions are given, we can set the auxiliary magnetization $\widetilde{\mathbf{m}}_E$ to the given values on the edges. If Neumann boundary conditions are given, we can set the magnetic fluxes $\mathbf{p}_E$ to given values on the edges.

The local mimetic formulation implies a global mimetic formulation. The local mimetic formulation is more suitable for implementation on computers, whereas the global mimetic formulation is more suitable for convergence analysis. The local and global discrete gradient operator are equivalent. This fact can be shown by summing up equations (3.21) and canceling out interface terms by flux continuity constraint (2.6).

2.3.3 Implicit-explicit time discretization

We consider a θ-scheme, $0 \le \theta \le 1$ by discretizing time derivative in (3.32). Let us denote the time $t^j = j \, k$ where k is the time stepsize and j is the index. We define the θ-scheme as

$$\mathbf{p}_E^{j+\theta} = -\mathbf{GRAD}_E \begin{pmatrix} \mathbf{m}_E^{j+\theta} \\ \widetilde{\mathbf{m}}_E^{j+\theta} \end{pmatrix},$$

$$\frac{\mathbf{m}_E^{j+1} - \mathbf{m}_E^j}{k} = \mathbf{m}_E^j \times \mathbf{DIV}_E \, \mathbf{p}_E^{j+\theta} + \alpha \, (\mathbf{m}_E^j \cdot (\mathbf{DIV}_E \, \mathbf{p}_E^{j+\theta})) \mathbf{m}_E^j - \alpha \mathbf{DIV}_E \, p_E^{j+\theta} + \mathbf{f}_E^j(\mathbf{m}_E^j). \tag{2.16}$$

For $\theta = 0$, (2.16) is an explicit method otherwise it is an implicit method. But it is not fully implicit as it requires only a linear solver for each time step. From now on, we only deal with the implicit case $\theta = 1$. For simplicity, we write $\mathbf{m}^j$ instead of $\mathbf{m}^{h,j}$. By plugging in the first equation in (2.16) into the second equation, and using flux continuity constraint (2.6) with appropriate boundary and initial conditions, we get a linear system of equations for element-based and edge-based magnetizations:

$$\mathbb{A}^j \begin{pmatrix} \mathbf{m}^{j+1} \\ \widetilde{\mathbf{m}}^{j+1} \end{pmatrix} = \begin{pmatrix} \mathbf{b}_1^j \\ \mathbf{b}_2^j \end{pmatrix}. \tag{2.17}$$

Here, the flux continuity conditions (2.6) can multiplied by $|f|$ for better symmetry. The vector on the right-hand side of the equation depends on $\mathbf{m}^j$, the external field, the stray field, and boundary conditions.

The stiffness matrix $\mathbb{A}^j$ is of the following form

$$\mathbb{A}^j = \sum_{E \in \Omega^h} \mathbb{N}_E \, \mathbb{A}_E^j \, \mathbb{N}_E^T. \tag{2.18}$$

where $\mathbb{N}_E$ is the conventional assembly matrix that maps local indices to global indices. It is a sparse matrix and is the sum of local matrices. The local $3(n+1) \times 3(n+1)$ matrix $\mathbb{A}_E^j$ has the following block structure

$$\mathbb{A}_E^j = \begin{pmatrix} \mathbb{A}^{EE} & \mathbb{A}^{Ef} \\ \mathbb{A}^{fE} & \mathbb{A}^{ff} \end{pmatrix} \tag{2.19}$$

where the first block row corresponds to element-based magnetizations and n is the number of edges of the element E.

Let $\mathbb{I}$ be a generic identity matrix, $\mathbb{C}_E$ be the $n \times n$ diagonal matrix $\mathbb{C}_E = \text{diag}\{|f_1|, \dots, |f_n|\}$, and $\mathbf{e} = (1, 1, \dots, 1)^T$. We could further represent block matrices of (2.19) using the tensor-product notation:

$$\begin{aligned} \mathbb{A}^{EE} &= \mathbb{I} + \frac{k}{|E|} \left(\mathbf{e}^T \mathbb{C}_E \, \mathbb{M}_{\mathcal{F},E}^{-1} \, \mathbb{C}_E \, \mathbf{e} \right) \hat{\mathbb{A}}^j, \quad \mathbb{A}^{Ef} = -\frac{k}{|E|} \left(\mathbf{e}^T \mathbb{C}_E \, \mathbb{M}_{\mathcal{F},E}^{-1} \, \mathbb{C}_E \right) \otimes \hat{\mathbb{A}}^j \\ \mathbb{A}^{fE} &= -\left(\mathbb{C}_E \, \mathbb{M}_{\mathcal{F},E}^{-1} \, \mathbb{C}_E \, \mathbf{e} \right) \otimes \mathbb{I}, \qquad \mathbb{A}^{ff} = \left(\mathbb{C}_E \, \mathbb{M}_{\mathcal{F},E}^{-1} \, \mathbb{C}_E \right) \otimes \mathbb{I}, \end{aligned} \tag{2.20}$$

and

$$\hat{\mathbb{A}}^j = \alpha \, \mathbb{I} - \alpha \, \mathbf{m}_E^j \, (\mathbf{m}_E^j)^T - \begin{pmatrix} 0 & -m_{z,E}^j & m_{y,E}^j \\ m_{z,E}^j & 0 & -m_{x,E}^j \\ -m_{y,E}^j & m_{x,E}^j & 0 \end{pmatrix}. \tag{2.21}$$

Our method is summarized in Algorithm 1. We project the magnetization onto the unit sphere in step 2b), to preserve the nonconvex constraint $|\mathbf{m}_E^{j+1}| = 1$. In the actual computation, we only require the matrix $\mathbb{M}_{\mathcal{F},E}^{-1}$. This can be calculated at the same cost as matrix $\mathbb{M}_{\mathcal{F},E}$. In Algorithm 1 step 2a), the right-hand side of (2.17) does not depend on $\widetilde{\mathbf{m}}^j$ (See (2.16) with $\theta = 1$). Thus, in practice, we don't need to renormalize $\widetilde{\mathbf{m}}_E^{j+1}$ in step 2b) of the algorithm to prepare for the next iteration.

Algorithm 1 The mimetic finite difference method for the Landau-Lifshitz equation

For a given final time $T > 0$, set $J = [\frac{T}{k}]$.

1. Set an initial discrete magnetization $\mathbf{m}^0$ at the centroids of mesh elements.

2. For $j = 0, \ldots, J - 1$,

   a) Form and solve the linear system (2.17) and denote the solution by $\begin{pmatrix} \hat{\mathbf{m}}^{j+1} \\ \widetilde{\mathbf{m}}^{j+1} \end{pmatrix}$.

   b) Renormalize the element-centered magnetizations,

$$\mathbf{m}_E^{j+1} := \frac{\hat{\mathbf{m}}_E^{j+1}}{|\hat{\mathbf{m}}_E^{j+1}|}, \qquad \forall E \in \Omega^h.$$

2.3.4 Construction of the matrices $\mathbb{M}_{\mathcal{F},E}$ and $\mathbb{M}_{\mathcal{F},E}^{-1}$

The inner product matrix $\mathbb{M}_{\mathcal{F},E}$ in (2.13) and its inverse $\mathbb{M}_{\mathcal{F},E}^{-1}$ are built to satisfy the consistency and stability conditions.

- (Consistency) Let $p_{u,E}^0$ and $q_{u,E}$ be vectors of the degrees of freedom for functions $\mathbf{p}_u^0$ and $\mathbf{q}_u$, respectively. Let $\mathbf{p}_u^0$ be any constant vector function and $\mathbf{q}_u$ be any sufficiently smooth function such that $\mathbf{div}\, \mathbf{q}_u$ is constant and $\mathbf{q}_u \cdot \mathbf{n}_f$ is constant on each edge f of the element E. Then the local mimetic inner product is exact with the integral of $\mathbf{p}_u^0$ and $\mathbf{q}_u$.

$$\left(p_{u,E}^0\right)^T \mathbb{M}_{\mathcal{F},E}\, q_{u,E} = \langle p_{u,E}^0,\, q_{u,E} \rangle_{\mathcal{F},E} = \int_E \mathbf{p}_u^0 \cdot \mathbf{q}_u \,\mathrm{d}x \tag{2.22}$$

- (Stability) There exists two positive constants $c_0, C_0 > 0$, independent of h and E, such that, for every $q_u \in \mathcal{F}^h|_E$ and every $E \in \Omega^h$, we have

$$c_0 \,|E|\, q_{u,E}^T \, q_{u,E} \leq q_{u,E}^T \, \mathbb{M}_{\mathcal{F},E}\, q_{u,E} = \langle q_{u,E},\, q_{u,E} \rangle_{\mathcal{F},E} \leq C_0 \,|E|\, q_{u,E}^T \, q_{u,E}. \tag{2.23}$$

Taking $\mathbf{p}_u^0$ as the gradient of a linear function m_u^1 with mean value zero on E and integrating by parts, we have

$$\int_E \mathbf{p}_u^0 \cdot \mathbf{q}_u \,\mathrm{d}x = -\int_E m_u^1 \,\mathrm{div}\, \mathbf{q}_u \,\mathrm{d}x + \int_{\partial E} (\mathbf{q}_u \cdot \mathbf{n}_E)\, m_u^1 \,\mathrm{d}x = \sum_{f \in \partial E} q_{u,E,f} \int_f m_u^1 \,\mathrm{d}x. \tag{2.24}$$

Let (x_E, y_E, z_E) be the centroid of the element E. By taking $m_u^1 = x - x_E,\ y - y_E$, and $z - z_E$, the formula in (2.22) becomes

$$q_{u,E}^T \, \mathbb{M}_{\mathcal{F},E}\, p_{u,E}^{0,(j)} = q_{u,E}^T \, r_{u,E}^{(j)}. \tag{2.25}$$

for $j = 1, 2, 3$. Let us take $\mathbb{N} = [p_{u,E}^{0,(1)}, \ p_{u,E}^{0,(2)}, \ p_{u,E}^{0,(3)}]$ and $\mathbb{R} = [r_{u,E}^{(1)}, \ r_{u,E}^{(2)}, \ r_{u,E}^{(3)}]$, to reformulate (2.22) as

$$\mathbb{M}_{\mathcal{F},E}\, \mathbb{N} = \mathbb{R}. \tag{2.26}$$

Let $f_1, \ldots, f_m$ be the edges of E. Using equation (2.4), we can calculate

$$p_{u,E}^{0,(1)}|_{f_i} = \frac{1}{|f_i|} \int_{f_i} \mathbf{p}_u \cdot \boldsymbol{n}_{f_i} \ \mathrm{d}x = \frac{1}{|f_i|} \int_{f_i} \nabla(x - x_E) \cdot \boldsymbol{n}_{f_i} \ \mathrm{d}x = n_{x_{f_i}}.$$

for $i = 1, \ldots, m$. Similary, we can calculate all the entries of $\mathbb{N}$, and we have

$$\mathbb{N} = \begin{pmatrix} n_{x_{f_1}} & n_{y_{f_1}} & n_{z_{f_1}} \\ n_{x_{f_2}} & n_{y_{f_2}} & n_{z_{f_2}} \\ \vdots & \vdots & \vdots \\ n_{x_{fm}} & n_{y_{fm}} & n_{z_{fm}} \end{pmatrix}.$$

Here n_{u_f} is the u-th component of the outward unit normal vector of the edge f of E. Let (x_f, y_f, z_f) be the centroid of the edge. By taking $q_{u,E} = \vec{e}_i$ in (2.24), we can calculate

$$r_{u,E}^{(1)}|_{f_i} = \int_{f_i} (x - x_E) \ \mathrm{d}x = |f_i|(x_{f_i} - x_E)$$

Similary, we can calculate all the entries of $\mathbb{R}$, and we have

$$\mathbb{R} = \begin{pmatrix} |f_1|(x_{f_1} - x_E) & |f_1|(y_{f_1} - y_E) & |f_1|(z_{f_1} - z_E) \\ |f_2|(x_{f_2} - x_E) & |f_2|(y_{f_2} - y_E) & |f_2|(z_{f_2} - z_E) \\ \vdots & \vdots & \vdots \\ |f_m|(x_{f_m} - x_E) & |f_m|(y_{f_m} - y_E) & |f_m|(z_{f_m} - z_E) \end{pmatrix}.$$

The symmetric positive definite matrix

$$\mathbb{M}_{\mathcal{F},E} = \frac{1}{|E|} \mathbb{R}\mathbb{R}^T + \gamma\, (\mathbb{I} - \mathbb{N}\, (\mathbb{N}^T\, \mathbb{N})^{-1}\, \mathbb{N}^T), \qquad \gamma > 0, \tag{2.27}$$

is a solution to matrix equation (2.26) which was shown in [21]. The second term includes the orthogonal projection, and we can set $\gamma = |E|$ or $\gamma = \frac{1}{2|E|}\, \mathrm{trace}(\mathbb{R}\,\mathbb{R}^T)$. The general solution to (2.26) is

$$\mathbb{M}_{\mathcal{F},E} = \frac{1}{|E|} \mathbb{R}\mathbb{R}^T + (\mathbb{I} - \mathbb{N}\, (\mathbb{N}^T\, \mathbb{N})^{-1}\, \mathbb{N}^T)\, \mathbb{G}\, (\mathbb{I} - \mathbb{N}\, (\mathbb{N}^T\, \mathbb{N})^{-1}\, \mathbb{N}^T) \tag{2.28}$$

where $\mathbb{G}$ is a symmetric positive definite matrix. This matrix is chosen to satisfy the stability condition (2.23).

We can easily derive a formula for $\mathbb{M}_{\mathcal{F},E}^{-1}$ used in the actual computation of Algorithm 1. The matrix equation (2.26) can be also written as

$$\mathbb{M}_{\mathcal{F},E}^{-1}\, \mathbb{R} = \mathbb{N}. \tag{2.29}$$

Because there are only changes in the role of the matrices $\mathbb{R}$ and $\mathbb{N}$ with the same equation structure, the symmetric positive definite matrix

$$\mathbb{M}_{\mathcal{F},E}^{-1} = \frac{1}{|E|}\mathbb{N}\mathbb{N}^T + \tilde{\gamma}(\mathbb{I} - \mathbb{R}\,(\mathbb{R}^T\,\mathbb{R})^{-1}\,\mathbb{R}^T) \tag{2.30}$$

is a solution to (2.29). The general solution to (2.29) is

$$\mathbb{M}_{\mathcal{F},E}^{-1} = \frac{1}{|E|}\mathbb{N}\mathbb{N}^T + (\mathbb{I} - \mathbb{R}\,(\mathbb{R}^T\,\mathbb{R})^{-1}\,\mathbb{R}^T)\,\tilde{\mathbb{G}}\,(\mathbb{I} - \mathbb{R}\,(\mathbb{R}^T\,\mathbb{R})^{-1}\,\mathbb{R}^T), \tag{2.31}$$

where $\tilde{\mathbb{G}}$ is symmetric positive definite matrix. We can set $\tilde{\gamma} = \frac{1}{|E|}$ or $\tilde{\gamma} = \frac{1}{2\,|E|}\,\text{trace}(\mathbb{N}\,\mathbb{N}^T)$.

Remark 3. *The matrix equations (2.26) and (2.29) both have multiple solutions. However, the matrices in (2.27) and (2.30) with $\gamma = \tilde{\gamma}^{-1} = |E|$ are not inverse to each other. They do not represent related members from two families of solutions.*

2.4 Stability analysis

In this section, we show that the discrete exchange energy decreases in time under certain conditions for both explicit ($\theta = 0$) and implicit time integration schemes, focusing on $\theta = 1$ in the latter case. We consider the case $\bar{\mathbf{h}} = 0$ and homogeneous Neumann boundary conditions. For the explicit scheme, the time step and the mesh size must satisfy a Courant condition, but for the implicit scheme, we do not have such constraint. In our results, we require all matrices $\mathbb{M}_{\mathcal{F},E}^{-1}$ to be M-matrices.

Let $\|\cdot\|_{\mathcal{F}}$ denote the norm induced by the global inner product in (2.8) and $\|\cdot\|_{\mathcal{F},E}$ denote the norm induced by local inner product in (2.8). We first give our main result and then prove two lemmas.

Theorem 1. *Let the assumptions from Lemmas 1 and 2 hold true. For the explicit scheme ($\theta = 0$), we further assume the Courant condition*

$$\frac{k}{h^2} \leq \frac{2\alpha}{C_1(1 + \alpha^2)}. \tag{2.32}$$

Then, for any j, we have the following energy estimate,

$$||\mathbf{GRAD}\,\mathbf{m}^{j+1}||_{\mathcal{F}} \leq ||\mathbf{GRAD}\,\mathbf{m}^j||_{\mathcal{F}}.$$

Proof. Let $\hat{\mathbf{m}}^{j+1}$ denote the element-based magnetization obtained from step 2a of Algorithm 1. Let $\mathbf{v}^j$ denote the velocity vector, i.e. $\hat{\mathbf{m}}^{j+1} = \mathbf{m}^j + k\mathbf{v}^j$. We have $\mathbf{m}_E^j \cdot \mathbf{v}_E^j = 0$ from (2.16) and $|\mathbf{m}_E^j| = 1$ from step 2b of Algorithm 1 for all E. Thus, we have $|\hat{\mathbf{m}}_E^j| \geq 1$ and we have energy decrease after normalization from Lemma 2 below, which is

$$||\mathbf{GRAD}\,\mathbf{m}^{j+1}||_{\mathcal{F}} \leq ||\mathbf{GRAD}\,\hat{\mathbf{m}}^{j+1}||_{\mathcal{F}}. \tag{2.33}$$

Now, we derive an upper bound for $\|\mathbf{GRAD}\,\hat{\mathbf{m}}^{j+1}\|_{\mathcal{F}}$, starting from the following identity,

$$\|\mathbf{GRAD}(\mathbf{m}^j + k\mathbf{v}^j)\|_{\mathcal{F}}^2 = \|\mathbf{GRAD}\,\mathbf{m}^j\|_{\mathcal{F}}^2$$
$$+ 2k\,\langle\mathbf{GRAD}\,\mathbf{m}^j,\,\mathbf{GRAD}\,\mathbf{v}^j\rangle_{\mathcal{F}} + k^2\|\mathbf{GRAD}\,\mathbf{v}^j\|_{\mathcal{F}}^2. \tag{2.34}$$

Next, we derive an expression for $\langle\mathbf{GRAD}\,\mathbf{m}^j,\,\mathbf{GRAD}\,\mathbf{v}^j\rangle_{\mathcal{F}}$. We get the definition of $\mathbf{v}_E^j$ from the second equation in the θ-scheme (2.16),

$$\mathbf{v}_E^j = -\mathbf{m}_E^j \times \mathbf{DIV}_E\,\mathbf{p}_E^{j+\theta} - \alpha\left(\mathbf{m}_E^j \cdot \mathbf{DIV}_E\,\mathbf{p}_E^{j+\theta}\right)\mathbf{m}_E^j + \alpha\,\mathbf{DIV}_E\,\mathbf{p}_E^{j+\theta}.$$

From this definition and the fact that $|\mathbf{m}_E^j| = 1$, we get

$$\alpha\mathbf{v}_E^j + \mathbf{m}_E^j \times \mathbf{v}_E^j = -(1+\alpha^2)\left((\mathbf{m}_E^j \cdot \mathbf{DIV}_E\,\mathbf{p}_E^{j+\theta})\,\mathbf{m}_E^j - \mathbf{DIV}_E\,\mathbf{p}_E^{j+\theta}\right). \tag{2.35}$$

Taking the dot product with $\mathbf{v}_E^j$, and summing over the element with weighted element volumes, we get

$$-\frac{\alpha}{1+\alpha^2}\langle\mathbf{v}^j,\,\mathbf{v}^j\rangle_{\mathcal{Q}} = -\langle\mathbf{DIV}\,\mathbf{p}^{j+\theta},\,\mathbf{v}^j\rangle_{\mathcal{Q}} \tag{2.36}$$

From the duality property of the mimetic operator, we have

$$-\langle\mathbf{DIV}\,\mathbf{p}^{j+\theta},\,\mathbf{v}^j\rangle_{\mathcal{Q}} = \langle\mathbf{GRAD}(\mathbf{m}^j + \theta k\mathbf{v}^j),\,\mathbf{GRAD}\mathbf{v}^j\rangle_{\mathcal{F}} \tag{2.37}$$

Equations (2.36) and (2.37) give

$$-\frac{\alpha}{1+\alpha^2}\langle\mathbf{v}^j,\,\mathbf{v}^j\rangle_{\mathcal{Q}} = \langle\mathbf{GRAD}\,\mathbf{m}^j,\,\mathbf{GRAD}\mathbf{v}^j\rangle_{\mathcal{F}} + \theta k\,\langle\mathbf{GRAD}\mathbf{v}^j,\,\mathbf{GRAD}\,\mathbf{v}^j\rangle_{\mathcal{F}} \tag{2.38}$$

Inserting (2.38) in (2.34), we obtain

$$\|\mathbf{GRAD}\,\hat{\mathbf{m}}^{j+1}\|_{\mathcal{F}}^2 = \|\mathbf{GRAD}\,\mathbf{m}^j\|_{\mathcal{F}}^2 - \frac{2\alpha\,k}{1+\alpha^2}\|\mathbf{v}^j\|_{\mathcal{Q}}^2 - k^2\,(2\theta - 1)\|\mathbf{GRAD}\,\mathbf{v}^j\|_{\mathcal{F}}^2.$$

This shows that for the implicit scheme, $\theta = 1$, we have the decrease of the energy using equation (2.33). For the explicit scheme $\theta = 0$, we have

$$\|\mathbf{GRAD}\,\hat{\mathbf{m}}^{j+1}\|_{\mathcal{F}}^2 \le \|\mathbf{GRAD}\,\mathbf{m}^j\|_{\mathcal{F}}^2 - k\left(\frac{2\alpha}{1+\alpha^2} - \frac{C_1\,k}{h^2}\right)\|\mathbf{v}^j\|_{\mathcal{Q}^h}^2$$

using Lemma 1 below. Thus, for the explicit scheme, we have the energy decrease under the Courant condition (2.32) using (2.33). $\qquad\square$

We now present two technical lemmas which are important in Theorem 1 above. The first lemma is the inverse estimate which uses the stability condition (2.23). This lemma is used only for the explicit scheme ($\theta = 0$). The second lemma shows that the exchange energy decreases even under nonlinear projection step in Algorithm 1 step 2b). It assumes that the family of elemental matrices $\mathbb{M}_{\mathcal{F},E}^{-1}$ contains M-matrices, which gives certain constraints on the shape of mesh cells. An M-matrix is a Z-matrix with eigenvalues whose real parts are positive; a Z-matrix is a matrix whose off-diagonal entries are less than or equal to zero. We refer to [14, 59] for more details about M-matrices.

Lemma 1. *Let mesh Ω^h be shape regular and quasi-uniform. Then, for any $\mathbf{v}^h \in (\mathcal{Q}^h)^3$, we have the inverse estimate,*

$$\|\mathbf{GRAD}\,\mathbf{v}^h\|_{\mathcal{F}}^2 \leq \frac{C_1}{h^2}\|\mathbf{v}^h\|_{\mathcal{Q}}^2, \tag{2.39}$$

where C_1 is a positive constant, independent of h and $\mathbf{v}^h$.

Proof. For each component $u \in \{x, y, z\}$, we have

$$\|\mathcal{GRAD}\,v_u^h\|_{\mathcal{F}} = \|\mathbb{M}_{\mathcal{F}}^{-1/2}\,\mathcal{DIV}^T\,\mathbb{M}_{\mathcal{Q}}v_u^h\| \leq \frac{C_2}{h^{d/2}}\|\mathcal{DIV}^T\,\mathbb{M}_{\mathcal{Q}}v_u^h\| \leq \frac{C_2}{h^{d/2}}\|\mathcal{DIV}^T\|\,\|\mathbb{M}_{\mathcal{Q}}v_u^h\|.$$

where C_2 depends on c_0 in (2.23) and the shape regularity of mesh Ω^h. Here, we used the definition of the discrete gradient operator in (2.10) in the first equality and the stability condition (2.23) in the first inequality. From the definition of the discrete divergence operator, we have $\|\mathcal{DIV}^T\| \leq C_3\,h^{-1}$, where C_3 depends only on the shape regularity of the mesh. Also, we have $\|\mathbb{M}_{\mathcal{Q}}^{1/2}\| \leq h^{d/2}$ from the definition of the inner product matrix. Thus, we get

$$\|\mathcal{GRAD}\,v_u^h\|_{\mathcal{F}}^2 \leq \frac{(C_2\,C_3)^2}{h^2}\|v_u^h\|_{\mathcal{Q}}^2.$$

Summing over $u \in \{x, y, z\}$, we obtain the above result with $C_1 = (C_2\,C_3)^2$. $\qquad\square$

Lemma 2. *Let each elemental matrix $\mathbb{M}_{\mathcal{F},E}$ satisfy two conditions: (a) $\mathbb{M}_{\mathcal{F},E}^{-1}$ is an M-matrix, and (b) vector $\mathbb{M}_{\mathcal{F},E}^{-1}\,\mathbb{C}_E\,\mathbf{e}$ has positive entries. Let $\hat{\mathbf{v}}^h \in (\mathcal{Q}^h)^3$ be a vector with $|\hat{\mathbf{v}}_E| \geq 1$ for all $E \in \Omega^h$. Also, let $\mathbf{v}^h$ be the normalization of $\hat{\mathbf{v}}^h$, that is $\mathbf{v}_E = \hat{\mathbf{v}}_E/|\hat{\mathbf{v}}_E|$ for all $E \in \Omega^h$. Then, we have energy decrease after the renormalization:*

$$\|\mathbf{GRAD}\,\mathbf{v}^h\|_{\mathcal{F}} \leq \|\mathbf{GRAD}\,\hat{\mathbf{v}}^h\|_{\mathcal{F}}. \tag{2.40}$$

Proof. First, we define the vectors

$$\mathbf{q}^h = \mathbf{GRAD}\,\mathbf{v}^h \quad \text{and} \quad \mathbf{q}_E = \mathbf{GRAD}_E\begin{pmatrix}\mathbf{v}_E \\ \widetilde{\mathbf{v}}_E\end{pmatrix}$$

using global and local discrete gradient operators. The global and local discrete gradient operators are equivalent from the flux continuity constraint, which is $q_{u,E_1,f} + q_{u,E_2,f} = 0$ on each internal edge f shared by two elements E_1 and E_2. From the additivity property of the inner products, we have

$$\|\mathbf{q}\|_{\mathcal{F}}^2 = \sum_{E \in \Omega^h} \|\mathbf{q}_E\|_{\mathcal{F},E}^2.$$

We then obtain

$$\|\mathbf{q}_{u,E}\|_{\mathcal{F},E}^2 = \begin{pmatrix}v_{u,E} \\ \widetilde{v}_{u,E}\end{pmatrix}^T \begin{pmatrix}\mathbf{e}^T\mathbb{T}_E\,\mathbf{e} & -\mathbf{e}^T\mathbb{T}_E \\ -\mathbb{T}_E\,\mathbf{e} & \mathbb{T}_E\end{pmatrix}\begin{pmatrix}v_{u,E} \\ \widetilde{v}_{u,E}\end{pmatrix}, \qquad \mathbb{T}_E = \mathbb{C}_E\,\mathbb{M}_{\mathcal{F},E}^{-1}\,\mathbb{C}_E \tag{2.41}$$

from formula (2.14) for the local discrete gradient operator and the definition of the diagonal matrix $\mathbb{C}_E$. The $\widetilde{v}_{u,E}^h$ are associated with edges and are defined completely by the flux continuity condition $q_{u,E_1,f} + q_{u,E_2,f} = 0$. We sum up equations (2.41) to get

$$\|\mathbf{q}_u\|_{\mathcal{F}}^2 = \sum_{E \in \Omega^h} \|\mathbf{q}_{u,E}\|_{\mathcal{F},E}^2 = \begin{pmatrix} v_u^h \\ \widetilde{v}_u^h \end{pmatrix}^T \begin{pmatrix} \mathbb{T}^{EE} & \mathbb{T}^{Ef} \\ \mathbb{T}^{fE} & \mathbb{T}^{ff} \end{pmatrix} \begin{pmatrix} v_u^h \\ \widetilde{v}_u^h \end{pmatrix}. \tag{2.42}$$

By multipling (2.14) by $|f|$ and using the flux continuity equation, we have

$$\mathbb{T}^{fE} v_u^h + \mathbb{T}^{ff} \widetilde{v}_u^h = 0.$$

Plugging this equation into (2.42), we have

$$\|\mathbf{q}_u\|_{\mathcal{F}}^2 = (v_u^h)^T \left(\mathbb{T}^{EE} - \mathbb{T}^{Ef} (\mathbb{T}^{ff})^{-1} \mathbb{T}^{fE} \right) v_u^h =: (v_u^h)^T \, \mathbb{S}^{EE} \, v_u^h.$$

The Schur complement $\mathbb{S}^{EE}$ has one important property. According to [59], the conditions (a) and (b) imply that the local matrices in (2.41) are singular irreducible M-matrices with the single null vector $\boldsymbol{e}$. Hence, the assembled matrix in (2.42) is a singular M-matrix. From linear algebra we know that the Schur complement is also a singular M-matrix. Since $\mathbb{S}^{EE} \boldsymbol{e} = 0$, the following vector-matrix-vector product can be broken into the assembly of 2×2 matrices,

$$(v_u^h)^T \, \mathbb{S}^{EE} \, v_u^h = \sum_{i<j} \beta_{ij} \begin{pmatrix} v_{u,E_i} \\ v_{u,E_j} \end{pmatrix}^T \begin{pmatrix} 1 & -1 \\ -1 & 1 \end{pmatrix} \begin{pmatrix} v_{u,E_i} \\ v_{u,E_j} \end{pmatrix}, \tag{2.43}$$

with non-negative weights β_{ij}. Recall that $v_{u,E_i} = \hat{v}_{u,E_i}/|\hat{\mathbf{v}}_{E_i}|$ and $|\hat{\mathbf{v}}_{E_i}| \geq 1$. Thus, we have the following estimate:

$$\sum_{u \in \{x,y,z\}} \left(\frac{(\hat{v}_{u,E_i})^2}{|\hat{\mathbf{v}}_{E_i}|^2} - 2 \frac{\hat{v}_{u,E_i}}{|\hat{\mathbf{v}}_{E_i}|} \frac{\hat{v}_{u,E_j}}{|\hat{\mathbf{v}}_{E_j}|} + \frac{(\hat{v}_{u,E_j})^2}{|\hat{\mathbf{v}}_{E_j}|^2} \right) = 2 - 2 \sum_{u \in \{x,y,z\}} \frac{\hat{v}_{u,E_i}}{|\hat{\mathbf{v}}_{E_i}|} \frac{\hat{v}_{u,E_j}}{|\hat{\mathbf{v}}_{E_j}|}$$

$$\leq |\hat{\mathbf{v}}_{E_i}| \, |\hat{\mathbf{v}}_{E_j}| \left(\frac{|\hat{\mathbf{v}}_{E_i}|}{|\hat{\mathbf{v}}_{E_j}|} + \frac{|\hat{\mathbf{v}}_{E_j}|}{|\hat{\mathbf{v}}_{E_i}|} - 2 \sum_{u \in \{x,y,z\}} \frac{\hat{v}_{u,E_i}}{|\hat{\mathbf{v}}_{E_i}|} \frac{\hat{v}_{u,E_j}}{|\hat{\mathbf{v}}_{E_j}|} \right) = \sum_{u \in \{x,y,z\}} (\hat{v}_{u,E_i} - \hat{v}_{u,E_j})^2.$$

We conclude that

$$\sum_{u \in \{x,y,z\}} (v_u^h)^T \, \mathbb{S}^{EE} \, v_u^h \leq \sum_{u \in \{x,y,z\}} (\hat{v}_u^h)^T \, \mathbb{S}^{EE} \, \hat{v}_u^h = \sum_{u \in \{x,y,z\}} \|\mathcal{GRAD} \, \hat{v}_u^h\|_{\mathcal{F}}^2,$$

and the assertion of the lemma follows. $\qquad \square$

2.5 Numerical Examples

In this section, we present several numerical tests on various meshes with different boundary conditions.

2.5.1 Analytical solution

As a first test, following [38], we present an analytical solution of the Landau-Lifshitz equation (1.8) with effective field involving only exchange energy term with $\mathbf{h} = \Delta\mathbf{m}$. The analytical solution $\mathbf{m} = (m_x, m_y, m_z)$ on the unit square is given by

$$m_x(x_1, x_2, t) = \frac{1}{d(t)} \sin\beta \cos(\kappa(x_1 + x_2) + g(t)),$$

$$m_y(x_1, x_2, t) = \frac{1}{d(t)} \sin\beta \sin(\kappa(x_1 + x_2) + g(t)), \tag{2.44}$$

$$m_z(x_1, x_2, t) = \frac{1}{d(t)} e^{2\kappa^2 \alpha t} \cos\beta,$$

where $\beta = \frac{\pi}{12}$, $\kappa = 2\pi$, $d(t) = \sqrt{\sin^2\beta + e^{4\kappa^2 \alpha t} \cos^2\beta}$ and $g(t) = \frac{1}{\alpha} \log\left(\frac{d(t) + e^{2\kappa^2 \alpha t} \cos\beta}{1 + \cos\beta}\right)$. Note that $\mathbf{m} \to (0, 0, 1)$ as $t \to \infty$. The analytical solution (2.44) at time 0 is shown in Fig. 2.1. We perform simulations on the time interval $[0, T]$, where $T = 0.001$.
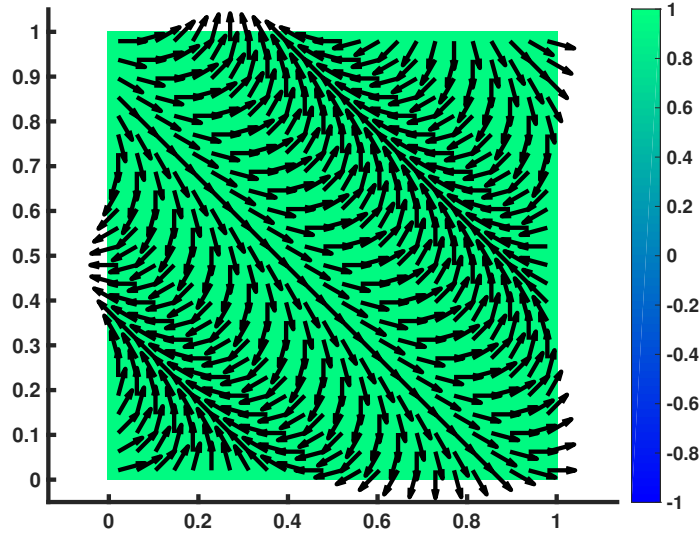
Figure 2.1: Analytical solution (2.44) of the Landau-Lifshitz equation at time 0. The vectors in the plot denote the m_x and m_y components, and the color denotes the m_z component.

2.5.1.1 Explicit time integration scheme ($\theta = 0$)

We consider a uniform square mesh on the unit square Ω with mesh size h and time step $k = 8 \cdot 10^{-7} h^2$. We measure errors in the magnetization $\mathbf{m}$ in the mesh dependent L^2-type norm $\|\cdot\|_{\mathcal{Q}}$ and the maximum norm

$$\|\mathbf{m^h} - \mathbf{m^I}\|_{L^\infty} = \max_{E \in \Omega^h} |\mathbf{m}_E - \mathbf{m}_E^I|.$$

We also measure error in the magnetization flux tensor $\mathbf{p}$ in the mesh dependent L^2-type norm $\|\cdot\|_{\mathcal{F}}$. The $\mathbf{m}^I \in (\mathcal{Q}^h)^3$ and $\mathbf{p}^I \in (\mathcal{F}^h)^3$ denote the projections of the analytical solution on the discrete spaces. For these projections, we simply take the values of $\mathbf{m}$ and $\mathbf{p}$ at centroids of elements E and edges (or faces) f, respectively.

The convergence rates of the magnetization and its flux are summarized in Table 2.1. It shows second order convergence for both the magnetization and its flux.

$1/h$	$\|\mathbf{m}^h - \mathbf{m}^I\|_{L^\infty}$	$\|\mathbf{m}^h - \mathbf{m}^I\|_{\mathcal{Q}}$	$\|\mathbf{p}^h - \mathbf{p}^I\|_{\mathcal{F}}$
32	8.222e-05	8.360e-05	2.967e-03
64	2.060e-05	2.092e-05	7.418e-04
128	5.154e-06	5.231e-06	1.854e-04
256	1.289e-06	1.308e-06	4.636e-05
rate	2.00	2.00	2.00

Table 2.1: **Explicit time integration scheme** $(\theta = 0)$: Error and convergence rates on uniform square mesh with mesh size h and time step $k = 8 \cdot 10^{-7} h^2$ and time 0.001.

2.5.1.2 Implicit time integration scheme ($\theta = 1$), uniform square meshes

In this section, we consider the implicit time integration scheme, i.e. $\theta = 1$ in (2.16), with the analytical solution (2.44). We set time step $k = 0.008\, h^2$ so that the first-order time integration error does not affect the convergence rate.

Table 2.2 shows the second-order convergence for the magnetization and the first-order convergence for its flux. The explanation of the lack of super-convergence of magnetization flux tensor $\mathbf{p}$ in this implicit scheme is required by conducting a rigorous convergence analysis of the Algorithm 1, which is beyond the scope of this work.

$1/h$	$\|\mathbf{m}^h - \mathbf{m}^I\|_{L^\infty}$	$\|\mathbf{m}^h - \mathbf{m}^I\|_{\mathcal{Q}}$	$\|\mathbf{p}^h - \mathbf{p}^I\|_{\mathcal{F}}$
32	9.082e-05	9.195e-05	2.531e-02
64	2.273e-05	2.302e-05	1.261e-02
128	5.687e-06	5.756e-06	6.301e-03
256	1.422e-06	1.439e-06	3.150e-03
rate	2.00	2.00	1.00

Table 2.2: **Implicit time integration scheme** $(\theta = 1)$: Error and convergence rates on a uniform square mesh with mesh size h and time step $k = 0.008h^2$ and time 0.001.

2.5.1.3 Smoothly distorted and randomized quadrilateral meshes

We consider the randomized and smoothly distorted meshes shown in Fig. 2.3.
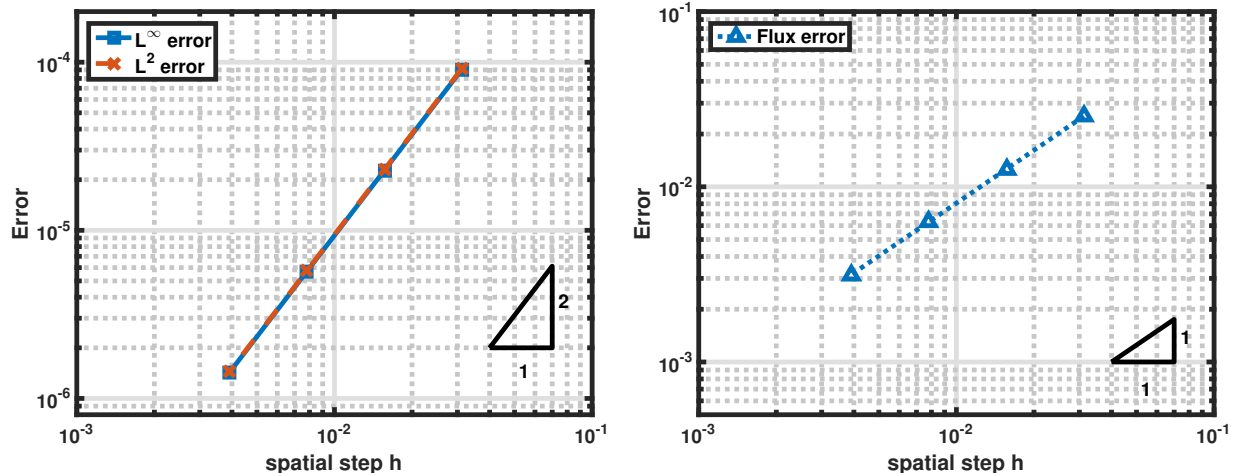
Figure 2.2: Error plot with respect to the mesh size h using Algorithm 1 on a uniform square mesh with $\theta = 1$. Left : $\left\| \mathbf{m^h} - \mathbf{m} \right\|_{L^\infty}$ and $\left\| \mathbf{m^h} - \mathbf{m} \right\|_{\mathcal{Q}}$, Right : $\left\| \mathbf{p^h} - \mathbf{p} \right\|_{\mathcal{F}}$.
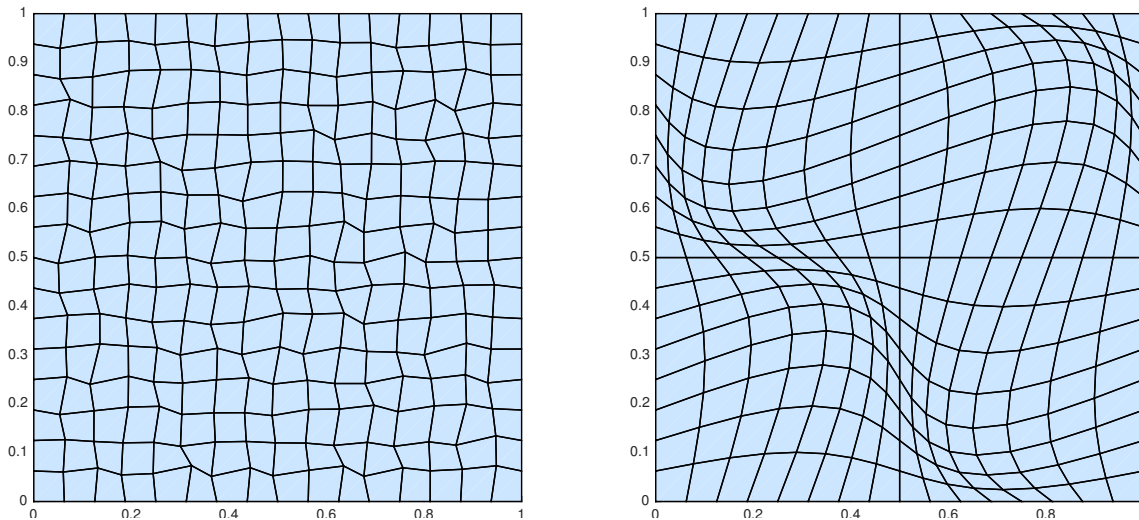
Figure 2.3: Left : Randomized mesh, Right : Smoothly distorted mesh.

The randomized mesh is constructed from the uniform square mesh by random distortion of its nodes. The map is given by

$$x := x + 0.2\,\xi_x\,h, \quad y := y + 0.2\,\xi_y\,h, \tag{2.45}$$

where ξ_x and ξ_y are random variables between -1 and 1. The nodes on the boundary were modified to satisfy periodic boundary conditions.

The smoothly distorted mesh is constructed from the uniform square mesh using a smooth map. The map is given by

$$x := x + 0.1\sin(2\pi x)\sin(2\pi y),$$
$$y := y + 0.1\sin(2\pi x)\sin(2\pi y). \tag{2.46}$$

In Table 2.3 and Fig. 2.4, the errors and the convergence rates are summarized. We observe *almost* second-order convergence rate for the magnetization and *almost* first-order convergence rate for its flux.

$1/h$	Randomized mesh		
	$\|\mathbf{m}^h - \mathbf{m}^I\|_{L^\infty}$	$\|\mathbf{m}^h - \mathbf{m}^I\|_{\mathcal{Q}}$	$\|\mathbf{p}^h - \mathbf{p}^I\|_{\mathcal{F}}$
16	3.121e-03	9.460e-04	6.560e-02
32	1.005e-03	2.988e-04	3.249e-02
64	2.585e-04	7.258e-05	1.615e-02
128	7.939e-05	1.807e-05	8.135e-03
rate	1.79	1.92	1.00
$1/h$	Smoothly distorted mesh		
	$\|\mathbf{m}^h - \mathbf{m}^I\|_{L^\infty}$	$\|\mathbf{m}^h - \mathbf{m}^I\|_{\mathcal{Q}}$	$\|\mathbf{p}^h - \mathbf{p}^I\|_{\mathcal{F}}$
16	1.751e-03	1.009e-03	7.611e-02
32	5.477e-04	2.809e-04	3.000e-02
64	1.432e-04	7.214e-05	1.362e-02
128	3.608e-05	1.816e-05	6.623e-03
rate	1.87	1.94	1.17

Table 2.3: **Implicit time integration scheme** $(\theta = 1)$: Error and convergence rates on randomly and smoothly distorted meshes shown in Fig. 2.3 with mesh size h and time step $k = 0.008h^2$ and time 0.001.

In these numerical tests, we used $\mathbb{M}_{\mathcal{F},E}^{-1}$ in (2.30) with constant $\tilde{\gamma}$ defined by the scaled trace of the first term. Thus, $\mathbb{M}_{\mathcal{F},E}^{-1}$ is not always an M-matrix. In section 2.4, we proved that exchange energy decreases under the condition that $\mathbb{M}_{\mathcal{F},E}^{-1}$ is an M-matrix. Fig. 2.5 shows exchange energy $\frac{1}{2}[\mathbf{p}^h, \mathbf{p}^h]_{\mathcal{F}}$ as a function of time for both randomized and smoothly distorted meshes and for two different mesh sizes $h = \frac{1}{32}$ and $h = \frac{1}{64}$. It shows that exchange energy decreases in time. This result suggests that the M-matrix conditions are sufficient but may not be necessary for the stability analysis.

We further investigate the influence of the constant $\tilde{\gamma}$ in (2.30) on the error. In Fig. 2.6, the errors are plotted as a function of γ_0 on the randomly distorted mesh with mesh size $h = 1/32$, where $\tilde{\gamma} = \gamma_0 \frac{1}{|E|} \text{trace}(\mathbb{N}\mathbb{N}^T)$. We were unable to minimize errors both in the magnetization and its flux with only one free parameter. The full matrix of parameters has to be used to minimize both errors.
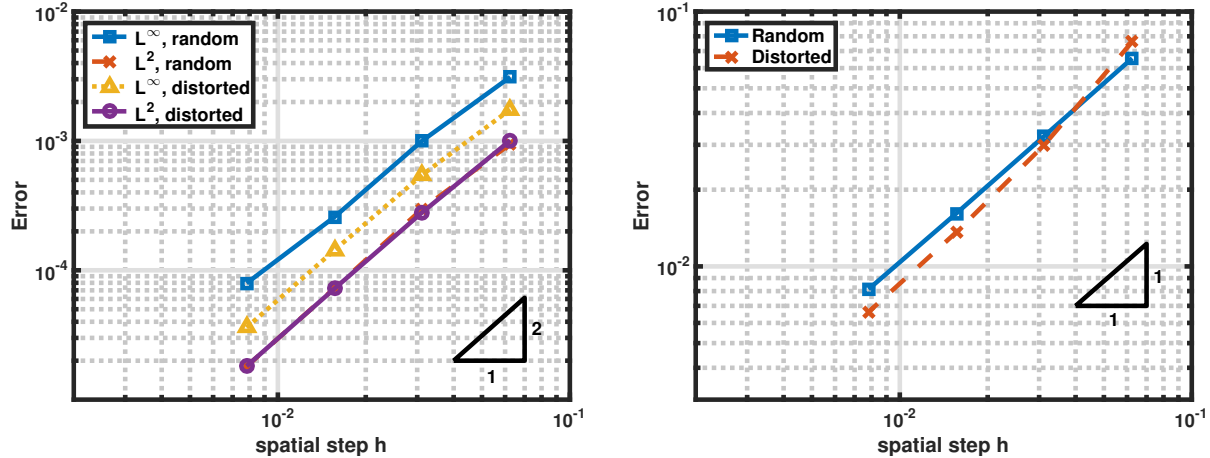
Figure 2.4: Error plot with respect to the mesh size h using Algorithm 1 and $\theta = 1$ on the randomized and smoothly distorted meshes shown in Fig. 2.3. Left : $\left\|\mathbf{m^h} - \mathbf{m}\right\|_{L^\infty}$ and $\left\|\mathbf{m^h} - \mathbf{m}\right\|_{\mathcal{Q}}$, Right : $\left\|\mathbf{p^h} - \mathbf{p}\right\|_{\mathcal{F}}$.
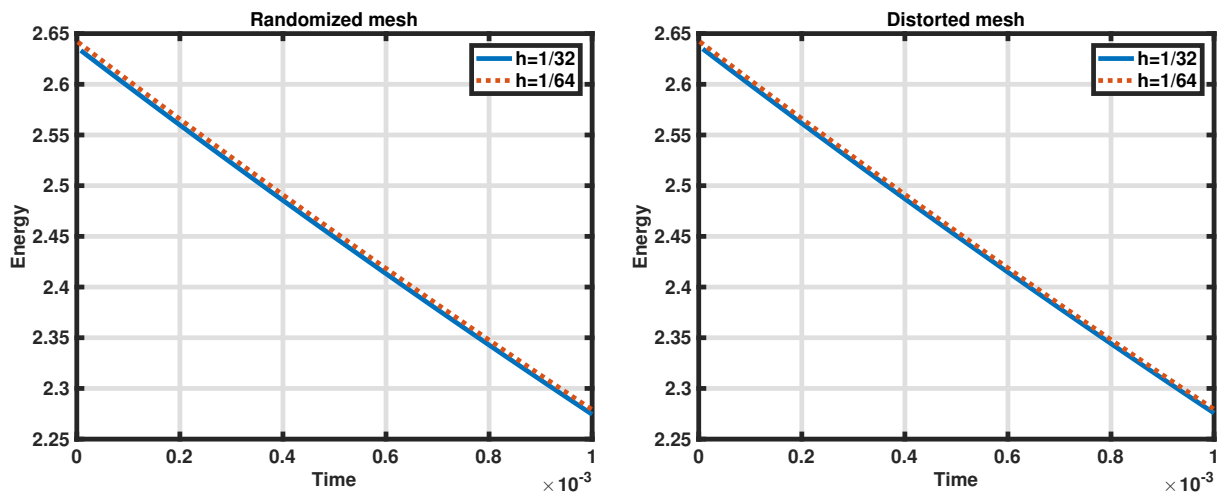
Figure 2.5: Decrease of the exchange energy. Left : Randomized mesh, Right : Smoothly distorted mesh.
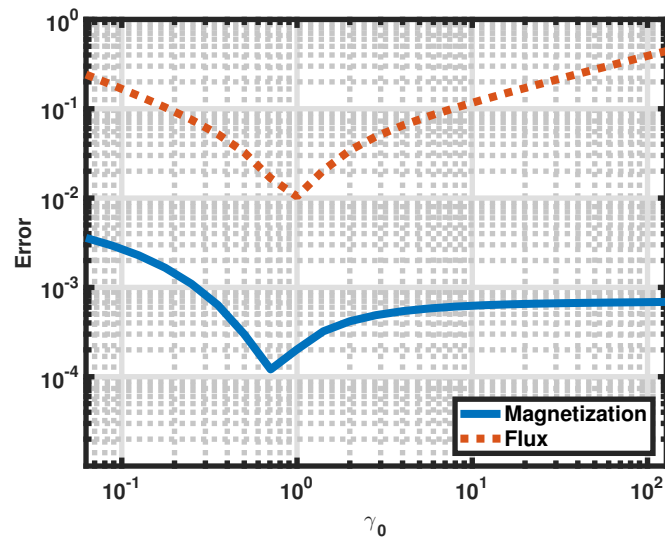
Figure 2.6: Errors as a function of γ_0 on the randomly distorted mesh shown in the left panel of Fig. 2.3 with mesh size $h = 1/32$.

2.5.2 Convergence analysis for problems with the Dirichlet boundary condition

In this section, we consider the implicit time integration scheme with $\theta = 1$ in (2.16) and the analytical solution (2.44), but now with the Dirichlet boundary condition.

We can consider more general domains such as the circular domain under the Dirichlet boundary condition. Fig. 2.7 shows a logically square mesh fitted to the circular domain with center $(0.5, 0.5)$ and radius 0.5. The four mesh elements at the four corners of this mesh are almost triangles. However, these elements are classified as shape regular in the mimetic framework and do not alter the convergence rates [21].
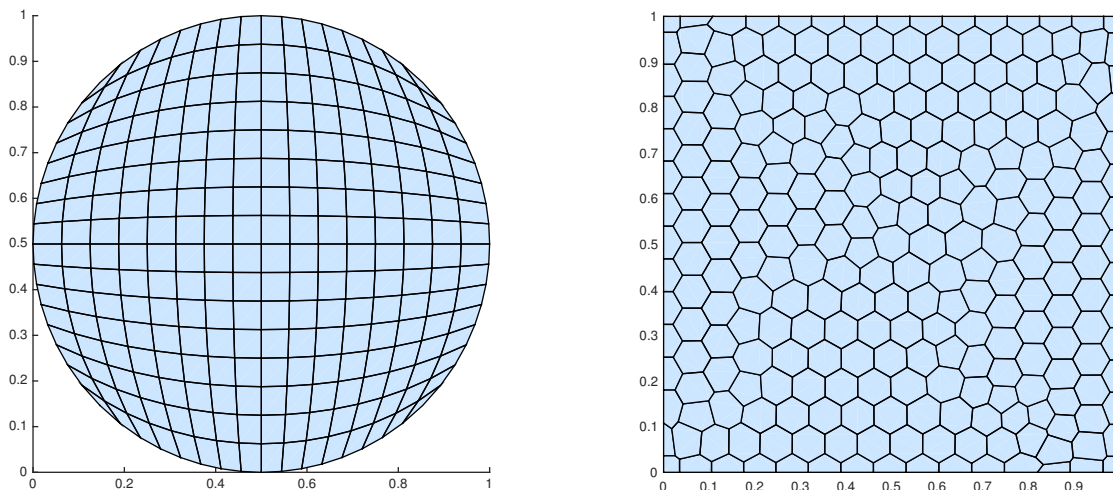
Figure 2.7: Left : Logically square mesh fitted to the circular domain, Right : Polygonal mesh.

In Table 2.4 and Fig. 2.8, the errors and the convergence rates are summarized. We conducted the numerical experiments on uniform square meshes, smoothly and randomly distorted meshes as in Fig. 2.3, logically square meshes fitted to the circle and polygonal meshes as in Fig. 2.7. The time step for the polygonal meshes is set to $k = 0.004\,h^2$ and all the other meshes set to $k = 0.008\,h^2$. We have an *almost* second-order convergence rate for the magnetization and an *almost* first-order convergence rate for its flux.

	Uniform square meshes					
$1/h$	$\|\mathbf{m}^h - \mathbf{m}^I\|_{L^\infty}$	ratio	$\|\mathbf{m}^h - \mathbf{m}^I\|_{\mathcal{Q}}$	ratio	$\|\mathbf{p}^h - \mathbf{p}^I\|_{\mathcal{F}}$	ratio
8	6.799e-03	0.83	3.239e-03	0.83	1.585e-01	1.40
16	3.812e-03	1.81	1.347e-03	1.73	6.021e-02	1.19
32	1.088e-03	2.00	4.061e-04	1.98	2.639e-02	1.05
64	2.717e-04		1.028e-04		1.275e-02	
	Randomized meshes					
8	6.889e-03	0.89	3.335e-03	1.09	1.795e-01	1.31
16	3.722e-03	1.62	1.566e-03	1.67	7.254e-02	1.12
32	1.212e-03	1.85	4.921e-04	2.01	3.348e-02	1.04
64	3.370e-04		1.221e-04		1.630e-02	
	Smoothly distorted meshes					
8	6.451e-03	0.57	3.562e-03	1.20	2.522e-01	1.52
16	4.349e-03	1.49	1.550e-03	1.52	8.808e-02	1.45
32	1.551e-03	1.61	5.414e-04	1.91	3.220e-02	1.21
64	5.073e-04		1.440e-04		1.393e-02	
	Polygonal meshes					
8	7.071e-03	0.72	4.029e-03	1.42	2.301e-01	1.32
16	4.288e-03	1.40	1.506e-03	1.60	9.242e-02	1.28
32	1.623e-03	1.71	4.970e-04	1.81	3.794e-02	1.10
64	4.957e-04	1.85	1.422e-04	2.28	1.765e-02	1.06
128	1.372e-04		2.929e-05		8.495e-03	
	Logically square meshes in the circular domain					
8	2.388e-02	1.68	3.689e-03	1.66	1.293e-01	1.35
16	7.451e-03	1.87	1.166e-03	1.90	5.086e-02	1.11
32	2.032e-03	1.95	3.120e-04	1.99	2.354e-02	1.02
64	5.268e-04		7.856e-05		1.159e-02	

Table 2.4: **Implicit time integration scheme** $(\theta = 1)$: Error and convergence rates on various meshes under the Dirichlet boundary condition with mesh size h and time step $k = 0.008h^2$ at time 0.001.
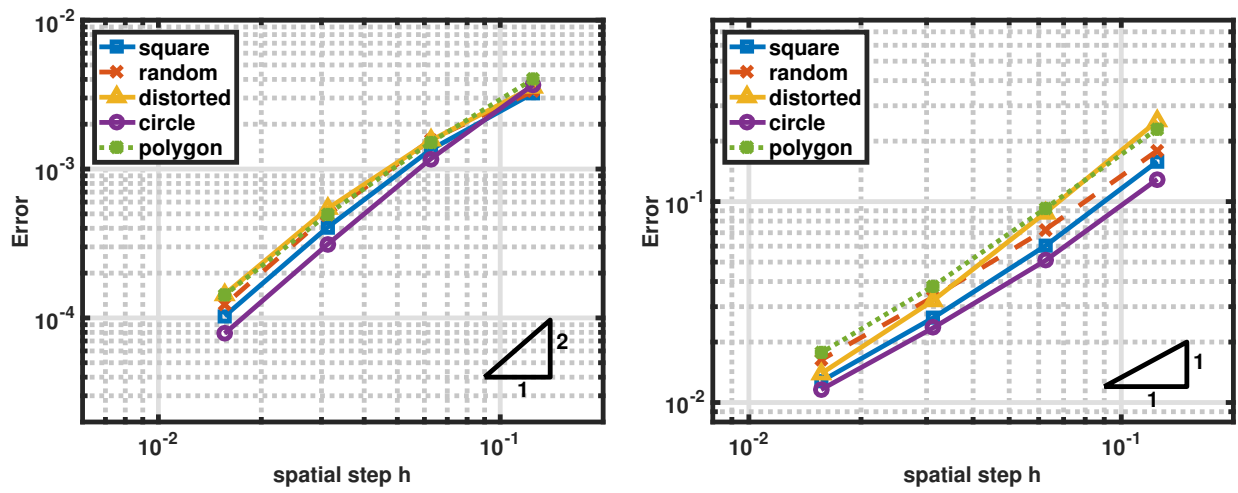
Figure 2.8: Error plot with respect to the mesh size h using Algorithm 1 and $\theta = 1$ with Dirichlet boundary conditions. Left : $\left\|\mathbf{m^h} - \mathbf{m}\right\|_{\mathcal{Q}}$, Right : $\left\|\mathbf{p^h} - \mathbf{p}\right\|_{\mathcal{F}}$.

2.5.3   NIST μmag standard problem 4

The μmag standard problem 4 is proposed by Micromagnetic Modeling Activity Group (μMAG) at the National Institute of Standards and Technology (NIST) [62]. The problem is to simulate the magnetization dynamics in a permalloy thin film of dimensions 500nm $\times$ 125nm $\times$ 3nm with two different applied fields.

Before its nondimensionalization, the Landau-Lifshitz equation [63] is

$$\frac{\partial \mathbf{M}}{\partial t'} = -\frac{\gamma}{1+\alpha^2}\mathbf{M} \times \mathbf{H} - \frac{\gamma\alpha}{M_s(1+\alpha^2)}\mathbf{M} \times (\mathbf{M} \times \mathbf{H}) \tag{2.47}$$

with homogeneous Neumann boundary condition and the initial condition described below. Here, the effective field is given by

$$\mathbf{H} = -\frac{1}{\mu_0 M_s}\frac{\delta E}{\delta \mathbf{m}}, \quad E(\mathbf{M}) = \int_\Omega \frac{A}{2M_s^2}|\nabla \mathbf{M}|^2 - \mu_0(\mathbf{H}_e \cdot \mathbf{M}) - \frac{1}{2}\mu_0(\mathbf{H}_s \cdot \mathbf{M}) \, \mathrm{d}x, \tag{2.48}$$

where $\mathbf{M} = M_s\mathbf{m}$, $\mathbf{H}_e$ is the external field and $\mathbf{H}_s$ is the stray field. The material parameters are the exchange constant $A = 2.6 \times 10^{-11} \, [\mathrm{J} \cdot \mathrm{m}^{-1}]$, saturation magnetization $M_s = 8 \times 10^5 \, [\mathrm{A} \cdot \mathrm{m}^{-1}]$, gyromagnetic ratio $\gamma = 2.21 \times 10^5 \, [\mathrm{m} \cdot \mathrm{A}^{-1} \cdot \mathrm{s}^{-1}]$, magnetic permeability of vacuum $\mu_0 = 4\pi \times 10^{-7} \, [\mathrm{N} \cdot \mathrm{A}^{-2}]$ and the dimensionless damping parameter $\alpha = 0.02$.

By taking $\mathbf{H} = M_s\mathbf{h}$, $\mathbf{H}_s = M_s\mathbf{h}_s$, $\mathbf{H}_e = M_s\mathbf{h}_e$, $x = Lx'$ with $L = 10^{-9}$, and $t = \frac{1+\alpha^2}{\gamma M_s}t'$, we obtain equation (1.8) with $\eta = \frac{A}{\mu_0 M_s^2 L^2}$ and equation (1.9) with $Q = 0$. The initial state is an equilibrium S-state as in Fig. 2.9. This is obtained by applying an external field of $2\,T$ along direction $[1,1,1]$ and slowly reducing it to zero by $0.02\,T$ each time step [62, 52].

For the thin film, we assume that the magnetization is constant along the OZ direction and solve the two-dimensional Landau-Lifshitz equation. We take spatial step size as $h_x = h_y = 5$nm. We use the explicit time integration scheme ($\theta = 0$) with the time step $\hat{k} = \frac{0.005}{\gamma M_s} \approx 28.28$ fs and implicit time discretization scheme ($\theta = 1$) with five different time steps $\hat{k} = \frac{0.01}{\gamma M_s} \approx 56.56$ fs, $\hat{k} \approx 0.14$ ps, $\hat{k} \approx 0.28$ ps, $\hat{k} \approx 0.57$ ps, and $\hat{k} \approx 1.13$ ps.
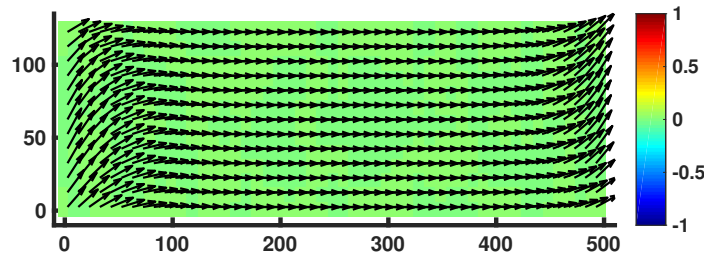
Figure 2.9: NIST μmag standard problem 4 : the initial equilibrium S-state. The vectors in the plot denote the m_x and m_y components, and the color denotes the m_z component.
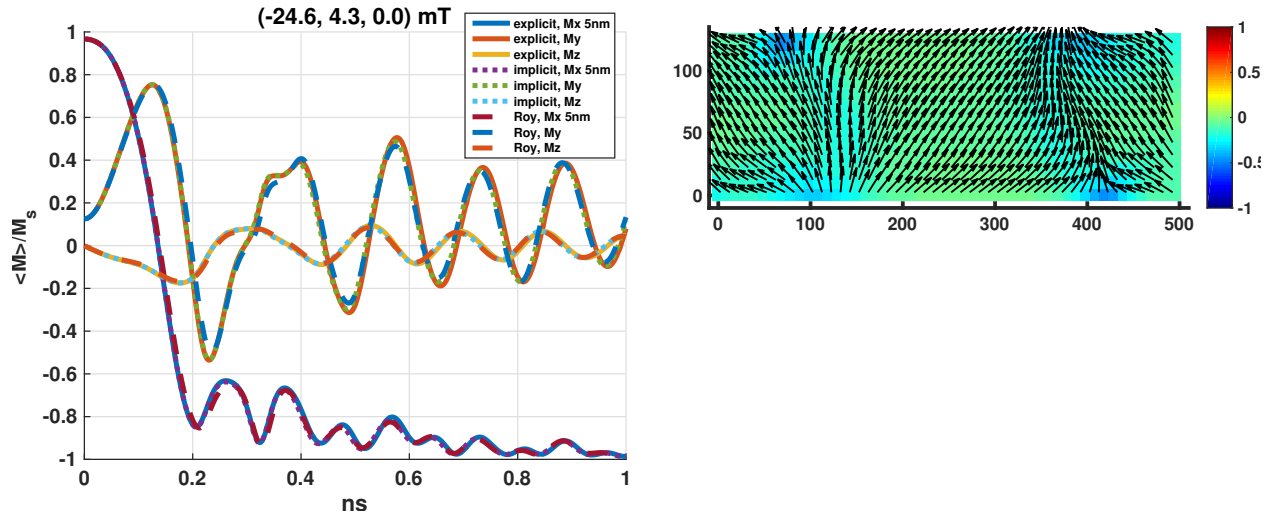
Figure 2.10: NIST μmag standard problem 4 with the external field $\mu_0\,\mathbf{H}_e = (-24.5, 4.3, 0.0)\,[\text{mT}]$. Left : The time evolution of the average magnetization calculated using the explicit and implicit mimetic schemes with the comparison of Roy and Svedlindh's results in [62], Right : The magnetization field when $\langle m_x \rangle$ first crosses zero. The vectors in the plot denote the m_x and m_y components, and the color denotes the m_z component.

With two different applied fields, we simulate the dynamics of the magnetization. The first field is $\mu_0\mathbf{H}_e = (-24.6, 4.3, 0.0)\,[\text{mT}]$ which makes angle of approximately 170 degrees with the positive direction of the x-axis. The second field is $\mu_0\mathbf{H}_e = (-35.5, 6.3, 0.0)\,[\text{mT}]$ which makes angles of approximately 190 degrees with the positive direction of the x-axis. We plot the time evolution of the average magnetization, where the average magnetization is computed by the formula

$$\langle \mathbf{m} \rangle = \frac{1}{N_E} \sum_{E \in \Omega_h} \mathbf{m}_E.$$

The evolution of the average magnetization and the magnetization field when $\langle m_x \rangle$ first crosses zero is shown in Fig. 2.10. The result is compared with the results obtained by Roy and Svedlindh in [62]. They used a finite difference method (leading to the conventional 5-point approximation for the Laplacian) and RK4 for the time-stepping with time step $\hat{k} \approx 11$ fs. The evolution of the magnetization is qualitatively in very good agreement.

With the second external field, the evolution of the average magnetization and the magnetization field when $\langle m_x \rangle$ first crosses zero is shown in Fig. 2.11. Solutions obtained with different schemes begin to diverge approximately after $0.35\,ns$ as reported in [62]. We have qualitatively good agreement until this time.

Furthermore, Fig. 2.12 shows the evolution of the magnetization for both applied fields with different time steps. This shows the stability and temporal convergence of the $\theta = 1$
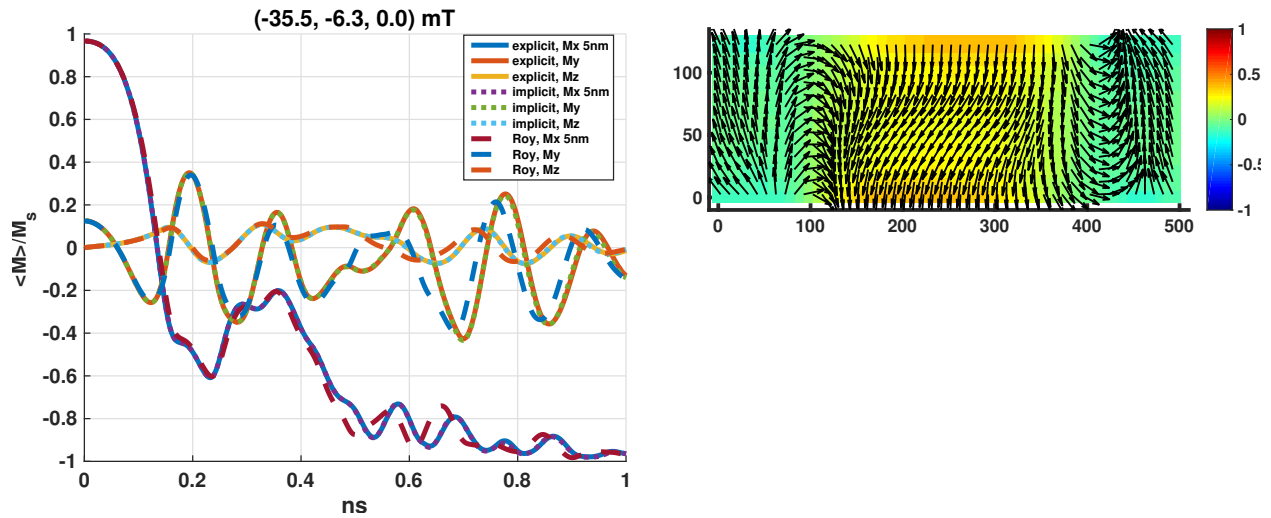
Figure 2.11: NIST μmag standard problem 4 with the external field $\mu_0 \mathbf{H}_e =$ $(-35.5, 6.3, 0.0)\,[\text{mT}]$. Left : The time evolution of the average magnetization calculated using the explicit and implicit mimetic schemes with comparison of Roy and Svedlindh's results in [62]. Right : The magnetization field when $\langle m_x \rangle$ first crosses zero. The vectors in the plot denote the m_x and m_y components, and the color denotes the m_z component.

implicit scheme of Algorithm 1.
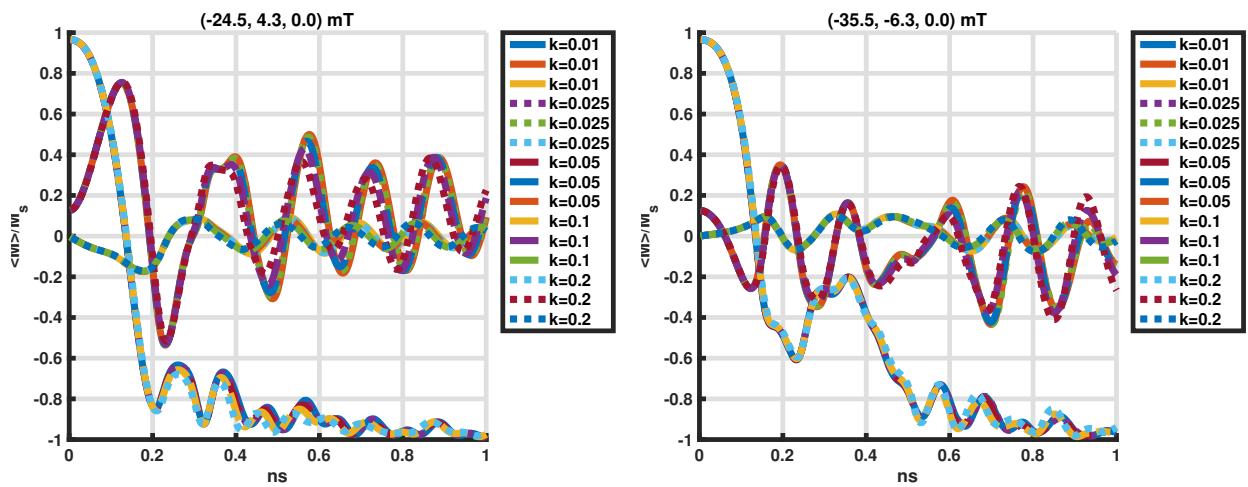
Figure 2.12: NIST μmag standard problem 4 : Evolution of average magnetization computed using Algorithm 1 with various time steps $\hat{k} = \frac{k}{\gamma M_s}$ with two different applied fields : Left : $\mu_0 \mathbf{H}_e = (-24.5, 4.3, 0.0)\,[\text{mT}]$, Right : $\mu_0 \mathbf{H}_e = (-35.5, 6.3, 0.0)\,[\text{mT}]$.

2.5.4   Domain wall structures in a thin film

In this section, we conduct numerical simulation of the domain wall structures in rectangular thin films of size 240nm × 480nm × 7nm using both explicit and implicit time integration schemes ($\theta = 0, 1$). In [89], a similar numerical experiment was conducted using the Gauss-Seidel projection method while gradually increasing the thickness of the film. Before its nondimensionalization, the Landau-Lifshitz equation [89] is given by

$$\frac{\partial \mathbf{M}}{\partial t'} = -\gamma \mu_0 \mathbf{M} \times \mathbf{H} - \frac{\gamma \alpha \mu_0}{M_s} \mathbf{M} \times (\mathbf{M} \times \mathbf{H}) \tag{2.49}$$

with homogeneous Neumann boundary conditions and the initial condition described below. The effective field $\mathbf{H}$ is given by (2.48). The material parameters are the exchange constant $A = 2.1 \times 10^{-11} \, [\text{J} \cdot \text{m}^{-1}]$, saturation magnetization $M_s = 1.71 \times 10^6 \, [\text{A} \cdot \text{m}^{-1}]$, gyromagnetic ratio $\gamma = 1.76 \times 10^{11} \, [\text{T}^{-1} \cdot \text{s}^{-1}]$, magnetic permeability of vacuum $\mu_0 = 4\pi \times 10^{-7} \, [\text{N} \cdot \text{A}^{-2}]$, and the dimensionless damping parameter $\alpha = 0.02$.

Using a slightly different rescaling than in section 2.5.3, $\mathbf{H} = M_s \mathbf{h}$, $\mathbf{H}_s = M_s \mathbf{h}_s$, $\mathbf{H}_e = M_s \mathbf{h}_e$, $x = Lx'$ with $L = 10^{-9}$, and $t = \frac{1}{\mu_0 \gamma M_s} t'$, we obtain equation (1.8) with $\eta = \frac{A}{\mu_0 M_s^2 L^2}$ and equation (1.9) with $Q = 0$. We may assume that the magnetization is constant along OZ direction and solve two-dimensional Landau-Lifshitz equation. We set spatial step size as $h_x = h_y = 3.75$nm.

For the explicit time integration scheme, we set time step $k = \frac{0.01}{\mu_0 \gamma M_s} \approx 26.44$ fs. For the implicit time discretization scheme, we set $k = \frac{0.25}{\mu_0 \gamma M_s} \approx 0.66$ ps. The initial state is a uniform Néel wall, with $\mathbf{m} = (0, 1, 0)$ for $0 < x < 120$nm and $\mathbf{m} = (0, -1, 0)$ for 120nm $< x < 240$nm as shown on the first panel in Fig. 2.13. The evolution of the magnetization is shown in other panels in Fig. 2.13. We observe a transition from the Néel wall to four 90° Néel walls connecting a vortex which is the equilibrium state. For better visualization, we plotted the magnetizations on a coarser grid in Fig. 2.13.
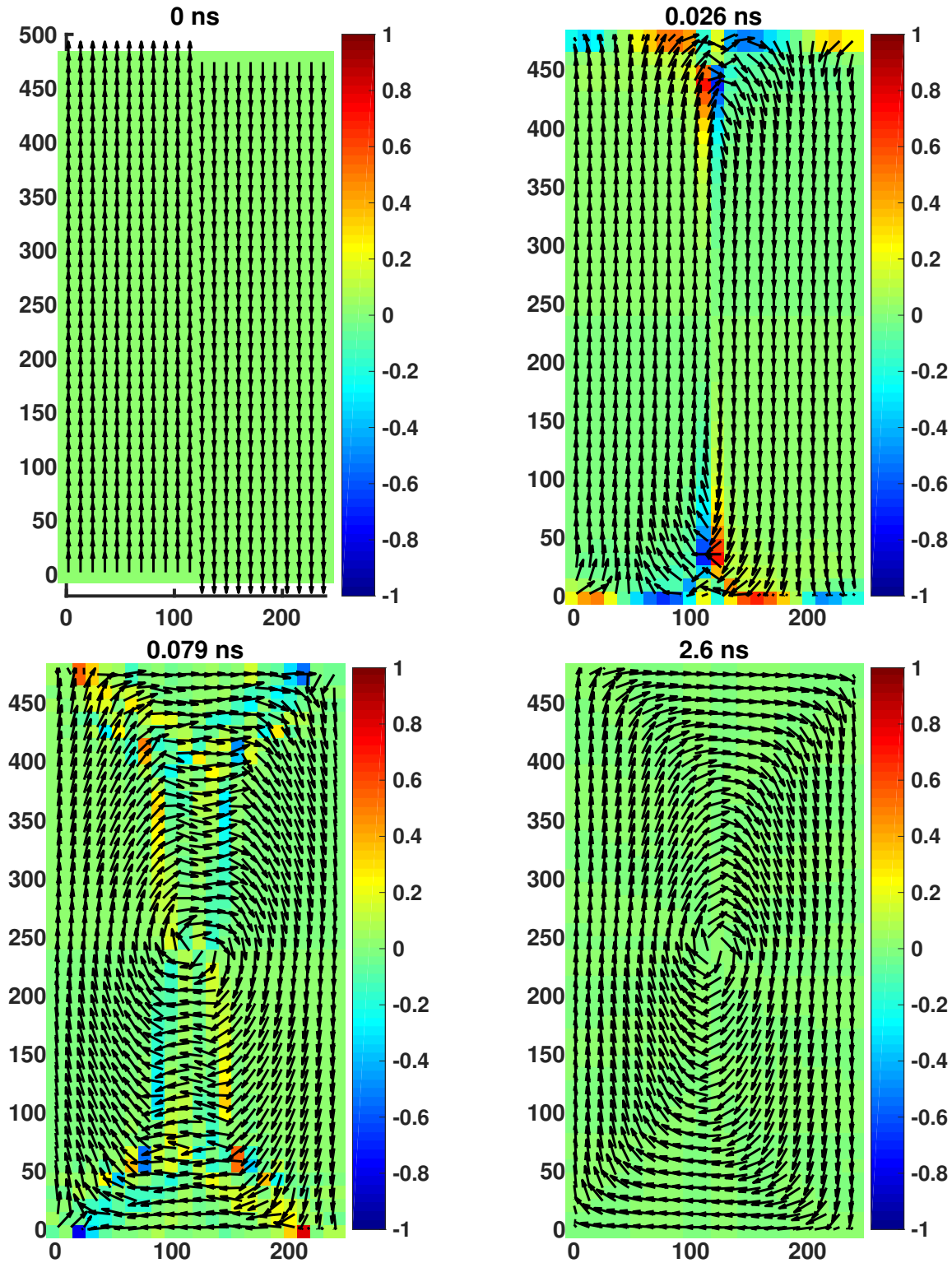
Figure 2.13: Transition from the Néel wall to vortex structure. The vectors in the plot denote the m_x and m_y components, and the color denotes the m_z component.

2.6   Adaptive mesh refinement

The simulation of domain walls in section 2.5.4 shows a strong need for adaptive meshes. We compare the performance of the MFD method on uniform and locally refined meshes with prescribed structure. We consider the 1D steady-state solution $\mathbf{m} = (m_x, m_y, m_z)$ with the Dirichlet boundary conditions given by

$$
\begin{aligned}
m_x(x_1, x_2, t) &= \sin(\phi(x_1, x_2, t)) \\
m_y(x_1, x_2, t) &= \cos(\phi(x_1, x_2, t)) \qquad \phi(x_1, x_2, t) = \pi \left(1 + e^{-s\pi(x_1 - b/2)}\right)^{-1}, \\
m_z(x_1, x_2, t) &= 0,
\end{aligned}
\tag{2.50}
$$

where $b = 1$ and $s = 20$. This is a steady-state solution of the Landau-Lifshitz equation (1.8)-(1.9) with the external field

$$
\begin{aligned}
(\mathbf{h_e})_x(x_1, x_2, t) &= \left(\frac{\partial \phi(x_1, x_2, t)}{\partial x}\right)^2 \sin(\phi(x_1, x_2, t)) - \frac{\partial^2 \phi(x_1, x_2, t)}{\partial x^2} \cos(\phi(x_1, x_2, t)) \\
(\mathbf{h_e})_y(x_1, x_2, t) &= \left(\frac{\partial \phi(x_1, x_2, t)}{\partial x}\right)^2 \cos(\phi(x_1, x_2, t)) + \frac{\partial^2 \phi(x_1, x_2, t)}{\partial x^2} \sin(\phi(x_1, x_2, t)) \\
(\mathbf{h_e})_z(x_1, x_2, t) &= 0,
\end{aligned}
\tag{2.51}
$$

$Q = 0$ and $\mathbf{h}_s = 0$. The magnetization $\mathbf{m}$ has a sharp transition on the interval $0.4 < x_1 < 0.6$ and is almost constant on the other regions as shown on the first panel in Fig 2.14. The locally refined meshes consist of squares and degenerate pentagons. They are shown on the other panels in Fig 2.14.

In Table 2.5, the convergence results are summarized. The locally refined meshes lead to more accurate results for about the same numerical cost. We expect even better results for adaptive meshes constructed using an error indicator.

Uniform square meshes				
Number of cells	$\|\mathbf{m}^h - \mathbf{m}^I\|_{L^\infty}$	ratio	$\|\mathbf{m}^h - \mathbf{m}^I\|_{\mathcal{Q}}$	ratio
256	9.170e-01	1.51	3.429e-01	1.67
1024	3.231e-01	2.67	1.081e-01	2.81
4096	5.072e-02	2.09	1.542e-02	2.10
16384	1.192e-02		3.605e-03	
Adaptive mesh				
220	8.993e-01	3.52	2.906e-01	3.60
952	6.846e-02	3.30	2.076e-02	3.36
3760	7.099e-03	1.39	2.062e-03	1.99
15904	2.609e-03		4.915e-04	

Table 2.5: Comparison of errors between uniform and locally refined meshes in Fig. 2.14.
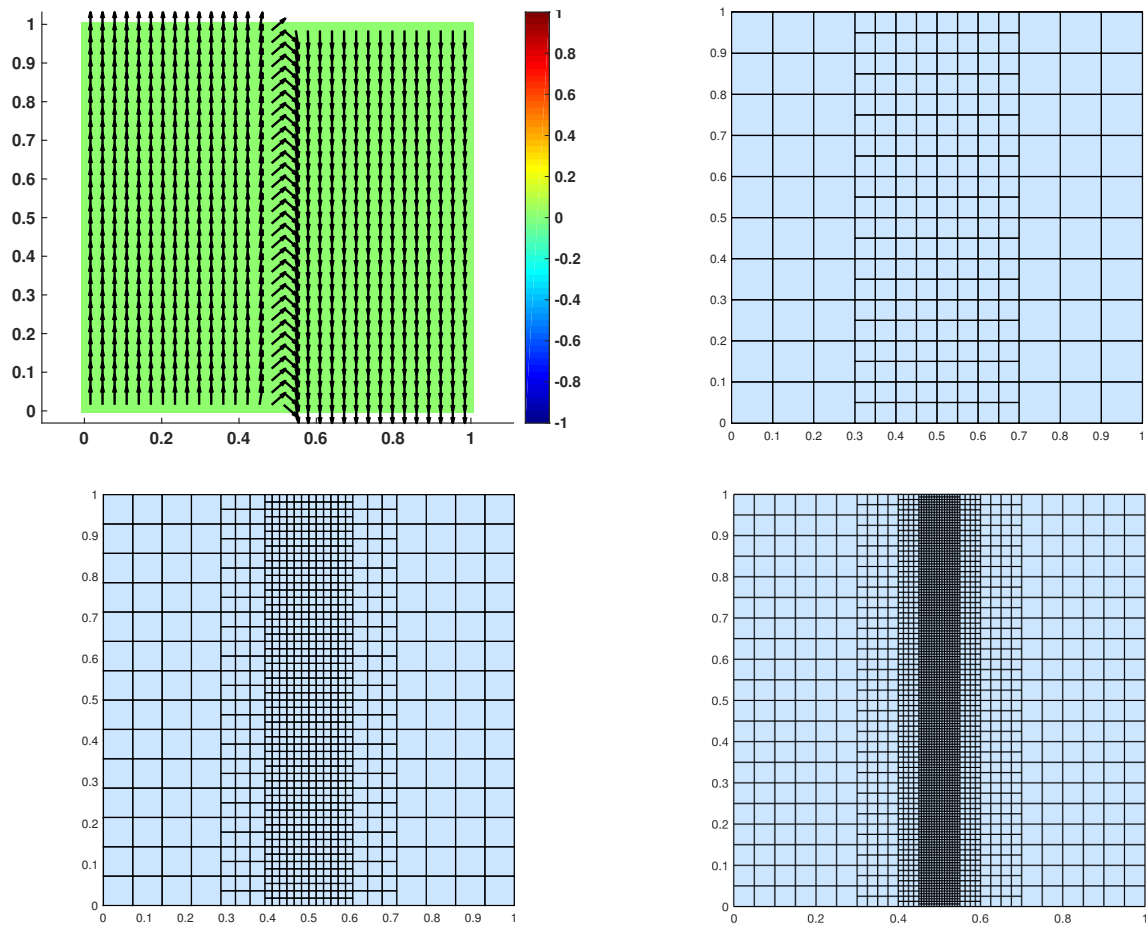
Figure 2.14: Steady state solution of the Landau-Lifshitz equation and three locally refined meshes.

Chapter 3

A high order mimetic finite difference method for the Landau-Lifshitz equation

In this chapter, we present a high order mimetic finite difference method (MFD) for the Landau-Lifshitz equation.

3.1 High order mimetic finite difference method for the Landau-Lifshitz equation

We consider the Landau-Lifshitz equation, written as a system of two equations, as in chapter 2 :

$$\mathbf{p} = -\nabla \mathbf{m},$$
$$\frac{\partial \mathbf{m}}{\partial t} = \mathbf{m} \times \mathbf{div}\ \mathbf{p} + \alpha \mathbf{m} \times (\mathbf{m} \times \mathbf{div}\ \mathbf{p}) + \mathbf{f}(\mathbf{m}). \tag{3.1}$$

where

$$\mathbf{f}(\mathbf{m}) = -\mathbf{m} \times \bar{\mathbf{h}}(\mathbf{m}) - \alpha \mathbf{m} \times (\mathbf{m} \times \bar{\mathbf{h}}(\mathbf{m})) \tag{3.2}$$

corresponds to the low-order terms (1.10). We refer to $\mathbf{p}$ as the magnetic flux tensor. Our high-order MFD method solves simultaneously for $\mathbf{m}$ and $\mathbf{p}$.

As before, we assume $\mathbf{m} \in \mathcal{Q} = (L^2(\Omega))^3$ and $\mathbf{p} \in \mathcal{F}$, where

$$\mathcal{F} = \{\mathbf{p} \mid \mathbf{p} \in (L^s(\Omega))^{d \times 3}, \ s > 2, \ \mathbf{div}\ \mathbf{p} \in (L^2(\Omega))^3\}.$$

Let Ω^h be the partitions of the domain Ω with N_E non-overlapping polygonal or polyhedral elements E with maximum diameter h. Let N_F be the total number of edges (or faces in 3D). Let $|E|$ denote the area of each element E (or volume in 3D), and $|f|$ denote the length of each edge f (or area in 3D).

We develop a high order MFD for the Landau-Lifshitz equation using similar framework to the high order MFD method for the diffusion equation in [47].

3.1.1 Orthogonal basis functions

In order to introduce the degrees of freedom associated with the magnetization vector and magnetic flux tensor, we introduce a family of orthogonal polynomials $\{\phi_{E,i}\}_{i=0,1,\ldots,n_k^E-1}$ of degree k on each element E and a family of orthogonal polynomials $\{\phi_{f,i}\}_{i=0,1,\ldots,n_k^f-1}$ of degree k associated with each edge f (or face in 3D). Here, $n_k^E = \frac{(k+1)(k+2)}{2}$ for $d = 2$, $n_k^E = \frac{(k+1)(k+2)(k+3)}{6}$ for $d = 3$ and $n_k^f = k + 1$ for $d = 2$, $n_k^f = \frac{(k+1)(k+2)}{2}$ for $d = 3$.

For each mesh element E, let $\mathbb{P}_k(E)$ be the space of polynomial functions defined on E with degree at most k. The orthogonal polynomials $\{\phi_{E,i}\}_{i=0,1,\ldots,n_k^E-1}$ associated with each element E form an orthogonal basis in $\mathbb{P}_k(E)$ and satisfy the orthogonality condition

$$\int_E \phi_{E,i}\,\phi_{E,j}\,\mathrm{d}x = |E|\,\delta_{ij}. \tag{3.3}$$

where δ_{ij} is a Kronecker delta function. We take $\phi_{E,0} = 1$. We define the projection $\Pi_k^E(\phi) \in \mathbb{P}_k(E)$ of a function $\phi \in L^2(E)$ by the orthogonality relation

$$\int_E (\Pi_k^E(\phi) - \phi)\,\psi\,\mathrm{d}x = 0 \quad \text{for all } \psi \in \mathbb{P}_k(E). \tag{3.4}$$

For each mesh edge f, let $\mathbb{P}_k(f)$ be the space of polynomial functions defined on f with degree at most k. The orthogonal polynomials $\{\phi_{f,i}\}_{i=0,1,\ldots n_k^f-1}$ associated with each edge f (or face in 3D) form an orthogonal basis in $\mathbb{P}_k(f)$, and satisfy the orthogonality condition

$$\int_f \phi_{f,i}\,\phi_{f,j}\,\mathrm{d}S = |f|\,\delta_{ij}. \tag{3.5}$$

and we take $\phi_{f,0} = 1$. We define the projection $\Pi_k^f(\phi) \in \mathbb{P}_k(f)$ of a function $\phi \in L^2(f)$ by the orthogonality relation

$$\int_f (\Pi_k^f(\phi) - \phi)\,\psi\,\mathrm{d}S = 0 \quad \text{for all } \psi \in \mathbb{P}_k(f). \tag{3.6}$$

3.1.2 Degrees of Freedom

For $\mathbf{m} = (m_x, m_y, m_z)$, we associate the degrees of freedom for each component of the magnetization $\mathbf{m}$ to each element E. They represent the moments of m_u with respect to the orthogonal polynomials $\phi_{E,i}$ of degree at most k. We define

$$m_{u,E,i} := \frac{1}{|E|} \int_E m_u\,\phi_{E,i}\,\mathrm{d}x, \quad \text{for } i = 0, 1, \ldots, n_k^E - 1, \quad u \in \{x, y, z\} \tag{3.7}$$

where $\phi_{E,i}$ are orthogonal polynomials of degree up to k. The vector space

$$\mathcal{Q}^h = \left\{ m_u^h \mid m_u^h = (m_{u,E,0}, m_{u,E,1}, \cdots, m_{u,E,n_k^E-1})_{E\in\Omega^h}^T \right\}. \tag{3.8}$$

has dimension equals to n_k^E times the number of elements. Then the discrete magnetization $\mathbf{m}^h$ may be written (m_x^h, m_y^h, m_z^h) with $m_u^h \in \mathcal{Q}^h$. The restriction of each component of the magnetization m_u^h to each element E is given by $m_{u,E}$ which is the set of n_k^E real numbers $(m_{u,E,0}, \; m_{u,E,1}, \cdots, \; m_{u,E,n_k^E-1})$, and the restriction of the magnetization to each element E is given by $\mathbf{m}_E = (m_{x,E}, m_{y,E}, m_{z,E})$. The restriction operator to each element E and ith degree is given by $(\cdot)_{E,i}$ and we have $(m_u^h)_{E,i} := m_{u,E,i}$ and $(\mathbf{m}^h)_{E,i} := \mathbf{m}_{E,i} = (m_{x,E,i}, m_{y,E,i}, m_{z,E,i})^T$.

Let $\mathbf{p} = (\mathbf{p}_x, \mathbf{p}_y, \mathbf{p}_z)$. We associate the degrees of freedom for each component of the magnetic flux $\mathbf{p}$ to each element E and edge f (or face f in 3D) :

$$p_{u,E,i} = \frac{1}{|E|^{d/2}} \int_E \mathbf{p}_u \cdot \nabla \phi_{E,i} \, \mathrm{d}x, \quad \text{for } i = 1, \ldots, n_k^E - 1, \quad u \in \{x, y, z\},$$

and

$$p_{u,E,f,i} = \frac{1}{|f|} \int_f \mathbf{p}_u \cdot \boldsymbol{n}_{E,f} \, \phi_{f,i} \, \mathrm{d}x, \quad \text{for } i = 0, \ldots, n_k^f - 1, \quad u \in \{x, y, z\},$$

where $\boldsymbol{n}_{E,f}$ is an outward unit normal vector. Consider the vector space

$$\mathcal{F}^h = \left\{ p_u^h \mid p_u^h = \left(\{p_{u,E,1}, p_{u,E,2}, \ldots, p_{u,E,n_k^E-1}\}_{E \in \Omega^h}, \; \{p_{u,E,f,0}, p_{u,E,f,1}, \ldots, p_{u,E,f,n_k^f-1}\}_{f \in \partial E} \right)^T \right\}.$$
(3.9)

The dimension of this space is equal to $n_k^E - 1$ times the number of elements plus $2n_k^f$ times the number of interior edges and n_k^f times the number of boundary edges (faces in 3D). Then the discrete magnetic flux $\mathbf{p}^h$ may be written (p_x^h, p_y^h, p_z^h) with $p_u^h \in \mathcal{F}^h$. The restriction of each component of the magnetic flux p_u^h to each element E consists of degrees of freedom associated with both the element and the edges (faces) of the element. It is denoted by $p_{u,E}$ which is $(p_{u,E,1}, \ldots, p_{u,E,n_k^E-1}, \{p_{u,E,f,0}, \ldots, p_{u,E,f,n_f^k-1}\}_{f \in \partial E})^T$, and the restriction of the magnetic flux is $\mathbf{p}_E = (p_{x,E}, p_{y,E}, p_{z,E})$. The restriction operator to each element E and ith degree is $(\cdot)_{E,i}$ given by $(p_u^h)_{E,i} := (p_{u,E,i})$, and the restriction operator to each edge (or face) $f \in \partial E$ and ith degree is $(\cdot)_{E,f,i}$ given by $(p_u^h)_{E,f,i} := (p_{u,E,f,i})_{f \in \partial E}$.

We have a continuity condition for the flux on the edge. Let f be an internal edge shared by two elements E_1 and E_2. Then it satisfies the flux continuity constraints,

$$p_{u,E_1,f,i} + p_{u,E_2,f,i} = 0, \quad \text{for } i = 0, \ldots, n_k^f - 1, \quad u \in \{x, y, z\}. \tag{3.10}$$

3.1.3 Interpolation Operators

The local interpolation for each component of the magnetization $m_u \in L^2(E)$ is $m_{u,E}^I \in \mathcal{Q}^h|_E$, whose components are the moments of m_u with respect to the orthogonal polynomials $\phi_{E,i}$,

$$m_{u,E,i}^I := (m^I)_{u,E,i} = \frac{1}{|E|} \int_E m_u \, \phi_{E,i} \, \mathrm{d}x \quad \text{for } i = 0, 1, \ldots, n_k^E - 1.$$

The global interpolation of m_u is denoted by $m_u^I \in \mathcal{Q}^h$, whose restriction to E is $m_{u,E}^I$.

The piecewise polynomial representation on each element using the degrees of freedom
for each component of the discrete magnetization is

$$\widetilde{m}_u^h(x) = \sum_{i=0}^{n_k^E-1} m_{u,E,i}\, \phi_{E,i}(x) \quad \text{for } x \in E, \quad u \in \{x, y, z\}. \tag{3.11}$$

Then we have $m_u^h = (\widetilde{m}_u^h)^I$. The piecewise polynomial representation on each element using
the degrees of freedoms for the discrete magnetization is

$$\widetilde{\mathbf{m}}^h(x) = \sum_{i=0}^{n_k^E-1} \begin{pmatrix} m_{x,E,i} \\ m_{y,E,i} \\ m_{z,E,i} \end{pmatrix} \phi_{E,i}(x) \quad \text{for } x \in E. \tag{3.12}$$

The local interpolation for each component of the magnetic flux $\mathbf{p}_u \in H(\text{div}, E) \cap (L^s(E))^d$
with $s > 2$ is $p_{u,E}^I \in \mathcal{F}^h|_E$ whose components have the moments of $\mathbf{p}_u$ with respect to the
gradient of the orthogonal polynomials $\nabla\phi_{E,i}$,

$$p_{u,E,i}^I = (p_u^I)_{E,i} = \frac{1}{|E|^{1/d}} \int_E \mathbf{p}_u \cdot \nabla\phi_{E,i} \, \mathrm{d}x \quad \text{for } i = 1, 2, \ldots, n_k^E - 1,$$

and the moments of $\mathbf{p}_u \cdot \boldsymbol{n}_{E,f}$ for each edge (or face) $f \in \partial E$ with respect to the orthogonal
polynomials $\phi_{f,i}$,

$$p_{u,E,f,i}^I = (p_u^I)_{E,f,i} = \frac{1}{|f|} \int_f \mathbf{p}_u \cdot \boldsymbol{n}_{E,f} \, \phi_{f,i} \, \mathrm{d}x \quad \text{for } i = 0, 1, \ldots, \ldots, n_k^f - 1,$$

where $\boldsymbol{n}_{E,f}$ is an outward unit normal vector. The global interpolation of $\mathbf{p}_u$ is denoted by
$p_u^I \in \mathcal{F}^h$, whose restriction to E is $p_{u,E}^I$.

The piecewise polynomial representation on each edge (or face) using the degrees of
freedoms for each component of the discrete flux is

$$\widetilde{p}_u^h(x) = \sum_{i=0}^{n_k^f-1} p_{u,E,f,i}\, \phi_{f,i}(x) \quad \text{for } x \in f, \quad u \in \{x, y, z\}. \tag{3.13}$$

The piecewise polynomial representation on each edge (or face) using the degrees of
freedoms for the discrete flux is

$$\widetilde{\mathbf{p}}^h(x) = \sum_{i=0}^{n_k^f-1} \begin{pmatrix} p_{x,E,f,i} \\ p_{y,E,f,i} \\ p_{z,E,f,i} \end{pmatrix} \phi_{f,i}(x) \quad \text{for } x \in f. \tag{3.14}$$

Remark 4. *We can define the degrees of freedom for the low order terms (1.10) similarly
as in (3.7). Let us denote $\bar{\mathbf{h}}_{E,i}(\mathbf{m}) = (\bar{h}_{x,E,i}(\mathbf{m}), \bar{h}_{y,E,i}(\mathbf{m}), \bar{h}_{z,E,i}(\mathbf{m}))^T$, where $\bar{h}_{u,E,i}(\mathbf{m})$ are
the degrees of freedom for each component of the low order term $\bar{\mathbf{h}}(\mathbf{m})$. That is,*

$$\bar{h}_{u,E,i}(\mathbf{m}) = \frac{1}{|E|} \int_E \bar{\mathbf{h}}_u(\mathbf{m})\, \phi_{E,i} \, \mathrm{d}x, \quad \text{for } i = 0, 1, \ldots, n_k^E - 1, \quad u \in \{x, y, z\}.$$

Similarly, the piecewise polynomial representation on each element using the degrees of freedoms for $\bar{\mathbf{h}}(\mathbf{m})$ *is*

$$\widetilde{\bar{\mathbf{h}}(\mathbf{m})}^h (x) = \sum_{i=0}^{n_k^E - 1} \begin{pmatrix} \bar{h}_{x,E,i}(\mathbf{m}) \\ \bar{h}_{y,E,i}(\mathbf{m}) \\ \bar{h}_{z,E,i}(\mathbf{m}) \end{pmatrix} \phi_{E,i}(x) \quad \textit{for } x \in E. \tag{3.15}$$

3.1.4   Mimetic Divergence Operator

The mimetic divergence operator $\mathcal{DIV} : \mathcal{F}^h \to \mathcal{Q}^h$ is defined on each element by the commutation property:

$$\mathcal{DIV}\ p_u^I = (\mathbf{div}\ \mathbf{p}_u)^I \text{ for all } \mathbf{p} \in \mathcal{F}.$$

Each degree of freedom can be computed by using integration by parts:

$$(\mathbf{div}\ \mathbf{p}_u)_{E,i}^I = \frac{1}{|E|} \int_E (\mathbf{div}\ \mathbf{p}_u)\ \phi_{E,i}\ \mathrm{d}x = \frac{1}{|E|}(-\int_E \mathbf{p}_u \cdot \nabla\phi_{E,i}\ \mathrm{d}x + \sum_{f \in \partial E} \int_f \mathbf{p}_u \cdot \mathbf{n}_{E,f}\ \phi_{E,i}\ \mathrm{d}x)$$

for $i = 0, 1, \ldots, n_k^E - 1$. The restriction of $\mathcal{DIV}\ p_u^h \in \mathcal{Q}^h$ to each element E is given by $\mathcal{DIV}_E\ p_{u,E}$ with components $((\mathcal{DIV}\ p_u^h)_{E,0}, (\mathcal{DIV}\ p_u^h)_{E,1}, \cdots, (\mathcal{DIV}\ p_u^h)_{E,n_k^E-1})^T$. Let us define

$$\mathbf{DIV}_E\ \mathbf{p}_E = \begin{pmatrix} \mathcal{DIV}_E\ p_{x,E} \\ \mathcal{DIV}_E\ p_{y,E} \\ \mathcal{DIV}_E\ p_{z,E} \end{pmatrix},$$

and

$$\mathbf{DIV}_E\ \mathbf{p}_{E,i} = \begin{pmatrix} (\mathcal{DIV}\ p_x^h)_{E,i} \\ (\mathcal{DIV}\ p_y^h)_{E,i} \\ (\mathcal{DIV}\ p_z^h)_{E,i} \end{pmatrix}.$$

for $i = 0, 1, \ldots, n_k^E - 1$.

The piecewise polynomial representation using the degrees of freedoms for each component of the divergence is

$$\widetilde{\mathcal{DIV}\ p_u^h} (x) = \sum_{i=0}^{n_k^E - 1} (\mathcal{DIV}\ p_u^h)_{E,i}\ \phi_{E,i}(x) \quad \text{for } x \in E. \tag{3.16}$$

The piecewise polynomial representation using the degrees of freedoms for the divergence is

$$\widetilde{\mathbf{DIV}\ \mathbf{p}}^h (x) = \sum_{i=0}^{n_k^E - 1} \begin{pmatrix} (\mathcal{DIV}\ p_x^h)_{E,i} \\ (\mathcal{DIV}\ p_y^h)_{E,i} \\ (\mathcal{DIV}\ p_z^h)_{E,i} \end{pmatrix} \phi_{E,i}(x) \quad \text{for } x \in E. \tag{3.17}$$

3.1.5 Mimetic Inner Products

We define the mimetic inner product in the discrete magnetization space $\mathcal{Q}^h$ by

$$\langle \mathbf{m}^h, \mathbf{w}^h \rangle_{\mathcal{Q}} = \sum_{u \in \{x,y,z\}} \langle m_u^h, w_u^h \rangle_{\mathcal{Q}}, \quad \langle m_u^h, w_u^h \rangle_{\mathcal{Q}} = \sum_{E \in V_h} \langle m_{u,E}^h, w_{u,E}^h \rangle_{\mathcal{Q},E} \tag{3.18}$$

The local inner product is defined by adding all degrees of freedom associated with the element,

$$\langle m_{u,E}^h, w_{u,E}^h \rangle_{\mathcal{Q},E} = |E| \left(\sum_{i=0}^{n_k^E - 1} m_{u,E,i} \, w_{u,E,i} \right).$$

This can be obtained from the L^2 inner product for piecewise polynomial functions of degree k associated with m_u^h and w_u^h. That is,

$$\int_E \widetilde{m}_u^h(x) \, \widetilde{w}_u^h(x) \, \mathrm{d}x = \sum_{i,j=0}^{n_k^E - 1} m_{u,E,i} \, w_{u,E,j} \int_E \phi_{E,i}(x) \phi_{E,j}(x) \, \mathrm{d}x$$

$$= |E| \left(\sum_{i,j=0}^{n_k^E - 1} m_{u,E,i} \, w_{u,E,j} \, \delta_{ij} \right) = |E| \left(\sum_{i=0}^{n_k^E - 1} m_{u,E,i} \, w_{u,E,i} \right). \tag{3.19}$$

We define the mimetic inner product in the space of discrete magnetic flux $\mathcal{F}^h$ by

$$\langle \mathbf{p}^h, \mathbf{q}^h \rangle_{\mathcal{F}} = \sum_{u \in \{x,y,z\}} \langle p_u^h, q_u^h \rangle_{\mathcal{F}}, \quad \langle p_u^h, q_u^h \rangle_{\mathcal{F}} = \sum_{E \in V_h} \langle p_{u,E}, q_{u,E} \rangle_{\mathcal{F},E}, \tag{3.20}$$

where $\langle \cdot, \cdot \rangle_{\mathcal{F},E}$ is an element-based inner product that requires special construction discussed later in section 3.1.7.

3.1.6 Mimetic Gradient Operator

To introduce the mimetic gradient operator, we start by discretizing the local Green formula

$$\int_E \mathbf{m} \cdot \mathbf{div} \, \mathbf{p} \, \mathrm{d}x = -\int_E \nabla \mathbf{m} : \mathbf{p} \, \mathrm{d}x + \int_{\partial E} (\mathbf{p} \cdot \mathbf{n}) \cdot \mathbf{m} \, \mathrm{d}x.$$

To discretize the last term, we introduce additional degrees of freedom associated with the magnetization on mesh edges (or faces) f for each element E. The components are

$$m_{u,f,i} = \frac{1}{|f|} \int_f m_u \, \phi_{f,i} \, \mathrm{d}x, \quad \text{for } i = 0, 1, \ldots, n_k^f - 1, \quad u \in \{x, y, z\}.$$

The restriction of each component of the magnetization to each edge (or face) f is denoted by $m_{u,f}$ and the restriction of the magnetization to each edge (or face) f is denoted by

$\mathbf{m}_f = (m_{x,f},\, m_{y,f},\, m_{z,f})$. Let $\widetilde{\mathbf{m}}_E = (\widetilde{m}_{x,E}, \widetilde{m}_{y,E}, \widetilde{m}_{z,E})^T$ be the additional degrees of freedom associated with each element E, where $\widetilde{m}_{u,E} = (m_{u,f,0}, \ldots, m_{u,f,n_k^f-1})_{f \in \partial E}$. The total number of degrees of freedom is equal to n_k^f times the number of edges (or faces) N_F. The local mimetic gradient operator is defined implicitly by a discrete duality property :

$$\langle \mathbf{m}_E,\, \mathbf{DIV}_E\, \mathbf{p}_E \rangle_{Q,E} = -\left\langle \mathbf{GRAD}_E \begin{pmatrix} \mathbf{m}_E \\ \widetilde{\mathbf{m}}_E \end{pmatrix},\, \mathbf{p}_E \right\rangle_{\mathcal{F},E} + \sum_{u \in \{x,\,y,\,z\}} \sum_{f \in \partial E} \sum_{i=0}^{n_k^f-1} |f|\, p_{u,E,f,i} \cdot m_{u,f,i}$$

(3.21)

for all $\mathbf{m}_E$, $\widetilde{\mathbf{m}}_E$, and $\mathbf{p}_E$. The local mimetic gradient operator is defined uniquely due to the properties of the inner products.

3.1.7   Construction of mimetic inner product for flux

We present the construction of the local mimetic inner products for magnetic fluxes. We consider a subspace $\mathcal{S}^h$ of $\bar{\mathcal{F}}^h$ defined as

$$\mathcal{S}^h = \{p \in \bar{\mathcal{F}}^h \mid (\mathbf{div}\, p)_E \in \mathbb{P}_k(E), p \cdot \mathbf{n}_{E,f} \in \mathbb{P}_{k+1}(f) \text{ for every } E \in \Omega^h\}, \tag{3.22}$$

where

$$\bar{\mathcal{F}}^h = \{v \mid \mathbf{div}\, v \in L^2(\Omega),\, (\mathbf{div}\, v)|_E \in L^2(E),\, v \in (L^s(E))^d, \\ \text{with } s > 2,\, E \in V^h \text{ for every } E \in \Omega^h\} \tag{3.23}$$

The local inner product $\langle p_{u,E},\, q_{u,E} \rangle_{\mathcal{F},E}$ in (3.20) is constructed to satisfy stability and consistency conditions :

- (Local Consistency) For every polynomial $p \in \mathbb{P}_{k+2}(E)$ and every $q \in \mathcal{S}^h$, we have

$$\langle \left(\Pi_{k+1}^E(\nabla p)\right)^I, q^I \rangle_E = \int_E \nabla p \cdot q \, \mathrm{d}x. \tag{3.24}$$

- (Stability) There exist two positive constants $c_0, C_0 > 0$ such that

$$c_0|E|\|p_{u,E}\|_E^2 \le \langle p_{u,E},\, p_{u,E} \rangle_{\mathcal{F},E} \le C_0|E|\|p_{u,E}\|_E^2 \tag{3.25}$$

for all $p_{u,E} \in \mathcal{F}^h|_E$, where

$$|p_{u,E}|_E^2 = h_E^2 \sum_{i=1}^{n_k^E} |p_{u,E,i}|^2 + \sum_{f \in \partial E} \sum_{i=0}^{n_k^f-1} |p_{u,E,f,i}|^2 \tag{3.26}$$

with h_E the diameter of E.

Using equation (3.24), we get

$$\langle\left(\Pi_{k+1}^E(\nabla p)\right)^I, q^I\rangle_E = \int_E \nabla p \cdot q \, \mathrm{d}x = -\int_E p \, \mathbf{div} \, q \, \mathrm{d}x + \sum_{f\in\partial E}\int_f q\cdot \boldsymbol{n}_{E,f} \, p \, dS$$

$$= -\int_E p \, \Pi_k^E(\mathbf{div} \, q) \, \mathrm{d}x + \sum_{f\in\partial E}\int_f \Pi_{k+1}^f(q\cdot\boldsymbol{n}_{E,f}) \, p \, dS$$

$$= -\int_E p \, (\widetilde{\mathcal{DIV}q^I}) \, \mathrm{d}x + \sum_{f\in\partial E}\int_f (\widetilde{q^I}) \, p \, dS. \tag{3.27}$$

Using equation (3.27), we can construct the mimetic inner product in $\mathcal{F}^h$ as in [47]. It is an $n_{k+1}^E \times n_{k+1}^E$ symmetric positive definite matrix $\mathbb{M}_{\mathcal{F},E}$ with

$$\langle p_{u,E}, q_{u,E}\rangle_{\mathcal{F},E} = (p_{u,E})^T \, \mathbb{M}_{\mathcal{F},E} \, (q_{u,E}). \tag{3.28}$$

The matrix $\mathbb{M}_{\mathcal{F},E}$ is defined by

$$\mathbb{M}_{\mathcal{F},E} = \mathbb{R}_E \, (\mathbb{N}_E^T \, \mathbb{R}_E)^{-1} \, \mathbb{R}_E^T + \mu_E \, (I - \mathbb{N}_E \, (\mathbb{N}_E^T \, \mathbb{N}_E)^{-1} \, \mathbb{N}_E^T), \tag{3.29}$$

where the ith column of $\mathbb{N}_E$ is given by

$$(\mathbb{N}_E)_i = (\Pi_{k+1}^E(\nabla\phi_{E,i}))^I \tag{3.30}$$

for $i = 1, \ldots, n_{k+2}^E - 1$ and the ith column of $\mathbb{R}_E$ satisfies

$$q_{u,E}^T \, (\mathbb{R}_E)_i = -\int_E \widetilde{\mathcal{DIV}q_u^h} \, \phi_{E,i} \, \mathrm{d}x + \sum_{f\in\partial E}\int_f \tilde{q}_u^h \, \phi_{E,i} dS \tag{3.31}$$

for every $q_E \in \mathcal{F}^h|_E$ and $\mu_E = \mathrm{trace} \, (\mathbb{R}_E \, (\mathbb{N}_E^T \, \mathbb{R}_E)^{-1} \, \mathbb{R}_E^T)$.

3.1.8   The Predictor-Corrector Scheme

We use the mimetic discretization to discretize in space. The semi-discrete mimetic formulation is to find $\mathbf{m}_E$, $\widetilde{\mathbf{m}}_E$, and $\mathbf{p}_E$, for $E \in V^h$, such that

$$\mathbf{p}_E = -\mathbf{GRAD}_E \begin{pmatrix}\mathbf{m}_E \\ \widetilde{\mathbf{m}}_E\end{pmatrix}$$

$$\sum_{i=0}^{n_k^E-1} a_{il}\frac{\partial\mathbf{m}_{E,i}}{\partial t} = \sum_{i,j=0}^{n_k^E-1} a_{ijl}\mathbf{m}_{E,i}\times(\mathbf{DIV}_E\mathbf{p}_{E,j} - \bar{\mathbf{h}}_{E,j}(\mathbf{m}))$$
$$+\alpha\sum_{i,j,k=0}^{n_k^E-1} a_{ijkl}(\mathbf{m}_{E,i}\cdot(\mathbf{DIV}_E\,\mathbf{p}_{E,j} - \bar{\mathbf{h}}_{E,j}(\mathbf{m}))\,\mathbf{m}_{E,k}$$
$$-\alpha\sum_{i,j,k=0}^{n_k^E-1} a_{ijkl}\,(\mathbf{m}_{E,i}\cdot\mathbf{m}_{E,k})\,(\mathbf{DIV}_E\,\mathbf{p}_{E,j} - \bar{\mathbf{h}}_{E,j}(\mathbf{m})) \tag{3.32}$$

where $a_{il} = \int_E \phi_{E,i} \, \phi_{E,l} \, \mathrm{d}x$, $a_{ijl} = \int_E \phi_{E,i} \, \phi_{E,j} \, \phi_{E,l} \, \mathrm{d}x$, and $a_{ijkl} = \int_E \phi_{E,i} \, \phi_{E,j} \, \phi_{E,k} \, \phi_{E,l} \, \mathrm{d}x$, for $l = 0, \ldots, n_k^E - 1$ and subject to flux continuity (3.10), initial and boundary conditions.

The Dirichlet boundary conditions are imposed by prescribing given values of the auxiliary magnetization $\widetilde{\mathbf{m}}_E$ on each edge (or face) f. The Neumann boundary conditions are imposed by setting the magnetic flux to the given values. In fact, the second equation in (3.32) can be derived from

$$
\begin{aligned}
\int_E \frac{\partial \widetilde{\mathbf{m}}^h}{\partial t} \cdot \widetilde{\mathbf{v}}^h \;=\; & \int_E (\widetilde{\mathbf{m}}^h \times (\widetilde{\mathbf{DIV}\ \mathbf{p}^h} - \widetilde{\bar{\mathbf{h}}(\mathbf{m})}^h)) \cdot \widetilde{\mathbf{v}}^h \\
& + \alpha \int_E (\widetilde{\mathbf{m}}^h \cdot (\widetilde{\mathbf{DIV}\ \mathbf{p}^h} - \widetilde{\bar{\mathbf{h}}(\mathbf{m})}^h))(\widetilde{\mathbf{m}}^h \cdot \widetilde{\mathbf{v}}^h) \\
& - \alpha \int_E (\widetilde{\mathbf{m}}^h \cdot \widetilde{\mathbf{m}}^h)((\widetilde{\mathbf{DIV}\ \mathbf{p}^h} - \widetilde{\bar{\mathbf{h}}(\mathbf{m})}^h) \cdot \widetilde{\mathbf{v}}^h)
\end{aligned}
\tag{3.33}
$$

We discretize in time using backward Euler time stepping, which is first order in time, and use it as the predictor step. To preserve the magnitude of the magnetization in a certain sense, we use a corrector step. This step preserves the magnitude of the magnetization in the sense that $\int_E |\widetilde{\mathbf{m}}^{h,J+1}|^2 = \int_E |\widetilde{\mathbf{m}}^{h,J}|^2$, that is, $\sum_{i=0}^{n_k^E-1} |\mathbf{m}_{E,i}^{J+1}|^2 = \sum_{i=0}^{n_k^E-1} |\mathbf{m}_{E,i}^J|^2$. We expect to be asymptotic conservation of the length. Note that, if we use a low order discretization in space, the predictor-corrector scheme would preserve the nonconvex constraint, i.e. $|\mathbf{m}_E^{J+1}| = |\mathbf{m}_E^J|$.

The resulting method is second order in time.

1. Predictor Step : Backward Euler

$$
\mathbf{p}_E^* \;=\; -\mathbf{GRAD}_E \left(\frac{\mathbf{m}_E^*}{\widetilde{\mathbf{m}}_E^*} \right)
$$

$$
\begin{aligned}
\sum_{i=0}^{n_k^E-1} a_{il} \frac{\mathbf{m}_{E,i}^* - \mathbf{m}_{E,i}^J}{k} \;=\; & \sum_{i,j=0}^{n_k^E-1} a_{ijl} \mathbf{m}_{E,i}^J \times (\mathbf{DIV}_E \mathbf{p}_{E,j}^* - \bar{\mathbf{h}}_{E,j}^*(\mathbf{m})) \\
& + \alpha \sum_{i,j,k=0}^{n_k^E-1} a_{ijkl}(\mathbf{m}_{E,i}^J \cdot (\mathbf{DIV}_E\ \mathbf{p}_{E,j}^* - \bar{\mathbf{h}}_{E,j}^*(\mathbf{m}))\, \mathbf{m}_{E,k}^J \\
& - \alpha \sum_{i,j,k=0}^{n_k^E-1} a_{ijkl}\, (\mathbf{m}_{E,i}^J \cdot \mathbf{m}_{E,k}^J)\, (\mathbf{DIV}_E\ \mathbf{p}_{E,j}^* - \bar{\mathbf{h}}_{E,j}^*(\mathbf{m}))
\end{aligned}
\tag{3.34}
$$

2. Corrector Step :

$$
\mathbf{p}_E^{J+\frac{1}{2}} \;=\; -\mathbf{GRAD}_E \left(\frac{\mathbf{m}_E^{J+\frac{1}{2}}}{\widetilde{\mathbf{m}}_E^{J+\frac{1}{2}}} \right)
$$

$$
\begin{aligned}
\sum_{i=0}^{n_k^E-1} a_{il} \frac{\mathbf{m}_{E,i}^{J+1} - \mathbf{m}_{E,i}^J}{k} \;=\; & \sum_{i,j=0}^{n_k^E-1} a_{ijl} \frac{\mathbf{m}_{E,i}^J + \mathbf{m}_{E,i}^{J+1}}{2} \times (\mathbf{DIV}_E \mathbf{p}_{E,j}^{J+\frac{1}{2}} - \bar{\mathbf{h}}_{E,j}^{J+\frac{1}{2}}(\mathbf{m})) \\
& + \alpha \sum_{i,j,k=0}^{n_k^E-1} a_{ijkl}(\frac{\mathbf{m}_{E,i}^J + \mathbf{m}_{E,i}^{J+1}}{2} \cdot (\mathbf{DIV}_E\ \mathbf{p}_{E,j}^{J+\frac{1}{2}} - \bar{\mathbf{h}}_{E,j}^{J+\frac{1}{2}}(\mathbf{m}))\, \mathbf{m}_{E,k}^{J+\frac{1}{2}} \\
& - \alpha \sum_{i,j,k=0}^{n_k^E-1} a_{ijkl}\, (\frac{\mathbf{m}_{E,i}^J + \mathbf{m}_{E,i}^{J+1}}{2} \cdot \mathbf{m}_{E,k}^{J+\frac{1}{2}})\, (\mathbf{DIV}_E\ \mathbf{p}_{E,j}^{J+\frac{1}{2}} - \bar{\mathbf{h}}_{E,j}^{J+\frac{1}{2}}(\mathbf{m}))
\end{aligned}
\tag{3.35}
$$

where $\mathbf{m}_E^{J+\frac{1}{2}} = \frac{\mathbf{m}_E^J + \mathbf{m}_E^*}{2}$ and $\widetilde{\mathbf{m}}_E^{J+\frac{1}{2}} = \frac{\widetilde{\mathbf{m}}_E^J + \widetilde{\mathbf{m}}_E^*}{2}$.

3.2 Numerical Examples 1

3.2.1 Periodic Boundary Conditions

In this section, we consider the predictor-corrector scheme and provide convergence tests on various meshes. A family of analytic solutions for the Landau-Lifshitz equation with effective field including only the exchange energy term, i.e. $\mathbf{h} = \Delta\mathbf{m}$, is given by [38]

$$m_x(x_1, x_2, t) = \frac{1}{d(t)} \sin\beta \cos(\kappa(x_1 + x_2) + g(t)),$$
$$m_y(x_1, x_2, t) = \frac{1}{d(t)} \sin\beta \sin(\kappa(x_1 + x_2) + g(t)), \qquad (3.36)$$
$$m_z(x_1, x_2, t) = \frac{1}{d(t)} e^{2\kappa^2 \alpha t} \cos\beta.$$

where $\beta = \frac{\pi}{12}$, $\kappa = 2\pi$, $d(t) = \sqrt{\sin^2\beta + e^{4\kappa^2\alpha t}\cos^2\beta}$ and $g(t) = \frac{1}{\alpha}\log\left(\frac{d(t) + e^{2\kappa^2\alpha t}\cos\beta}{1 + \cos\beta}\right)$. This family was also used in section 2.5.1 .

   We perform simulations on the time interval $[0, T]$ with $T = 0.001$. We have $(m_x, m_y, m_z) \to (0, 0, 1)$ as $t \to \infty$. We measure errors by calculating mesh dependent L^2-type norms $\|\cdot\|_{\mathcal{Q}}$ for the magnetization, and $\|\cdot\|_{\mathcal{F}}$ for the magnetic flux.

3.2.1.1 Uniform square meshes

In this section, we consider predictor-corrector scheme with the analytic solution given by (3.36) on a unit square $\Omega = [0, 1] \times [0, 1]$ with periodic boundary conditions. We perform the simulation on a uniform square mesh with mesh size h and set $k = Ch^{3/2}$ so that the second order time integration does not affect our conclusions. Specifically, we set $C = \sqrt{2} \cdot 10^{-4}$ for $h = 1/8, 1/32, 1/128$ and $C = 10^{-4}$ for $h = 1/16, 1/64$. The result is shown in Table 3.1 and Fig 3.2 which shows both third order convergence in h and second order convergence in k for the magnetization.

$1/h$	$\|\mathbf{m}^h - \mathbf{m}^I\|_{\mathcal{Q}}$
8	5.830e-04
16	7.427e-05
32	9.404e-06
64	1.178e-06
128	1.474e-07
rate	2.99

Table 3.1: Convergence analysis of predictor-corrector scheme on a uniform square mesh.

3.2.1.2 Smoothly distorted and randomized quadrilateral meshes

In this section, we continue the convergence analysis for the predictor-corrector scheme with two different meshes. We consider randomly and smoothly distorted mesh as shown in Fig. 3.1. The randomized mesh is constructed by random perturbation of the interior nodes in a uniform mesh, The nodes of the randomized mesh are given by

$$x := x + 0.2\,\xi_x\,h, \quad y := y + 0.2\,\xi_y\,h, \tag{3.37}$$

where ξ_x and ξ_y are random variables between -1 and 1. The smoothly distorted mesh is constructed from a uniform square mesh using a smooth map to calculate the positions of the new nodes. The smooth map is given by

$$
\begin{aligned}
x &:= x + 0.1\sin(2\pi x)\sin(2\pi y), \\
y &:= y + 0.1\sin(2\pi x)\sin(2\pi y).
\end{aligned}
\tag{3.38}
$$

As before, for a given mesh size h, we set $k = Ch^{3/2}$ with $C = \sqrt{2} \cdot 10^{-4}$ for $h =$
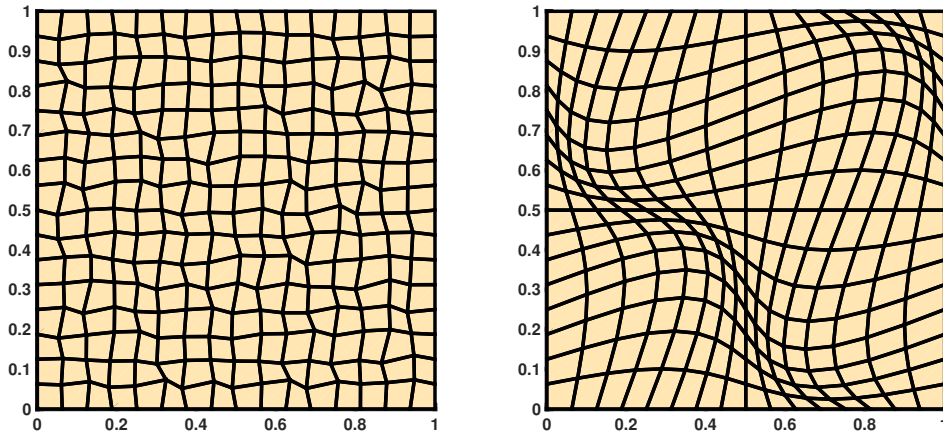
Figure 3.1: Left : Randomized mesh, Right : Smoothly distorted mesh.

$1/8, 1/32, 1/128$ and $C = 10^{-4}$ for $h = 1/16, 1/64$. The results are shown in Table 3.2 and Fig 3.2 which shows third order convergence in h for the magnetization.

3.2.1.3 Convergence analysis for problems with Dirichlet boundary conditions

In this section, we consider the predictor-corrector scheme for the Landau-Lifshitz equation with effective field including only the exchange energy term, i.e. $\mathbf{h} = \Delta\mathbf{m}$. We consider the analytic solution in (3.36) with Dirichlet boundary condition. We consider not only uniform and distorted meshes on a unit square, but also structured meshes on a circular domain

	Randomized mesh	Smoothly distorted mesh
$1/h$	$\|\mathbf{m}^h - \mathbf{m}^I\|_{\mathcal{Q}}$	$\|\mathbf{m}^h - \mathbf{m}^I\|_{\mathcal{Q}}$
8	1.504e-03	2.748e-03
16	1.740e-04	3.253e-04
32	2.294e-05	4.346e-05
64	2.799e-06	5.537e-06
128	3.600e-07	6.955e-07
rate	3.00	2.96

Table 3.2: Convergence analysis of predictor-corrector scheme on distorted meshes.
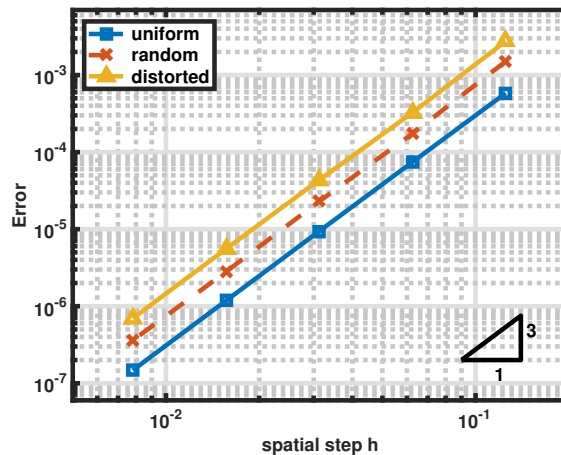
Figure 3.2: Error plot of $\|\mathbf{m}^h - \mathbf{m}^I\|_{\mathcal{Q}}$ with respect to the mesh size h on the uniform, randomized and smoothly distorted meshes shown in Fig. 3.1.

with center $(0.5, 0.5)$ and radius 0.5, shown in Fig. 3.3. The Dirichlet boundary conditions allows us to consider more general domains such as circular domains. In Fig. 3.3, it shows a logically square mesh fitted to the circular domain.

For a given mesh size h, we set $k = Ch^{3/2}$ with $C = \sqrt{2} \cdot 10^{-4}$ for $h = 1/8, 1/32, 1/128$ and $C = 10^{-4}$ for $h = 1/16, 1/64$. The errors and convergence rates are summarized in Table 3.3 and Fig. 3.4. We observe again the third-order convergence rate for the magnetization.
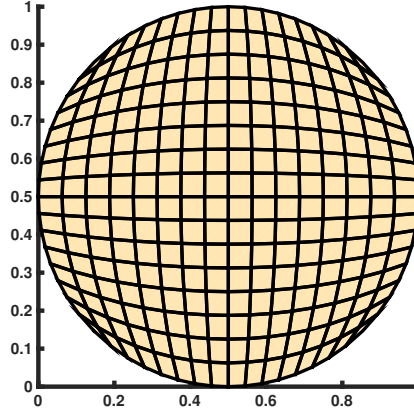
Figure 3.3: Logically square mesh fitted to the circular domain.

Uniform square mesh			Randomized mesh		
$1/h$	$\|\mathbf{m}^h - \mathbf{m}^I\|_\mathcal{Q}$	ratio	$1/h$	$\|\mathbf{m}^h - \mathbf{m}^I\|_\mathcal{Q}$	ratio
8	8.478e-04	3.26	8	1.549e-03	3.08
16	8.824e-05	3.14	16	1.830e-04	2.97
32	9.985e-06	3.05	32	2.338e-05	3.05
64	1.206e-06		64	2.825e-06	
Smoothly distorted mesh			Logically square mesh in the circular domain		
8	3.363e-03	3.13	8	9.318e-04	3.26
16	3.843e-04	3.08	16	9.719e-05	3.24
32	4.547e-05	3.02	32	1.027e-05	3.11
64	5.588e-06		64	1.189e-06	

Table 3.3: Convergence analysis of predictor-corrector scheme with Dirichlet boundary conditions.

3.3 Static skyrmions and efficiency of the high order method

In this section, we compute a static skyrmion [50], which is a local minimizer of the energy functional

$$E(\mathbf{m}) = \frac{1}{2} \int_\Omega |\nabla \mathbf{m}|^2 \, \mathrm{d}x + \frac{\kappa}{2} \int_\Omega (m_1^2 + m_2^2) \, \mathrm{d}x + \lambda \int_\Omega \mathbf{m} \cdot (\nabla \times \mathbf{m}) \, \mathrm{d}x, \qquad (3.39)$$

where λ is a chirality constant and κ is a dimensionless anisotropy constant. The energy of a skyrmion in a chiral ferromagnet is given by the above equation (3.39). The first term is the exchange energy, the second term is the anisotropy energy and the last term
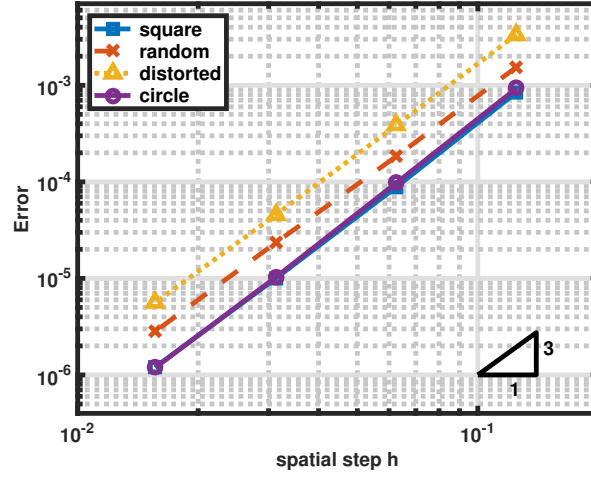
Figure 3.4: Error plot of $\|\mathbf{m}^h - \mathbf{m}^I\|_{\mathcal{Q}}$ with respect to the mesh size h for predictor-corrector scheme with Dirichlet boundary conditions.

is the Dzyaloshinskii-Moriya (DM) interaction [95, 66, 57]. In order to compute a static skyrmion, we use both low order and high order predictor-corrector scheme on a square domain $[-15, 15] \times [-15, 15]$ with Neumann boundary conditions and evolve to steady-state. The initial state of the magnetization is given by

$$
\begin{aligned}
m_x(x_1, x_2) &= \sin \Theta(r) \cos \Phi(\phi) \\
m_y(x_1, x_2) &= \sin \Theta(r) \sin \Phi(\phi) \\
m_z(x_1, x_2) &= \cos \Theta(r),
\end{aligned}
\tag{3.40}
$$

where $\Theta(r) = 2 \arctan(\frac{r}{r-a}) + \pi$ and $\Phi(\phi) = \phi$, with $a = 5$, $r = \sqrt{x_1^2 + x_2^2}$ and $\phi = \arctan(\frac{x_2}{x_1})$. The skyrmion number is given by

$$
\mathcal{Q} = \frac{1}{4\pi} \int_V \mathbf{m} \cdot (\frac{\partial \mathbf{m}}{\partial x} \times \frac{\partial \mathbf{m}}{\partial y}) \, \mathrm{d}x,
$$

which is the integral of the solid angle and counts how many times the magnetization wraps around the unit sphere. The initial state has spin configuration with $\mathcal{Q} = 1$ and eventually converges to a static skyrmion with $\mathcal{Q} = 1$. The energy of the numerical solution is shown in Fig. 3.5; it monotonically decreases as the solution converges to a stationary state. Table 3.4 summarizes the error in skyrmion number $\mathcal{Q}$ at time 6 with $k = 1.28h$. It shows second order convergence for the low order method and more than second order convergence for the high order method. We compared the efficiency of the two methods in Fig. 3.6, where the x-axis is the cost of the numerical method, which is proportional to the number of nonzero entries of the matrix, and the y-axis is the error in the skyrmion number $\mathcal{Q}$ at time 6. It shows that the high order method is more efficient than the low order method already for coarse meshes.
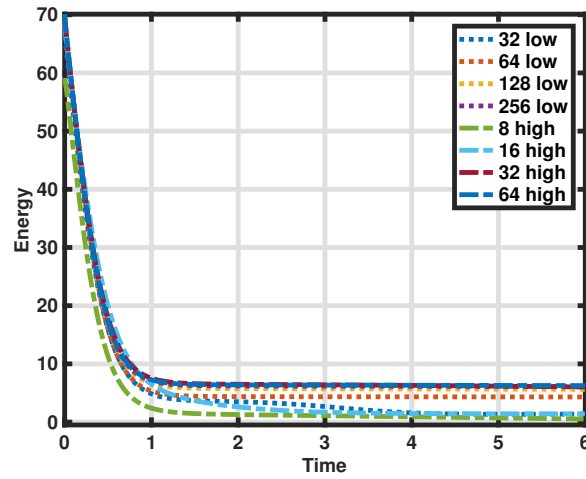
Figure 3.5: Energy of solutions as a function of time.

Low order method			High order method		
$1/h$	Error in $\mathcal{Q}$ at time 6	rate	$1/h$	Error in $\mathcal{Q}$ at time 6	rate
32	4.246e-01	1.92	8	5.683e-01	0.46
64	1.123e-01	1.89	16	4.135e-01	3.32
128	3.026e-02	1.97	32	4.134e-02	5.23
256	7.723e-03		64	1.103e-03	

Table 3.4: Error in skyrmion number and rate of convergence.
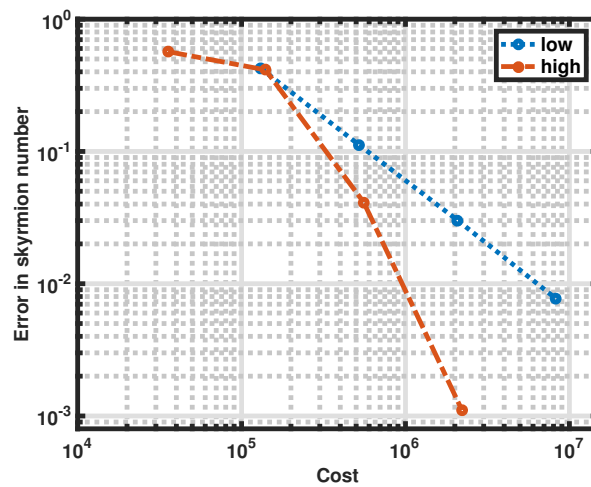
Figure 3.6: Comparison of the efficiency of high and low order methods.

Chapter 4

The mass-lumped finite element method for the Landau-Lifshitz equation

In this chapter, we present a family of mass-lumped finite element methods for the Landau-Lifshitz equation. We provide a rigorous convergence proof that the numerical solution of our scheme has a subsequence that converges weakly to a weak solution of the Landau-Lifshitz-Gilbert equation. We develop a simple proof technique that cancels out the product of weakly convergent sequences. Our proofs use tools introduced in [7].

   Our scheme has several advatanges over previous finite element methods for the Landau-Lifshitz equation [6, 5, 7, 52, 9, 13, 30] (See section 1.7.3). For our implicit scheme, we only need to solve a sparse linear system for each time step, which is of similar complexity to the algorithms in Alouges et al's scheme [6, 5, 7]. By contrast, Bartels and Prohl's scheme and Cimák's scheme require the solution of a nonlinear system. For the explicit scheme, our approach is more efficient in that it is completely explicit : the effective mass matrix is diagonal. Furthermore, we built our scheme based on the Landau-Lifshitz equation instead of the Landau-Lifshitz-Gilbert equation so that we can naturally extend the method to limiting case, such as the Schrödinger map or the harmonic map heat flow. In contrast, Alouges et al's scheme and Bartels and Prohl's schemes are based on other forms of the Landau-Lifshitz equation.

4.1   Weak solutions, meshes and the finite element space

Let us denote $\Omega_T = \Omega \times (0, T)$. We first introduce the definition of a weak solution of the Landau-Lifshitz-Gilbert equation :

Definition 1. *Let $\mathbf{m}_0(x) \in H^1(\Omega)^3$ with $|\mathbf{m}_0(x)| = 1$ a.e. Then $\mathbf{m}$ is a weak solution of (1.12) if for all $T > 0$,*

(i) $\mathbf{m}(x,t) \in H^1(\Omega_T)^3$ *and* $|\mathbf{m}(x,t)| = 1$ *a.e.,*

(ii) $\mathbf{m}(x,0) = \mathbf{m}_0(x)$ *in the trace sense,*

(iii) $\mathbf{m}$ *satisfies*

$$\int_{\Omega_T} \frac{\partial \mathbf{m}}{\partial t} \cdot \mathbf{w} - \alpha \int_{\Omega_T} (\mathbf{m} \times \frac{\partial \mathbf{m}}{\partial t}) \cdot \mathbf{w} \tag{4.1}$$

$$= (1 + \alpha^2)\eta \sum_{l=1}^{d} \int_{\Omega_T} (\mathbf{m} \times \frac{\partial \mathbf{m}}{\partial x_l}) \cdot \frac{\partial \mathbf{w}}{\partial x_l} - (1 + \alpha^2) \sum_{l=1}^{d} \int_{\Omega_T} (\mathbf{m} \times \bar{\mathbf{h}}(\mathbf{m})) \cdot \mathbf{w}.$$

for all $\mathbf{w} \in H^1(\Omega_T)^3$.

(iv) $\mathbf{m}$ *satisfies an energy inequality*

$$C \int_{\Omega_T} |\frac{\partial \mathbf{m}}{\partial t}|^2 + E(\mathbf{m}(x,T)) \leq E(\mathbf{m}(x,0)). \tag{4.2}$$

for some constant $C > 0$, where the energy $E(\mathbf{m})$ is defined in equation (1.2).

The value C in *(iv)* is taken to be $C = \frac{\alpha}{1+\alpha^2}$ in [6, 13].

Let the domain $\Omega \subset \mathbb{R}^d$ where $d = 2$ or 3 be discretized into triangular or tetrahedral elements $\{\mathcal{T}_h\}_h$ of mesh size at most h, with vertices $(x_i)_{i=1}^N$. Let the family of partitions $\mathcal{T} = \{\mathcal{T}_h\}_h$ be admissible, shape regular and uniform. We review the definition of *admissible, shape regular* and *uniform* (taken from [20]) :

Definition 2.   *1. A family of partitions $\mathcal{T} = \{\mathcal{T}_h\}_h$ is called <u>admissible</u> provided that*

    a) $\bar{\Omega} = \cup_h \mathcal{T}_h$.

    b) If $\mathcal{T}_{h_i} \cap \mathcal{T}_{h_j}$ consists of exactly one point, then it is a common vertex of $\mathcal{T}_{h_i}$ and $\mathcal{T}_{h_j}$.

    c) If for $i \neq j$, $\mathcal{T}_{h_i} \cap \mathcal{T}_{h_j}$ consists of more than one point, then $\mathcal{T}_{h_i} \cap \mathcal{T}_{h_j}$ is a common edge of $\mathcal{T}_{h_i}$ and $\mathcal{T}_{h_j}$.

  2. A family of partitions $\mathcal{T} = \{\mathcal{T}_h\}_h$ is called <u>shape regular</u> provided that there exists a positive constant $\kappa > 0$ such that every $\mathcal{T}_h \in \mathcal{T}$ contains a circle of radius $\rho_{\mathcal{T}}$ with

$$\rho_{\mathcal{T}} \geq \frac{h_{\mathcal{T}}}{\kappa}$$

  where $h_{\mathcal{T}}$ is half the diameter of $\mathcal{T}_h$.

3. *A family of partitions $\mathcal{T} = \{\mathcal{T}_h\}_h$ is called <u>uniform</u> provided that there exists a positive constant $\kappa > 0$ such that every $\mathcal{T}_h \in \mathcal{T}$ contains a circle of radius $\rho_\mathcal{T}$ with*

$$\rho_\mathcal{T} \geq \frac{h}{\kappa}.$$

Let $\{\phi_i\}_{1 \leq i \leq N}$ be piecewise linear nodal basis functions for $\mathcal{T}$, such that $\phi_i(x_j) = \delta_{ij}$, where δ_{ij} is a Kronecker delta function. The vector-valued finite element space F^h is defined by

$$F^h = \{\mathbf{w}^h \mid \mathbf{w}^h(x) = \sum_{i=1}^{N} \mathbf{w}_i^h \phi_i(x), \ \mathbf{w}_i^h \in \mathbb{R}^3\}.$$

Because of the nonconvex constraint, we consider a submanifold M^h of F^h defined by

$$M^h = \{\mathbf{m}^h \in F^h \mid \mathbf{m}^h(x) = \sum_{i=1}^{N} \mathbf{m}_i^h \phi_i(x), \ |\mathbf{m}_i^h| = 1\},$$

where the discrete magnetization $\mathbf{m}^h$ belongs to M^h. Moreover, we define the nodal interpolation operator $I_h : C^0(\Omega, \mathbb{R}^3) \to F^h$ by

$$I_h(\mathbf{m}) = \sum_{i=1}^{N} \mathbf{m}(x_i) \phi_i(x). \tag{4.3}$$

We make some additional assumptions for our finite element method: There exist some positive constants C_1, C_2, C_3, C_4 such that

$$
\begin{aligned}
C_1 h^d &\leq b_i = \int_\Omega \phi_i \leq C_2 h^d, \\
|M_{ij}| &= \left| \int_\Omega \phi_i \phi_j \right| \leq C_3 h^d, \\
\left| \frac{\partial \phi_i}{\partial x_l} \right| &\leq \frac{C_4}{h} \\
\int_\Omega &\nabla \phi_i \cdot \nabla \phi_j \leq 0, \quad \text{for } i \neq j,
\end{aligned}
\tag{4.4}
$$

for all $h > 0$, $i, j = 1, \ldots, N$ and $l = 1, \ldots, d$.

4.2 The finite element scheme, the main algorithm, and the main theorem

We consider the simple case with the effective field $\mathbf{h}$ containing only the exchange energy term, i.e. $\mathbf{h} = \eta \triangle \mathbf{m}$ from (1.9), to illustrate how we obtain Algorithm 2 below. The weak

form of the Landau-Lifshitz equation with $\mathbf{h} = \eta \triangle \mathbf{m}$ is

$$
\int_{\Omega_T} \frac{\partial \mathbf{m}}{\partial t} \cdot \mathbf{w} = \eta \sum_{l=1}^{d} \int_{\Omega_T} \left(\mathbf{m} \times \frac{\partial \mathbf{m}}{\partial x_l} \right) \cdot \frac{\partial \mathbf{w}}{\partial x_l}
$$

$$
- \alpha\eta \sum_{l=1}^{d} \int_{\Omega_T} \frac{\partial \mathbf{m}}{\partial x_l} \cdot \frac{\partial \mathbf{w}}{\partial x_l} + \alpha\eta \sum_{l=1}^{d} \int_{\Omega_T} \left(\frac{\partial \mathbf{m}}{\partial x_l} \cdot \frac{\partial \mathbf{m}}{\partial x_l} \right) (\mathbf{m} \cdot \mathbf{w}). \tag{4.5}
$$

Taking this weak form as a hint, we would like to find $\mathbf{v} = \sum_{j=1}^{N} \mathbf{v}_j \phi_j \in F^h$ such that

$$
\int_{\Omega} \sum_{j=1}^{N} \mathbf{v}_j \phi_j \cdot \mathbf{w}_i \phi_i = \eta \sum_{l=1}^{d} \sum_{j=1}^{N} \int_{\Omega} \left(\mathbf{m}_i \times \mathbf{m}_j \frac{\partial \phi_j}{\partial x_l} \right) \cdot \left(\frac{\partial \phi_i}{\partial x_l} \mathbf{w}_i \right)
$$

$$
- \alpha\eta \sum_{l=1}^{d} \sum_{j=1}^{N} \int_{\Omega} \left(\mathbf{m}_j \frac{\partial \phi_j}{\partial x_l} \right) \cdot \left(\mathbf{w}_i \frac{\partial \phi_i}{\partial x_l} \right) + \alpha\eta \sum_{l=1}^{d} \sum_{j=1}^{N} \int_{\Omega} \left(\frac{\partial \phi_j}{\partial x_l} \mathbf{m}_j \cdot \mathbf{m}_i \right) \left(\mathbf{m}_i \cdot \mathbf{w}_i \frac{\partial \phi_i}{\partial x_l} \right)
$$
$$\tag{4.6}$$

for $i = 1, \ldots, N$, where $\mathbf{m} = \sum_{j=1}^{N} \mathbf{m}_j \phi_j(x) \in M^h$, $\mathbf{w} \in (C^\infty(\Omega))^3$ and $\mathbf{w}_i = I_h(\mathbf{w})(x_i) = \mathbf{w}(x_i)$. Then, with $\mathbf{w}_i$ as $(1, 0, 0)$, $(0, 1, 0)$ or $(0, 0, 1)$ in equation (4.6), we obtain

$$
(\mathbf{M}\mathbf{v})_i = \eta \, \mathbf{m}_i \times (\mathbf{A}\mathbf{m})_i + \alpha\eta \, \mathbf{m}_i \times (\mathbf{m}_i \times (\mathbf{A}\mathbf{m})_i) \tag{4.7}
$$

for $i = 1, \ldots, N$, where $\mathbf{M} = \begin{bmatrix} M & 0 & 0 \\ 0 & M & 0 \\ 0 & 0 & M \end{bmatrix}$ and $\mathbf{A} = \begin{bmatrix} A & 0 & 0 \\ 0 & A & 0 \\ 0 & 0 & A \end{bmatrix}$ are $3N \times 3N$ block diagonal matrices with each block M and A a mass or stiffness matrix, i.e. $M_{ij} = \int_\Omega \phi_i \, \phi_j$, and $A_{ij} = \sum_{l=1}^{d} \int_\Omega \frac{\partial \phi_i}{\partial x_l} \frac{\partial \phi_j}{\partial x_l}$. Note that $\mathbf{m}_i \cdot (\mathbf{M}\mathbf{v})_i = 0$, so approximating $\mathbf{v}$ by $\hat{\mathbf{v}} = \frac{\mathbf{M}\mathbf{v}}{b}$ yields a tangent vector to the constraint manifold M^h, where $b_i = \int_\Omega \phi_i$. The left-hand side of (4.7) is then $b_i \hat{\mathbf{v}}_i$ which is a mass-lumping approximation. This suggests Algorithm 2 below.

Next we define the time-interpolated magnetization and velocity as in [7]:

Definition 3. *For $(x, t) \in \Omega \times [jk, (j+1)k) \subset \Omega \times [0, T)$, where $T = Jk$, define*

$$
\mathbf{m}^{h,k}(x, t) = \mathbf{m}^j(x),
$$
$$
\bar{\mathbf{m}}^{h,k}(x, t) = \frac{t - jk}{k} \mathbf{m}^{j+1}(x) + \frac{(j+1)k - t}{k} \mathbf{m}^j(x),
$$
$$
\hat{\mathbf{v}}^{h,k}(x, t) = \hat{\mathbf{v}}^j(x),
$$
$$
\mathbf{v}^{h,k}(x, t) = \mathbf{v}^j(x).
$$

The main theoretical result of this chapter is the following theorem, which is proved in section 4.4.

Theorem 2. *Let $\mathbf{m}_0 \in H^1(\Omega, \mathbb{S}^2)$ and suppose $\mathbf{m}_0^h \to \mathbf{m}_0$ in $H^1(\Omega)$ as $h \to 0$. Let $\theta \in [0, 1]$, and for $0 \le \theta < \frac{1}{2}$, assume that $\frac{k}{h^2} \le C_0$, for some $C_0 > 0$. If the triangulation $\mathcal{T} = \{\mathcal{T}_h\}_h$ satisfies condition (4.4), then the sequence $\{\mathbf{m}^{h,k}\}$, constructed by Algorithm 2 and definition 3, has a subsequence that converges weakly to a weak solution of the Landau-Lifshitz equation.*

Algorithm 2 The mass-lumped finite element method

Set an initial discrete magnetization $\mathbf{m}^0$ at the nodes of the finite element mesh described in section 4.1 above.

For $j = 0, \ldots, J$,

a. compute a velocity vector $\hat{\mathbf{v}}_i^j$ at each node by

$$
\begin{aligned}
\hat{\mathbf{v}}_i^j = \frac{(\mathbf{M}\mathbf{v}^j)_i}{b_i} = {} & \frac{\eta\, \mathbf{m}_i^j \times (\mathbf{Am} + \theta k \mathbf{A}\hat{\mathbf{v}})_i^j + \alpha\eta\, \mathbf{m}_i^j \times (\mathbf{m}_i^j \times (\mathbf{Am} + \theta k \mathbf{A}\hat{\mathbf{v}})_i^j)}{b_i} \\
& - \frac{\mathbf{m}_i^j \times (\mathbf{M}\bar{\mathbf{h}}(\mathbf{m}) + \theta k \mathbf{M}\bar{\mathbf{h}}(\hat{\mathbf{v}}))_i^j + \alpha\mathbf{m}_i^j \times (\mathbf{m}_i^j \times (\mathbf{M}\bar{\mathbf{h}}(\mathbf{m}) + \theta k \mathbf{M}\bar{\mathbf{h}}(\hat{\mathbf{v}}))_i^j)}{b_i}.
\end{aligned}
\tag{4.8}
$$

for $\theta \in [0,1]$ and for $i = 1, \ldots, N$.

b. Compute $\mathbf{m}_i^{j+1} = \frac{\mathbf{m}_i^j + k\hat{\mathbf{v}}_i^j}{|\mathbf{m}_i^j + k\hat{\mathbf{v}}_i^j|}$ for $i = 1, \ldots, N$.

4.3 Numerical Results

Before giving a proof for Theorem 2, we demonstrate the effectiveness of the scheme on a test problem. We conduct a numerical test for the Landau-Lifshitz equation (1.8) with effective field involving only the exchange energy term, i.e. $\mathbf{h} = \Delta\mathbf{m}$ in equation (1.9), on the unit square with periodic boundary conditions. This corresponds to setting $\eta = 1$ and $\bar{\mathbf{h}} = 0$ in equation (4.8) in Algorithm 2. For the convergence study, we used an explicit method ($\theta = 0$) and an implicit method ($\theta = 0.5$) on a structured and unstructured mesh. The unstructured mesh was generated using DistMesh [68], with an example shown in Figure 4.1. The L^∞ and L^2 errors were measured relative to an exact solution of the Landau-Lifshitz equation with $\mathbf{h} = \Delta\mathbf{m}$ from [38], namely

$$
\begin{aligned}
\mathbf{m}^x(x_1, x_2, t) &= \frac{1}{d(t)} \sin\beta \cos(k(x_1 + x_2) + g(t)), \\
\mathbf{m}^y(x_1, x_2, t) &= \frac{1}{d(t)} \sin\beta \sin(k(x_1 + x_2) + g(t)), \\
\mathbf{m}^z(x_1, x_2, t) &= \frac{1}{d(t)} e^{2k^2\alpha t} \cos\beta.
\end{aligned}
\tag{4.9}
$$

Here $\beta = \frac{\pi}{24}$, $k = 2\pi$, $d(t) = \sqrt{\sin^2\beta + e^{4k^2\alpha t}\cos^2\beta}$ and $g(t) = \frac{1}{\alpha}\log\left(\frac{d(t) + e^{2k^2\alpha t}\cos\beta}{1 + \cos\beta}\right)$. These exact solutions were used in sections 2.5.1 and 3.2.1 for the numerical tests. The numerical results are summarized in the Tables 4.1 and 4.2. Figure 4.2 shows the convergence rate of the method, which is first order in the time step k and second order in the mesh size h.
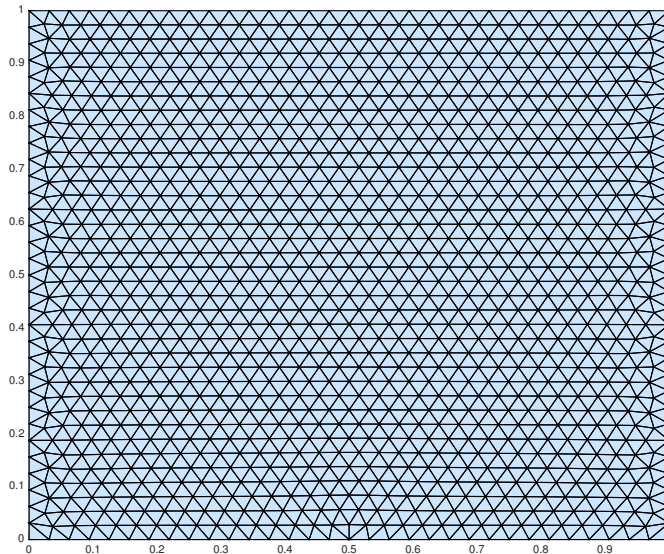
Figure 4.1: Unstructured mesh, with $h = 1/32$.

	structured mesh		unstructured mesh	
$\frac{1}{h}$	$\|\|\mathbf{m} - \mathbf{m}^h\|\|_{L^\infty}$	$\|\|\mathbf{m} - \mathbf{m}^h\|\|_{L^2}$	$\|\|\mathbf{m} - \mathbf{m}^h\|\|_{L^\infty}$	$\|\|\mathbf{m} - \mathbf{m}^h\|\|_{L^2}$
32	8.22e-05	7.40e-04	9.93e-04	1.11e-03
64	2.06e-05	1.85e-04	2.09e-04	2.75e-04
128	5.15e-06	4.63e-05	5.18e-05	6.88e-05
256	1.29e-06	1.16e-05	1.60e-05	1.73e-05
Slope	2.00	2.00	2.04	2.00

Table 4.1: **Explicit method** ($\theta = 0$) : L^∞ and L^2 error and convergence rates on a structured and unstructured mesh with spatial step h, time step $k = 8 \cdot 10^{-7} h^2$ and time 0.001.

4.3.1   Going beyond first order in time

In this section, we propose a method which is second order in time, by replacing the nonlinear projection step 2 (b) in Algorithm 2 by a linear projection step, and test the convergence order. In Algorithm 2, step 2 (a) can be viewed as the predictor step and 2 (b) as the corrector step. The corrector step was used to conserve the length of the magnetization at each node. By replacing this nonlinear projection by a linear projection step, it not only preserves the length of the magnetization at each node, but also makes the method higher order. Moreover, it has a similar complexity to the nonlinear projection step in that one
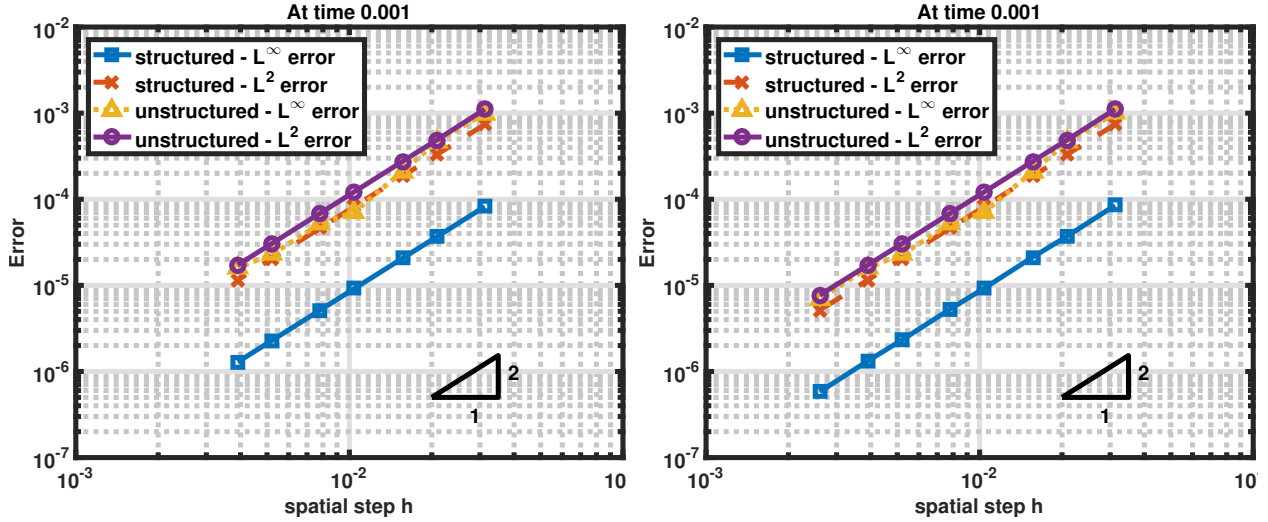
Figure 4.2: Convergence plot, Left : Explicit method, Right : Implicit method.

	structured mesh		unstructured mesh	
$\frac{1}{h}$	$\|\|\mathbf{m} - \mathbf{m}^h\|\|_{L^\infty}$	$\|\|\mathbf{m} - \mathbf{m}^h\|\|_{L^2}$	$\|\|\mathbf{m} - \mathbf{m}^h\|\|_{L^\infty}$	$\|\|\mathbf{m} - \mathbf{m}^h\|\|_{L^2}$
32	8.50e-05	7.40e-04	9.94e-04	1.11e-03
64	2.13e-05	1.85e-04	2.10e-04	2.75e-04
128	5.32e-06	4.63e-05	5.19e-05	6.88e-05
256	1.33e-06	1.16e-05	1.60e-05	1.73e-05
Slope	2.00	2.00	2.00	2.00

Table 4.2: **Implicit method** $(\theta = \frac{1}{2})$: L^∞ and L^2 error and convergence rates on structured and unstructured meshes, with spatial step h, time step $k = 0.02048h^2$ and time 0.001.

only needs to solve a 3×3 matrix equation for each node. We defer a rigorous analysis to future work and present here the modified algorithm and some convergence test results.

The length of the magnetization at each node is preserved, because by taking a dot product in (4.10) with $\frac{\mathbf{m}_i^{j+1}+\mathbf{m}_i^j}{2}$, we have $|\mathbf{m}_i^{j+1}|^2 = |\mathbf{m}_i^j|^2$. As before, we conduct a numerical test for the Landau-Lifshitz equation (1.8) with effective field involving only the exchange energy term, with $\mathbf{h} = \Delta\mathbf{m}$ in equation (1.9), on the unit square with periodic boundary conditions, to compare the two algorithms. For the convergence study, we used an implicit method ($\theta = 0.5$) on a structured and unstructured mesh. One of the unstructured meshes was shown in Figure 4.1. The L^2 errors are measured relative to the analytical solution (4.9) for the Landau-Lifshitz equation with $\mathbf{h} = \Delta\mathbf{m}$. The numerical results are summarized in the Table 4.3. Figure 4.3 shows the convergence rates of the methods, which shows first order in k for Algorithm 2 and second order convergence for Algorithm 3.

Algorithm 3 Modified mass-lumped finite element method

For a given time $\bar{T} > 0$, set $J = [\frac{\bar{T}}{k}]$.

Set an initial discrete magnetization $\mathbf{m}^0$ at the nodes of the finite element mesh described in section 4.1 above.

For $j = 0, \ldots, J$,

a. compute an intermediate magnetization vector $\mathbf{m}_i^*$ at each node by

$$
\begin{aligned}
\frac{\mathbf{m}_i^* - \mathbf{m}_i^j}{k} &= \hat{\mathbf{v}}_i^j = \frac{(\mathbf{Mv}^j)_i}{b_i} \\
&= \frac{\eta\, \mathbf{m}_i^j \times (\mathbf{Am} + \theta k \mathbf{A}\hat{\mathbf{v}})_i^j + \alpha\eta\, \mathbf{m}_i^j \times (\mathbf{m}_i^j \times (\mathbf{Am} + \theta k \mathbf{A}\hat{\mathbf{v}})_i^j)}{b_i} \\
&\quad - \frac{\mathbf{m}_i^j \times (\mathbf{M\bar{h}}(\mathbf{m}) + \theta k \mathbf{M\bar{h}}(\hat{\mathbf{v}}))_i^j + \alpha\mathbf{m}_i^j \times (\mathbf{m}_i^j \times (\mathbf{M\bar{h}}(\mathbf{m}) + \theta k \mathbf{M\bar{h}}(\hat{\mathbf{v}}))_i^j)}{b_i}
\end{aligned}
$$

for $\theta \in [0, 1]$ and for $i = 1, \ldots, N$.

b. Compute $\mathbf{m}_i^{j+1}$

$$
\begin{aligned}
\frac{\mathbf{m}_i^{j+1} - \mathbf{m}_i^j}{k} &= \\
&= \frac{\eta\, \frac{\mathbf{m}_i^{j+1} + \mathbf{m}_i^j}{2} \times (\mathbf{Am}_i^{j+1/2}) + \alpha\eta\, \frac{\mathbf{m}_i^{j+1} + \mathbf{m}_i^j}{2} \times (\mathbf{m}_i^{j+1/2} \times (\mathbf{Am}_i^{j+1/2}))}{b_i} \\
&\quad - \frac{\frac{\mathbf{m}_i^{j+1} + \mathbf{m}_i^j}{2} \times \mathbf{M\bar{h}}(\mathbf{m}_i^{j+1/2}) + \alpha\frac{\mathbf{m}_i^{j+1} + \mathbf{m}_i^j}{2} \times (\mathbf{m}_i^{j+1/2} \times (\mathbf{M\bar{h}}(\mathbf{m}_i^{j+1/2})))}{b_i}
\end{aligned}
\tag{4.10}
$$

where $\mathbf{m}_i^{j+1/2} = \frac{\mathbf{m}_i^j + \mathbf{m}_i^*}{2}$ for $i = 1, \ldots, N$.

4.4   Proof of Theorem 2

In this section, we present the proof of the theorem, which states that the sequence $\{\mathbf{m}^{h,k}\}$, constructed by Algorithm 2 and Definition 3, has a subsequence that converges weakly to a weak solution $\mathbf{m}$ of the Landau-Lifshitz-Gilbert equation under some conditions. That is, we show that the limit $\mathbf{m}$ satisfies Definition 1. In section 4.4.1, we derive a discretization of the weak form of the Landau-Lifshitz-Gilbert equation satisfied by the $\{\mathbf{m}^{h,k}\}$, namely (4.13). In section 4.4.2, we derive energy estimates to show that the sequences $\mathbf{m}^{h,k}$, $\bar{\mathbf{m}}^{h,k}$ converge to $\mathbf{m}$ and $\hat{\mathbf{v}}^{h,k}$ converges to $\frac{\partial \mathbf{m}}{\partial t}$ in a certain sense made precise in section 4.4.3. In section 4.4.4, we show that each term of the discretization of the weak form converges to the appropriate limit, so that the limit $\mathbf{m}$ satisfies the weak form of the Landau-Lifshitz-Gilbert equation. In section 4.4.5, we show that the limit $\mathbf{m}$ satisfies the energy inequality (4.2) in Definition 1 (iv). Finally, in section 4.4.6, we establish that the magnitude of $\mathbf{m}$ is 1 a.e. in
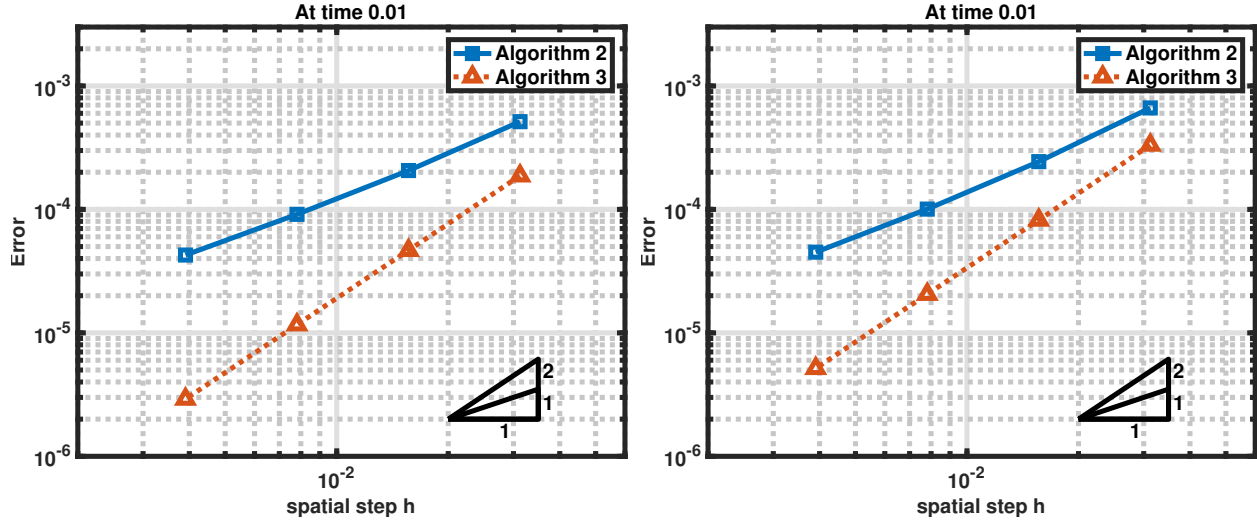
Figure 4.3: Convergence plot, Left : Structured mesh, Right : Unstructured mesh.

$\frac{1}{h}$	Structured mesh				Unstructured mesh			
	Alg. 2	rate	Alg. 3	rate	Alg. 2	rate	Alg. 3	rate
32	5.14e-04	1.32	1.87e-04	2.01	6.64e-04	1.44	3.32e-04	2.02
64	2.06e-04	1.18	4.66e-05	2.00	2.44e-04	1.28	8.21e-05	2.00
128	9.12e-05	1.10	1.16e-05	2.00	1.01e-04	1.16	2.06e-05	2.00
256	4.27e-05		2.91e-06		4.51e-05		5.16e-06	

Table 4.3: **Implicit method** $(\theta = \frac{1}{2})$: L^2 error and convergence rates on structured and unstructured meshes, with spatial step h, time step $k = 0.04h$ and time 0.01.

Ω_T.

4.4.1 Equations that $\mathbf{m}^{h,k}$ and $\mathbf{v}^{h,k}$ satisfy

In this section, we derive a discretization of the weak form of the Landau-Lifshitz-Gilbert equation. This form is easier to use for the proof of Theorem 2, since it does not involve the product of weakly convergent sequences. In general, a product of weakly convergent sequences is not weakly convergent. It is convergent only in some certain cases, such as when the sequences satisfy the hypothesis of the div-curl lemma [82, 28].

The generalized version of equation (4.6), including all the terms in the effective field $\mathbf{h}$

in (1.9) and with $0 \le \theta \le 1$ is

$$
\begin{aligned}
\int_\Omega \mathbf{v}^{h,k} \cdot \mathbf{w}^h = {} & \eta \sum_{l,i} \int_\Omega \left(\left(\mathbf{m}_i^{h,k} \times \frac{\partial(\mathbf{m}^{h,k} + \theta k \hat{\mathbf{v}}^{h,k})}{\partial x_l} \right) \cdot \mathbf{w}_i^h \right) \frac{\partial \phi_i}{\partial x_l} \\
& - \alpha\eta \sum_{l,i} \int_\Omega \left(\frac{\partial(\mathbf{m}^{h,k} + \theta k \hat{\mathbf{v}}^{h,k})}{\partial x_l} \cdot \mathbf{w}_i^h \right) \frac{\partial \phi_i}{\partial x_l} \\
& + \alpha\eta \sum_{l,i} \int_\Omega \left(\frac{\partial(\mathbf{m}^{h,k} + \theta k \hat{\mathbf{v}}^{h,k})}{\partial x_l} \cdot \mathbf{m}_i^{h,k} \right) (\mathbf{m}_i^{h,k} \cdot \mathbf{w}_i^h) \frac{\partial \phi_i}{\partial x_l} \\
& - \sum_i \int_\Omega (\mathbf{m}_i^{h,k} \times \bar{\mathbf{h}}(\mathbf{m}^{h,k} + \theta k \hat{\mathbf{v}}^{h,k})) \cdot \phi_i \mathbf{w}_i^h \\
& + \alpha \sum_i \int_\Omega \bar{\mathbf{h}}(\mathbf{m}^{h,k} + \theta k \hat{\mathbf{v}}^{h,k}) \cdot \phi_i \mathbf{w}_i^h \\
& - \alpha \sum_i \int_\Omega (\bar{\mathbf{h}}(\mathbf{m}^{h,k} + \theta k \hat{\mathbf{v}}^{h,k}) \cdot \mathbf{m}_i)(\mathbf{m}_i \cdot \mathbf{w}_i^h \phi_i).
\end{aligned}
\tag{4.11}
$$

In fact, by taking $\mathbf{w}_i^h$ as $(1,0,0), (0,1,0)$ and $(0,0,1)$ in (4.11), we get (4.8) in Algorithm 2. Setting $\mathbf{w}^h = \sum_{j=1}^{N} (\mathbf{m}_j^{h,k} \times \mathbf{u}_j^h) \phi_j$ in (4.11), we have

$$
\begin{aligned}
- \sum_i \int_\Omega (\mathbf{m}_i^{h,k} \times \mathbf{v}^{h,k}) \cdot \mathbf{u}_i^h \phi_i = {} & \eta \sum_l \int_\Omega \frac{\partial(\mathbf{m}^{h,k} + \theta k \hat{\mathbf{v}}^{h,k})}{\partial x_l} \cdot \frac{\partial \mathbf{u}^h}{\partial x_l} \\
& - \eta \sum_{l,i} \int_\Omega \left(\frac{\partial(\mathbf{m}^{h,k} + \theta k \hat{\mathbf{v}}^{h,k})}{\partial x_l} \cdot \mathbf{m}_i^{h,k} \right) (\mathbf{m}_i^{h,k} \cdot \mathbf{u}_i^h) \frac{\partial \phi_i}{\partial x_l} \\
& + \alpha\eta \sum_{l,i} \int_\Omega \left(\left(\mathbf{m}_i^{h,k} \times \frac{\partial(\mathbf{m}^{h,k} + \theta k \hat{\mathbf{v}}^{h,k})}{\partial x_l} \right) \cdot \mathbf{u}_i^h \right) \frac{\partial \phi_i}{\partial x_l} \\
& - \sum_i \int_\Omega (\bar{\mathbf{h}}(\mathbf{m}^{h,k} + \theta k \hat{\mathbf{v}}^{h,k})) \cdot \phi_i \mathbf{u}_i^h \\
& + \sum_i \int_\Omega (\bar{\mathbf{h}}(\mathbf{m}^{h,k} + \theta k \hat{\mathbf{v}}^{h,k}) \cdot \mathbf{m}_i^{h,k}) (\mathbf{m}_i^{h,k} \cdot \mathbf{u}_i^h) \phi_i \\
& - \alpha \sum_i \int_\Omega (\mathbf{m}_i^{h,k} \times \bar{\mathbf{h}}(\mathbf{m}^{h,k} + \theta k \hat{\mathbf{v}}^{h,k})) \cdot \mathbf{u}_i^h \phi_i.
\end{aligned}
\tag{4.12}
$$

Equations (4.11) and (4.12) have terms that contain the product of weakly convergent sequences, namely the third term of the right hand side of (4.11), and the second term of the right hand side of (4.12), $\alpha\eta \sum_{l,i} \int_\Omega \left(\frac{\partial(\mathbf{m}^{h,k}+\theta k \hat{\mathbf{v}}^{h,k})}{\partial x_l} \cdot \mathbf{m}_i^{h,k} \right) (\mathbf{m}_i^{h,k} \cdot \mathbf{w}_i^h) \frac{\partial \phi_i}{\partial x_l}$. By adding α times

equation (4.12) to equation (4.11), we eliminate the terms that contain such products :

$$
\int_\Omega \left[\mathbf{v}^{h,k} \cdot \mathbf{w}^h - \alpha \sum_i (\mathbf{m}_i^{h,k} \times \mathbf{v}^{h,k}) \cdot (\mathbf{w}_i^h \phi_i) \right]
$$

$$
= (1 + \alpha^2) \left[\eta \sum_{l,i} \int_\Omega \left[\left(\mathbf{m}_i^{h,k} \times \frac{\partial \mathbf{m}}{\partial x_l}^{h,k} \right) \cdot \left(\mathbf{w}_i^h \frac{\partial \phi_i}{\partial x_l} \right) + \theta k \left(\mathbf{m}_i^{h,k} \times \frac{\partial \hat{\mathbf{v}}}{\partial x_l}^{h,k} \right) \cdot \left(\mathbf{w}_i^h \frac{\partial \phi_i}{\partial x_l} \right) \right] \right.
$$

$$
\left. - \sum_i \int_\Omega \left[(\mathbf{m}_i^{h,k} \times \bar{\mathbf{h}}(\mathbf{m}^{h,k})) \cdot (\mathbf{w}_i^h \phi_i) + \theta k (\mathbf{m}_i^{h,k} \times \bar{\mathbf{h}}(\hat{\mathbf{v}}^{h,k})) \cdot (\mathbf{w}_i^h \phi_i) \right] \right].
$$

$$(4.13)$$

This is a similar procedure to subtracting α times the following equation

$$
\mathbf{m} \times \frac{\partial \mathbf{m}}{\partial t} = -\mathbf{m} \times (\mathbf{m} \times \mathbf{h}) + \alpha \mathbf{m} \times \mathbf{h} \tag{4.14}
$$

from the Landau-Lifshitz equation (1.8) to get the Landau-Lifshitz-Gilbert equation (1.12). Here, equation (4.14) is obtained by taking $\mathbf{m} \times$ the Landau-Lifshitz equation (1.8).

4.4.2 Energy inequality

In this section, we derive the energy inequalities we will need to prove Theorem 2, namely (4.27) for $0 \le \theta < \frac{1}{2}$ and (4.28) for $\frac{1}{2} \le \theta \le 1$. We will use Theorem 1 from [7], which states that the exchange energy is decreased after renormalization. This result goes back to [10, 12, 7] :

Theorem 3. *For the P^1 approximation in $\Omega \subset \mathbb{R}^2$, if*

$$
\int_\Omega \nabla \phi_i \cdot \nabla \phi_j \le 0, \quad \text{for } i \ne j, \tag{4.15}
$$

then for all $\mathbf{w} = \sum_{i=1}^N \mathbf{w}_i \phi_i \in F^h$ such that $|\mathbf{w}_i| \ge 1$ for $i = 1, \ldots, N$, we have

$$
\int_\Omega \left| \nabla I_h \left(\frac{\mathbf{w}}{|\mathbf{w}|} \right) \right|^2 \le \int_\Omega |\nabla \mathbf{w}|^2. \tag{4.16}
$$

In 3D, (4.16) holds if an additional condition that all dihedral angles of the tetrahedra of the mesh are smaller than $\frac{\pi}{2}$ is satisfied, along with (4.15); see [86, 7]. Also, we will use inequality (14) of [7],

$$
\left\| \bar{\mathbf{h}}(\mathbf{m}) \right\|_{L^2} \le C_5 \left\| \mathbf{m} \right\|_{L^2} + C_5, \tag{4.17}
$$

and equation (25) from [9],

$$
\left\| \mathbf{h}_s(\mathbf{m}) \right\|_{L^2} \le C_5 \left\| \mathbf{m} \right\|_{L^2}, \tag{4.18}
$$

where C_5 is a positive constant, depending only on Ω. Furthermore, we will use an inequality (20) of [7] in the proof, which states there exists $C_6 > 0$ such that for all $1 \leq p < \infty$ and all $\phi_h \in F^h$, we have

$$\frac{1}{C_6} \|\phi_h\|_{L^p}^p \leq h^d \sum_{i=1}^{N} |\phi_h(x_i)|^p \leq C_6 \|\phi_h\|_{L^p}^p .$$ (4.19)

Moreover, we will assume that there exists $C_7 > 0$ such that

$$\int_{\Omega} |\nabla \mathbf{v}^h|^2 \leq \frac{C_7}{h^2} \int_{\Omega} |\mathbf{v}^h|^2$$ (4.20)

for all $\mathbf{v}^h \in F^h$.

Taking $\mathbf{w}^h = \sum_{j=1}^{N} (\mathbf{m}_j^{h,k} \times \mathbf{u}_j^h) \, \phi_j$ in (4.13), and setting $\mathbf{u}^h = \hat{\mathbf{v}}^{h,k}$, we have

$$-\alpha \sum_i \int_{\Omega} \mathbf{v}_i^{h,k} \cdot \hat{\mathbf{v}}_i \phi_i = (1+\alpha^2)\Bigg[\eta \sum_{l,i} \int_{\Omega} \Bigg[\left(\frac{\partial \mathbf{m}^{h,k}}{\partial x_l} \cdot \frac{\partial \phi_i}{\partial x_l} \hat{\mathbf{v}}_i \right) + \theta k \left(\frac{\partial \hat{\mathbf{v}}^{h,k}}{\partial x_l} \cdot \frac{\partial \phi_i}{\partial x_l} \hat{\mathbf{v}}_i \right) \Bigg]$$
$$- \sum_i \int_{\Omega} \Big[(\bar{\mathbf{h}}(\mathbf{m}^{h,k}) \cdot \hat{\mathbf{v}}_i)\phi_i + \theta k(\bar{\mathbf{h}}(\hat{\mathbf{v}}^{h,k}) \cdot \hat{\mathbf{v}}_i)\phi_i \Big]\Bigg]$$ (4.21)

where we have used the fact $\mathbf{m}_i^{h,k} \cdot \hat{\mathbf{v}}_i^{h,k} = 0$ for $i = 1, \ldots, N$. This equation can be written as

$$(\nabla \mathbf{m}, \nabla \hat{\mathbf{v}}) = -\theta k \|\nabla \hat{\mathbf{v}}\|_{L^2}^2 - \frac{\alpha}{1+\alpha^2} \frac{1}{\eta} \sum_i \frac{|(\mathbf{M}\mathbf{v})_j|^2}{b_j} + \frac{1}{\eta}(\bar{\mathbf{h}}(\mathbf{m}), \hat{\mathbf{v}}) + \frac{\theta k}{\eta}(\bar{\mathbf{h}}(\hat{\mathbf{v}}), \hat{\mathbf{v}}).$$ (4.22)

We now derive an energy estimate. We have

$$\frac{1}{2} \|\nabla \mathbf{m}^{j+1}\|_{L^2}^2 \leq \frac{1}{2} \|\nabla \mathbf{m}^j + k\nabla \hat{\mathbf{v}}^j\|_{L^2}^2 = \frac{1}{2} \|\nabla \mathbf{m}^j\|_{L^2}^2 + k(\nabla \mathbf{m}^j, \nabla \hat{\mathbf{v}}^j) + \frac{1}{2} k^2 \|\nabla \hat{\mathbf{v}}^j\|_{L^2}^2$$
$$\leq \frac{1}{2} \|\nabla \mathbf{m}^j\|_{L^2}^2 - k \left(\frac{\alpha}{1+\alpha^2}\right) \frac{1}{\eta} \sum_i \frac{|(\mathbf{M}\mathbf{v})_i^j|^2}{b_i^2} b_i + \frac{1}{2} k^2 \|\nabla \hat{\mathbf{v}}^j\|_{L^2}^2 - \theta k^2 \|\nabla \hat{\mathbf{v}}^j\|_{L^2}^2$$
$$+ \frac{k}{\eta}(\bar{\mathbf{h}}(\mathbf{m}^j), \hat{\mathbf{v}}^j) + \theta \frac{k^2}{\eta}(\bar{\mathbf{h}}(\hat{\mathbf{v}}^j), \hat{\mathbf{v}}^j)$$
$$\leq \frac{1}{2} \|\nabla \mathbf{m}^j\|_{L^2}^2 - k \left(\frac{\alpha}{1+\alpha^2}\right) \frac{1}{\eta} \frac{C_1}{C_6} \|\hat{\mathbf{v}}^j\|_{L^2}^2 - \left(\theta - \frac{1}{2}\right) k^2 \|\nabla \hat{\mathbf{v}}^j\|_{L^2}^2 + \frac{k}{\eta}(\bar{\mathbf{h}}(\mathbf{m}^j), \hat{\mathbf{v}}^j)$$
$$+ \theta \frac{k^2}{\eta}(\bar{\mathbf{h}}_e, \hat{\mathbf{v}}^j)$$ (4.23)

where the first inequality is obtained by Theorem 3, the second inequality by equation (4.22), and the last inequality by the fact $(\mathbf{h}_s(\hat{\mathbf{v}}^j), \hat{\mathbf{v}}^j) < 0$. We have the estimate for the last two terms of the above inequality :

$$\left|(\bar{\mathbf{h}}(\mathbf{m}^j) + \theta k\bar{\mathbf{h}}_e, \hat{\mathbf{v}}^j)\right| \leq \|\bar{\mathbf{h}}(\mathbf{m}^j) + \theta k\bar{\mathbf{h}}_e\|_{L^2} \|\hat{\mathbf{v}}^j\|_{L^2} \leq C_8 \|\hat{\mathbf{v}}^j\|_{L^2} \leq \epsilon \|\hat{\mathbf{v}}^j\|_{L^2}^2 + \frac{1}{4\epsilon}C_8^2$$ (4.24)

for some $C_8 > 0$, where the second inequality is obtained by equation (4.17) and the last
inequality by Young's inequality with $\epsilon = \frac{1}{2}\frac{\alpha}{1+\alpha^2}\frac{C_1}{C_6}$. Summing the inequality (4.23) from
$j = 0, \ldots, J - 1$ and using (4.24), we get

$$
\frac{1}{2}\left\|\nabla\mathbf{m}^J\right\|_{L^2}^2 + k\left(\frac{1}{2\eta}\left(\frac{\alpha}{1+\alpha^2}\right)\frac{C_1}{C_6} - C_7\left(\frac{1}{2}-\theta\right)\frac{k}{h^2}\right)\sum_{j=0}^{J-1}\left\|\hat{\mathbf{v}}^j\right\|_{L^2}^2 \le \frac{1}{2}\left\|\nabla\mathbf{m}^0\right\|_{L^2}^2 + C_9 T
\tag{4.25}
$$

with $\frac{k}{h^2} \le C_0 < \frac{1}{2}\frac{\alpha}{1+\alpha^2}\frac{C_1}{C_6}\frac{1}{C_7\eta}$, for $0 \le \theta < \frac{1}{2}$, and

$$
\frac{1}{2}\left\|\nabla\mathbf{m}^J\right\|_{L^2}^2 + k\left(\frac{1}{2\eta}\left(\frac{\alpha}{1+\alpha^2}\right)\frac{C_1}{C_6}\right)\sum_{j=0}^{J-1}\left\|\hat{\mathbf{v}}^j\right\|_{L^2}^2 + \left(\theta - \frac{1}{2}\right)k^2\sum_{j=0}^{J-1}\left\|\nabla\hat{\mathbf{v}}^j\right\|_{L^2}^2
$$
$$
\le \frac{1}{2}\left\|\nabla\mathbf{m}^0\right\|_{L^2}^2 + C_9 T
\tag{4.26}
$$

for $\frac{1}{2} \le \theta \le 1$, and for some $C_9 > 0$.

In summary, we have the energy inequalities

$$
\frac{1}{2}\int_\Omega|\nabla\mathbf{m}^{h,k}(\cdot,T)|^2 + \left(\frac{1}{2\eta}\left(\frac{\alpha}{1+\alpha^2}\right)\frac{C_1}{C_6} - C_7 C_0\right)\int_{\Omega_T}|\hat{\mathbf{v}}^{h,k}|^2
$$
$$
\le \frac{1}{2}\int_\Omega|\nabla\mathbf{m}^{h,k}(\cdot,0)|^2 + C_9 T
\tag{4.27}
$$

with $C_0 < \frac{1}{2}\frac{\alpha}{1+\alpha^2}\frac{C_1}{C_6}\frac{1}{C_7\eta}$, for $0 \le \theta < \frac{1}{2}$ and

$$
\frac{1}{2}\int_\Omega\left|\nabla\mathbf{m}^{h,k}(\cdot,T)\right|^2 + \left(\frac{1}{2\eta}\left(\frac{\alpha}{1+\alpha^2}\right)\frac{C_1}{C_6}\right)\int_{\Omega_T}\left|\hat{\mathbf{v}}^{h,k}\right|^2
$$
$$
+ \left(\theta - \frac{1}{2}\right)k\int_{\Omega_T}\left|\nabla\hat{\mathbf{v}}^{h,k}\right|^2 \le \frac{1}{2}\int_\Omega\left|\nabla\mathbf{m}^{h,k}(\cdot,0)\right|^2 + C_9 T.
\tag{4.28}
$$

for $\frac{1}{2} \le \theta \le 1$.

4.4.3 Weak convergence of $\mathbf{m}^{h,k}$, $\bar{\mathbf{m}}^{h,k}$ and $\hat{\mathbf{v}}^{h,k}$

In this section, we show the weak convergence of $\bar{\mathbf{m}}^{h,k}$ and $\hat{\mathbf{v}}^{h,k}$ and strong convergence of
$\mathbf{m}^{h,k}$ in some sense, based on the energy estimates (4.27) and (4.28). We follow similar
arguments from section 6 of [9].

Since we have

$$
\left|\frac{\mathbf{m}_i^{j+1} - \mathbf{m}_i^j}{k}\right| \le \left|\hat{\mathbf{v}}_i^j\right|
\tag{4.29}
$$

for $i = 1, \ldots, N$ and $j = 0, \ldots, J - 1$, we have

$$
\left\|\frac{\partial\bar{\mathbf{m}}^{h,k}}{\partial t}\right\|_{L^2(\Omega)} = \left\|\frac{\mathbf{m}^{j+1} - \mathbf{m}^j}{k}\right\|_{L^2(\Omega)} \le C_6\left\|\hat{\mathbf{v}}^{h,k}\right\|_{L^2(\Omega)}.
\tag{4.30}
$$

Thus, we have

$$\left\| \frac{\partial \bar{\mathbf{m}}^{h,k}}{\partial t} \right\|_{L^2(\Omega_T)} = \left\| \frac{\mathbf{m}^{j+1} - \mathbf{m}^j}{k} \right\|_{L^2(\Omega_T)} \leq C_6 \left\| \hat{\mathbf{v}}^{h,k} \right\|_{L^2(\Omega_T)} \tag{4.31}$$

which is bounded by the energy inequalities, (4.27) for $0 \leq \theta < \frac{1}{2}$ and (4.28) for $\frac{1}{2} \leq \theta \leq 1$. Hence, $\bar{\mathbf{m}}^{h,k}$ is bounded in $H^1(\Omega_T)$ and $\hat{\mathbf{v}}^{h,k}$ is bounded in $L^2(\Omega_T)$ by (4.31) and by the energy inequalities, (4.27) for $0 \leq \theta < \frac{1}{2}$ and (4.28) for $\frac{1}{2} \leq \theta \leq 1$. Thus, by passing to subsequences, there exist $\mathbf{m} \in H^1(\Omega_T)$ and $\hat{\mathbf{v}} \in L^2(\Omega_T)$ such that

$$\begin{aligned} \bar{\mathbf{m}}^{h,k} &\to \mathbf{m} \text{ weakly in } H^1(\Omega_T), \\ \bar{\mathbf{m}}^{h,k} &\to \mathbf{m} \text{ strongly in } L^2(\Omega_T), \\ \hat{\mathbf{v}}^{h,k} &\to \hat{\mathbf{v}} \text{ weakly in } L^2(\Omega_T). \end{aligned} \tag{4.32}$$

Moreover, we have

$$\left| \mathbf{m}_i^{j+1} - \mathbf{m}_i^j - k\hat{\mathbf{v}}_i^j \right| = \left| \frac{\mathbf{m}_i^j + k\hat{\mathbf{v}}_i^j}{|\mathbf{m}_i^j + k\hat{\mathbf{v}}_i^j|} - \mathbf{m}_i^j - k\hat{\mathbf{v}}_i^j \right| = \left| 1 - |\mathbf{m}_i^j + k\hat{\mathbf{v}}_i^j| \right| \leq \frac{1}{2} k^2 \left| \hat{\mathbf{v}}_i^j \right|^2, \quad (4.33)$$

since $|\mathbf{m}_i^j + k\hat{\mathbf{v}}_i^j| = \sqrt{1 + k^2 |\hat{\mathbf{v}}_i^j|^2} \leq 1 + \frac{1}{2} k^2 |\hat{\mathbf{v}}_i^j|^2$, for $i = 1, \ldots, N$ and $j = 0, \ldots, J - 1$. Thus,

$$\left\| \frac{\partial \bar{\mathbf{m}}^{h,k}}{\partial t} - \hat{\mathbf{v}}^{h,k} \right\|_{L^1(\Omega_T)} \leq \frac{1}{2} k C_2 C_6 \left\| \hat{\mathbf{v}}^{h,k} \right\|_{L^2(\Omega_T)}^2 \tag{4.34}$$

which converges to 0 as $h, k \to 0$, so

$$\frac{\partial \mathbf{m}}{\partial t} = \hat{\mathbf{v}}. \tag{4.35}$$

Furthermore, since

$$\left\| \mathbf{m}^{h,k} - \bar{\mathbf{m}}^{h,k} \right\|_{L^2(\Omega_T)} = \left\| (t - jk) \frac{\mathbf{m}^{j+1} - \mathbf{m}^j}{k} \right\|_{L^2(\Omega_T)} \leq k \left\| \frac{\partial \bar{\mathbf{m}}^{h,k}}{\partial t} \right\|_{L^2(\Omega_T)} \tag{4.36}$$

and the right hand side goes to 0 as $h, k \to 0$, we have

$$\mathbf{m}^{h,k} \to \mathbf{m} \text{ strongly in } L^2(\Omega_T). \tag{4.37}$$

In summary, we have shown that there exist a subsequence of $\{\bar{\mathbf{m}}^{h,k}\}$ that converges weakly in $H^1(\Omega \times (0,T))$, a subsequence of $\{\hat{\mathbf{v}}^{h,k}\}$ that converges weakly in $L^2(\Omega \times (0,T))$, and a subsequence of $\{\mathbf{m}^{h,k}\}$ converges strongly in $L^2(\Omega_T)$ based on the energy estimates (4.27) and (4.28). However, in our numerical tests in section 4.3, it was not necessary to take subsequences and the method was in fact second order in space and first order in time. Thus, there is still a gap in what we are able to prove and the practical performance of the algorithm in cases where the weak solution is unique and sufficiently smooth.

4.4.4 The proof that the limit m actually satisfies Landau-Lifshitz-Gilbert equation

In this section, we show that each term of equation (4.13) converges to the appropriate limit, so that the limit $\mathbf{m}$ of the sequences $\{\bar{\mathbf{m}}^{h,k}\}$ and $\{\mathbf{m}^{h,k}\}$ satisfies the weak form of the Landau-Lifshitz-Gilbert equation (4.1) in Definition 1. The Bramble-Hilbert lemma, or classical interpolation inequality, is extensively used in this proof. We state the Bramble-Hilbert lemma for our proof [20, 6, 5].

Lemma 3 (Bramble-Hilbert lemma). *For each element E, for any function $\phi \in H^2(E)$, we have*

$$\|\phi - I_h(\phi)\|_{L^2(E)} \leq Ch^2 \|\triangle\phi\|_{L^2(E)},$$

and

$$\|\phi - I_h(\phi)\|_{H^1(E)} \leq Ch\|\triangle\phi\|_{L^2(E)}.$$

Lemma 4. *Let the sequences $\{\mathbf{m}^{h,k}\}$, $\{\bar{\mathbf{m}}^{h,k}\}$, $\{\hat{\mathbf{v}}^{h,k}\}$, and $\{\mathbf{v}^{h,k}\}$ be defined by Definition 3. Also, let $\mathbf{m} \in H^1(\Omega_T)$ be the limit as in (4.32) and (4.37). Moreover, let's assume $\mathbf{w} \in (C^\infty(\Omega_T))^3 \cap (H^1(\Omega_T))^3$, and $\mathbf{w}^h = I_h(\mathbf{w}) \in F_h$ as in equation (4.3). Then we have*

$$\lim_{h,k\to 0} \int_{\Omega_T} \mathbf{v}^{h,k} \cdot \mathbf{w}^h = \lim_{h,k\to 0} \int_0^T \sum_{j=1}^N \hat{\mathbf{v}}_j^{h,k} \cdot \mathbf{w}_j^h \int_\Omega \phi_j = \int_{\Omega_T} \frac{\partial \mathbf{m}}{\partial t} \cdot \mathbf{w}. \tag{4.38}$$

Proof. The difference between the last two terms is bounded by

$$\left| \int_{\Omega_T} I_h(\hat{\mathbf{v}}^{h,k} \cdot \mathbf{w}^h) - \hat{\mathbf{v}}^{h,k} \cdot \mathbf{w}^h \right| + \left| \int_{\Omega_T} \hat{\mathbf{v}}^{h,k} \cdot \mathbf{w}^h - \frac{\partial \mathbf{m}}{\partial t} \cdot \mathbf{w} \right|. \tag{4.39}$$

The first term of (4.39) has the following estimate. For each element E, we have $\hat{\mathbf{v}}^{h,k}(\cdot, t) \cdot \mathbf{w}^h(\cdot, t) \in C^\infty(E)$ and

$$\left\| I_h(\hat{\mathbf{v}}^{h,k} \cdot \mathbf{w}^h) - \hat{\mathbf{v}}^{h,k} \cdot \mathbf{w}^h \right\|_{L^2(E)}^2 \leq C_{10} h^4 \left\| \Delta(\hat{\mathbf{v}}^{h,k} \cdot \mathbf{w}^h) \right\|_{L^2(E)}^2$$

$$\leq C_{10} h^4 \left(\left\| \Delta\hat{\mathbf{v}}^{h,k} \cdot \mathbf{w}^h \right\|_{L^2(E)}^2 + \left\| \nabla\hat{\mathbf{v}}^{h,k} \cdot \nabla\mathbf{w}^h \right\|_{L^2(E)}^2 + \left\| \hat{\mathbf{v}}^{h,k} \cdot \Delta\mathbf{w}^h \right\|_{L^2(E)}^2 \right) \tag{4.40}$$

$$\leq C_{10} h^4 \left(\left(\left\| \nabla\hat{\mathbf{v}}^{h,k} \cdot \nabla\mathbf{w}^h \right\|_{L^2(E)}^2 \right) \right.$$

for some $C_{10} > 0$, where the first inequality is obtained by the Bramble-Hilbert lemma [20], and in the last inequality we have used $\Delta\hat{\mathbf{v}}^{h,k} = 0$ and $\Delta\mathbf{w}^h = 0$ in E, since $\hat{\mathbf{v}}^{h,k}$ and $\mathbf{w}^h$ are the sum of piecewise linear functions. We have the estimate

$$\left\| \nabla\hat{\mathbf{v}}^{h,k} \right\|_{L^2(\Omega)}^2 \leq \sum_E \int_E |\sum_i (\hat{\mathbf{v}}^{h,k})_i \nabla\phi_i|^2 \leq \frac{C_{11}}{h^2} \sum_E |\sum_{i\in I_E} (\hat{\mathbf{v}}^{h,k})_i|^2 |E|$$

$$\leq C_{12} h^{d-2} \sum_{i=1}^N |(\hat{\mathbf{v}}^{h,k})_i|^2 \leq \frac{C_{13}}{h^2} \left\| \hat{\mathbf{v}}^{h,k} \right\|_{L^2(\Omega)}^2. \tag{4.41}$$

for some constants $C_{11}, C_{12}, C_{13} > 0$ and I_E is the index of nodes of E, where the second inequality is obtained by (4.20), and the last inequality by (4.19). Hence,

$$\left\| I_h(\hat{\mathbf{v}}^{h,k} \cdot \mathbf{w}^h) - \hat{\mathbf{v}}^{h,k} \cdot \mathbf{w}^h \right\|_{L^2(\Omega_T)}^2 \leq C_{10} h^4 \left\| \nabla \hat{\mathbf{v}}^{h,k} \cdot \nabla \mathbf{w}^h \right\|_{L^2(\Omega_T)}^2 \leq C_{14} h^2 \left\| \hat{\mathbf{v}}^{h,k} \right\|_{L^2(\Omega_T)} \tag{4.42}$$

for some constant $C_{14} > 0$. Therefore, the first term of (4.39) goes to 0 as $h, k \to 0$. Moreover, the second term of (4.39) goes to 0 by the weak convergence of $\hat{\mathbf{v}}^{h,k}$ to $\frac{\partial \mathbf{m}}{\partial t}$ which are equations (4.32) and (4.35) . $\qquad \square$

Lemma 5. *Under the same assumptions of Lemma 4, we have*

$$\lim_{h,k \to 0} \int_{\Omega_T} \sum_i (\mathbf{m}_i^{h,k} \times \mathbf{v}^{h,k}) \cdot \mathbf{w}_i^h \phi_i = \lim_{h,k \to 0} \int_{\Omega_T} \sum_i (\mathbf{m}_i^{h,k} \times \hat{\mathbf{v}}_i^{h,k}) \cdot \mathbf{w}_i^h \phi_i$$

$$= \int_{\Omega_T} \left(\mathbf{m} \times \frac{\partial \mathbf{m}}{\partial t} \right) \cdot \mathbf{w} \tag{4.43}$$

Proof. The difference between the last two terms is bounded by

$$\left| \int_{\Omega_T} I_h((\mathbf{m}^{h,k})^a (\hat{\mathbf{v}}^{h,k})^b (\mathbf{w}^h)^c) - (\mathbf{m}^{h,k})^a (\hat{\mathbf{v}}^{h,k})^b (\mathbf{w}^h)^c \right|$$

$$+ \left| \int_{\Omega_T} (\mathbf{m}^{h,k})^a (\hat{\mathbf{v}}^{h,k})^b (\mathbf{w}^h)^c - \mathbf{m}^a \left(\frac{\partial \mathbf{m}}{\partial t} \right)^b \mathbf{w}^c \right| \tag{4.44}$$

for some $a, b, c \in \{1, 2, 3\}$. The first term of (4.44), has the following estimate. For each element E, we have $(\mathbf{m}^{h,k})^a (\hat{\mathbf{v}}^{h,k})^b (\mathbf{w}^h)^c \in C^\infty(E)$ and

$$\left\| I_h((\mathbf{m}^{h,k})^a (\hat{\mathbf{v}}^{h,k})^b (\mathbf{w}^h)^c) - (\mathbf{m}^{h,k})^a (\hat{\mathbf{v}}^{h,k})^b (\mathbf{w}^h)^c \right\|_{L^1(E)}$$

$$\leq C_{15} h^2 (\left\| \Delta((\mathbf{m}^{h,k})^a (\hat{\mathbf{v}}^{h,k})^b (\mathbf{w}^h)^c) \right\|_{L^1(E)})$$

$$\leq C_{15} h^2 (\left\| \nabla(\mathbf{m}^{h,k})^a \nabla(\hat{\mathbf{v}}^{h,k})^b (\mathbf{w}^h)^c \right\|_{L^1(E)} + \left\| \nabla(\mathbf{m}^{h,k})^a (\hat{\mathbf{v}}^{h,k})^b \nabla(\mathbf{w}^h)^c \right\|_{L^1(E)}$$

$$+ \left\| (\mathbf{m}^{h,k})^a \nabla(\hat{\mathbf{v}}^{h,k})^b \nabla(\mathbf{w}^h)^c \right\|_{L^1(E)}) \tag{4.45}$$

for some constant $C_{15} > 0$, where the first inequality is obtained by Bramble-Hilbert lemma, and in the last inequality we have used $\Delta \hat{\mathbf{m}}^{h,k} = 0$, $\Delta \hat{\mathbf{v}}^{h,k} = 0$ and $\Delta \mathbf{w}^h = 0$ in E, since $\mathbf{m}^{h,k}$, $\hat{\mathbf{v}}^{h,k}$ and $\mathbf{w}^h$ are the sum of piecewise linear functions. Hence, we have the estimate

$$\left\| I_h((\mathbf{m}^{h,k})^a (\hat{\mathbf{v}}^{h,k})^b (\mathbf{w}^h)^c) - (\mathbf{m}^{h,k})^a (\hat{\mathbf{v}}^{h,k})^b (\mathbf{w}^h)^c \right\|_{L^1(\Omega_T)}$$

$$\leq C_{16} h \left\| (\hat{\mathbf{v}}^{h,k})^b \right\|_{L^2(\Omega_T)} (\left\| \nabla(\mathbf{m}^{h,k})^a \right\|_{L^2(\Omega_T)} + h \left\| \nabla(\mathbf{m}^{h,k})^a \right\|_{L^2(\Omega_T)}$$

$$+ \left\| (\mathbf{m}^{h,k})^a \right\|_{L^2(\Omega_T)}). \tag{4.46}$$

for some constant $C_{16} > 0$, where we have used Hölder's inequality for all the terms and used (4.41) for the first and the third terms. Therefore, the first term of (4.44) goes to 0 as $h, k \to 0$. Moreover, the second term of (4.44) goes to 0 by the weak convergence of $(\hat{\mathbf{v}}^{h,k})^b$ to $\left(\frac{\partial \mathbf{m}}{\partial t} \right)^b$ established in (4.32) and (4.35), and strong convergence of $(\mathbf{m}^{h,k})^a$ to $\mathbf{m}^a$. $\qquad \square$

Lemma 6. *Under the same assumptions of Lemma 4, we have*

$$\lim_{h,k\to 0} \sum_{l,i} \int_{\Omega_T} \left(\mathbf{m}_i^{h,k} \times \frac{\partial \mathbf{m}^{h,k}}{\partial x_l} \right) \cdot \left(\mathbf{w}_i^h \frac{\partial \phi_i}{\partial x_l} \right) = \sum_l \int_{\Omega_T} \left(\mathbf{m} \times \frac{\partial \mathbf{m}}{\partial x_l} \right) \cdot \frac{\partial \mathbf{w}}{\partial x_l}. \tag{4.47}$$

Proof. The difference between the last two terms is bounded by

$$\left| \int_{\Omega_T} \left(\frac{\partial \mathbf{m}^{h,k}}{\partial x_l} \right)^b \left(\frac{\partial I_h((\mathbf{m}^{h,k})^c(\mathbf{w}^h)^a)}{\partial x_l} \right) - \int_{\Omega_T} \left(\frac{\partial \mathbf{m}^{h,k}}{\partial x_l} \right)^b (\mathbf{m}^{h,k})^c \left(\frac{\partial \mathbf{w}^h}{\partial x_l} \right)^a \right|$$

$$+ \left| \int_{\Omega_T} (\mathbf{m}^{h,k})^c \left(\frac{\partial \mathbf{m}^{h,k}}{\partial x_l} \right)^b \left(\frac{\partial \mathbf{w}^h}{\partial x_l} \right)^a - \int_{\Omega_T} \mathbf{m}^c \left(\frac{\partial \mathbf{m}}{\partial x_l} \right)^b \left(\frac{\partial \mathbf{w}}{\partial x_l} \right)^a \right|, \tag{4.48}$$

for some $a, b, c \in \{1, 2, 3\}$. The first term is bounded by

$$\left\| \left(\frac{\partial \mathbf{m}^{h,k}}{\partial x_l} \right)^b \right\|_{L^2(\Omega_T)} \left\| \frac{\partial I_h((\mathbf{m}^{h,k})^c(\mathbf{w}^h)^a)}{\partial x_l} - \frac{\partial((\mathbf{m}^{h,k})^c(\mathbf{w}^h)^a)}{\partial x_l} \right\|_{L^2(\Omega_T)}. \tag{4.49}$$

For each element E, we have $(\mathbf{m}^{h,k})^c(\mathbf{w}^h)^a \in C^\infty(E)$, and we have the estimate,

$$\left\| \frac{\partial I_h((\mathbf{m}^{h,k})^c(\mathbf{w}^h)^a)}{\partial x_l} - \frac{\partial((\mathbf{m}^{h,k})^c(\mathbf{w}^h)^a)}{\partial x_l} \right\|_{L^2(E)}^2 \le C_{17} h^2 |(\mathbf{m}^{h,k})^c(\mathbf{w}^h)^a|_{H^2(E)}^2 \tag{4.50}$$

for some constant $C_{17} > 0$, by the Bramble-Hilbert lemma. Moreover, we have the estimate,

$$|(\mathbf{m}^{h,k})^c(\mathbf{w}^h)^a|_{H^2(E)}^2 = \int_E |\Delta((\mathbf{m}^{h,k})^c(\mathbf{w}^h)^a)|^2 \le C_{18} \int_E |\nabla(\mathbf{m}^{h,k})^c|^2 |\nabla(\mathbf{w}^h)^a|^2$$

$$\le C_{19} \left\| (\mathbf{m}^{h,k})^c \right\|_{H^1(E)}^2 \tag{4.51}$$

for some constants $C_{18}, C_{19} > 0$, since $\Delta\mathbf{m}^{h,k} = 0$ and $\Delta\mathbf{w}^h = 0$ in E, since $\mathbf{m}^{h,k}$ and $\mathbf{w}^h$ are the sum of piecewise linear functions. We get the estimate

$$\left\| \frac{\partial I_h((\mathbf{m}^{h,k})^c(\mathbf{w}^h)^a)}{\partial x_l} - \frac{\partial((\mathbf{m}^{h,k})^c(\mathbf{w}^h)^a)}{\partial x_l} \right\|_{L^2(\Omega_T)}^2 \le C_{17} C_{19} h^2 \left\| (\mathbf{m}^{h,k})^c \right\|_{H^1(\Omega_T)}^2. \tag{4.52}$$

Therefore, we may conclude that the first term of (4.48) goes to 0 as $h, k \to 0$. Moreover, the second term of (4.48) goes to 0 by the weak convergence of $\left(\frac{\partial \mathbf{m}^{h,k}}{\partial x_l} \right)^b$ to $\left(\frac{\partial \mathbf{m}}{\partial x_l} \right)^b$ and strong convergence of $(\mathbf{m}^{h,k})^c$ to $\mathbf{m}^c$, which gives (4.32) and (4.37). $\qquad \square$

Lemma 7. *Under the same assumptions of Lemma 4, we have*

$$\lim_{h,k\to 0} \left| k \sum_i \int_{\Omega_T} \left(\mathbf{m}_i^{h,k} \times \frac{\partial \hat{\mathbf{v}}^{h,k}}{\partial x_l} \right)^a \left(\frac{\partial \mathbf{w}_i^h}{\partial x_l} \right)^a \right| = 0. \tag{4.53}$$

for $0 \le \theta \le 1$.

Proof. An upper bound for the sequence above is

$$\sqrt{k} \left\| \sqrt{k} \, \frac{\partial (\hat{\mathbf{v}}^{h,k})^c}{\partial x_l} \right\|_{L^2(\Omega_T)} \left\| \nabla (I_h(\mathbf{m}^{h,k})^b (\mathbf{w}^h)^a) \right\|_{L^2(\Omega_T)}. \tag{4.54}$$

for some $a, b, c \in \{1, 2, 3\}$. The term $\left\| \sqrt{k} \, \frac{\partial (\hat{\mathbf{v}}^{h,k})^c}{\partial x_l} \right\|_{L^2(\Omega_T)}$ in (4.54) is uniformly bounded, since $\left\| \sqrt{k} \frac{\partial (\hat{\mathbf{v}}^{h,k})^c}{\partial x_l} \right\|_{L^2(\Omega)} \leq C_7 \frac{\sqrt{k}}{h} \left\| (\hat{\mathbf{v}}^{h,k})^c \right\|_{L^2(\Omega)}$ is uniformly bounded by (4.27) for $0 \leq \theta < \frac{1}{2}$, which is obtained by (4.20), and $\left\| \sqrt{k} \frac{\partial (\hat{\mathbf{v}}^{h,k})^c}{\partial x_l} \right\|_{L^2(\Omega)}$ is uniformly bounded by equation (4.28) for $\frac{1}{2} \leq \theta \leq 1$. For each element E, we have $(\mathbf{m}^{h,k})^b (\mathbf{w}^h)^a \in C^\infty(E)$, so

$$\left\| \nabla I_h((\mathbf{m}^{h,k})^b (\mathbf{w}^h)^a) - \nabla ((\mathbf{m}^{h,k})^b (\mathbf{w}^h)^a) \right\|_{L^2(E)}^2 \leq C_{20} h^2 (\left\| (\nabla (\mathbf{m}^{h,k})^b) \right\|_{L^2(E)}^2), \tag{4.55}$$

for some constant $C_{20} > 0$, by the Bramble-Hilbert lemma, and using $\Delta \mathbf{m}^{h,k} = 0$ and $\Delta \mathbf{w}^h = 0$ in E, since $\mathbf{m}^{h,k}$ and $\mathbf{w}^h$ are the sum of piecewise linear functions. Thus, we have

$$\left\| \nabla (I_h(\mathbf{m}^{h,k})^b (\mathbf{w}^h)^a) \right\|_{L^2(\Omega_T)}^2 \leq \left\| \nabla (\mathbf{m}^{h,k})^b \right\|_{L^2(\Omega_T)}^2 + C_{20} h^2 (\left\| (\nabla (\mathbf{m}^{h,k})^b) \right\|_{L^2(\Omega_T)}^2), \tag{4.56}$$

which is uniformly bounded. Hence, (4.54) goes to 0 as $h, k \to 0$. $\qquad \square$

Lemma 8. *Under the same assumptions of Lemma 4, we have*

$$\lim_{h,k \to 0} \sum_i \int_{\Omega_T} (\mathbf{m}_i^{h,k} \times \bar{\mathbf{h}}(\mathbf{m}^{h,k})) \cdot \mathbf{w}_i^h \phi_i = \int_{\Omega_T} (\mathbf{m} \times \bar{\mathbf{h}}(\mathbf{m})) \cdot \mathbf{w}. \tag{4.57}$$

Proof. An upper bound for the difference between the sequence and the limit is given by

$$\left| \int_{\Omega_T} (\bar{\mathbf{h}}(\mathbf{m}^{h,k}))^a I_h((\mathbf{m}^{h,k})^b (\mathbf{w}^h)^c) - \int_{\Omega_T} (\bar{\mathbf{h}}(\mathbf{m}^{h,k}))^a (\mathbf{m}^{h,k})^b (\mathbf{w}^h)^c \right|$$
$$+ \left| \int_{\Omega_T} (\bar{\mathbf{h}}(\mathbf{m}^{h,k}))^a (\mathbf{m}^{h,k})^b (\mathbf{w}^h)^c - \int_{\Omega_T} (\bar{\mathbf{h}}(\mathbf{m}))^a \mathbf{m}^b \mathbf{w}^c \right| \tag{4.58}$$

for some $a, b, c \in \{1, 2, 3\}$. The first term of (4.58) is bounded by

$$\left\| \bar{\mathbf{h}}(\mathbf{m}^{h,k})^a \right\|_{L^2(\Omega_T)} \left\| I_h((\mathbf{m}^{h,k})^b (\mathbf{w}^h)^c) - (\mathbf{m}^{h,k})^b (\mathbf{w}^h)^c \right\|_{L^2(\Omega_T)} \tag{4.59}$$

For each element E, we have $(\mathbf{m}^{h,k})^b (\mathbf{w}^h)^c \in C^\infty(E)$, and we get the estimate,

$$\left\| I_h((\mathbf{m}^{h,k})^b (\mathbf{w}^h)^c) - ((\mathbf{m}^{h,k})^b (\mathbf{w}^h)^c) \right\|_{L^2(E)}^2 \leq C_{21} h^4 |(\mathbf{m}^{h,k})^b (\mathbf{w}^h)^c|_{H^2(E)}^2 \tag{4.60}$$

for some constant $C_{21} > 0$, by the Bramble-Hilbert lemma. Moreover,

$$|(\mathbf{m}^{h,k})^b(\mathbf{w}^h)^c|^2_{H^2(E)} \le C_{21} \int_E |\nabla(\mathbf{m}^{h,k})^b|^2|\nabla(\mathbf{w}^h)^c|^2 + |(\mathbf{m}^{h,k})^b|^2|\Delta(\mathbf{w}^h)^c|^2$$

$$\le C_{22} \left\|(\mathbf{m}^{h,k})^b\right\|^2_{H^1(E)} \tag{4.61}$$

for some constant $C_{22} > 0$, and using the fact $\Delta\mathbf{m}^{h,k} = \Delta\mathbf{w}^h = 0$ in E, since $\mathbf{m}^{h,k}$ and $\mathbf{w}^h$ are the sum of piecewise linear functions. We get the estimate

$$\left\|I_h((\mathbf{m}^{h,k})^b(\mathbf{w}^h)^c) - ((\mathbf{m}^{h,k})^b(\mathbf{w}^h)^c)\right\|^2_{L^2(\Omega_T)} \le C_{23}h^4 \left\|(\mathbf{m}^{h,k})^b\right\|^2_{H^1(\Omega_T)}. \tag{4.62}$$

for some constant $C_{23} > 0$. Thus, the first term of (4.58) goes to 0 as $h, k \to 0$, and the second term of (4.58) converges to 0 as $h, k \to 0$, because of the strong convergence of $(\bar{\mathbf{h}}(\mathbf{m}^{h,k}))^a$ and $(\mathbf{m}^{h,k})^b$. $\qquad \square$

Lemma 9. *Under the same assumptions of Lemma 4, we have*

$$\lim_{h,k\to 0} \left| k \sum_i \int_{\Omega_T} (\mathbf{m}^{h,k}_i \times \bar{\mathbf{h}}(\hat{\mathbf{v}}^{h,k})) \cdot \mathbf{w}^h_i \phi_i \right| = 0. \tag{4.63}$$

Proof. An upper bound for the sequence above is

$$k \left\|\bar{\mathbf{h}}(\hat{\mathbf{v}}^{h,k})\right\|_{L^2(\Omega_T)} \left\|\mathbf{w}^h\right\|_{L^2(\Omega_T)}. \tag{4.64}$$

Since, $\left\|\bar{\mathbf{h}}(\hat{\mathbf{v}}^{h,k})\right\|_{L^2(\Omega_T)} \le (C_5 \left\|\hat{\mathbf{v}}^{h,k}\right\|_{L^2(\Omega_T)} + C_5)$ by (4.17), the term $\left\|\bar{\mathbf{h}}(\hat{\mathbf{v}}^{h,k})\right\|_{L^2(\Omega_T)}$ in (4.64) is uniformly bounded. Therefore, (4.64) goes to 0 as $h, k \to 0$. $\qquad \square$

4.4.5 Energy of m

Recall the definition of the energy $E(\mathbf{m})$ in (1.2). We follow the same arguments in section 6 of [9]. We have an energy estimate of $\mathbf{m}^{h,k}$ as

$$E(\mathbf{m}^{j+1}) - E(\mathbf{m}^j) \le -k\left(\frac{\alpha}{1+\alpha^2}\right)\frac{C_1}{C_6}||\hat{\mathbf{v}}^j||^2_{L^2} - \left(\theta - \frac{1}{2}\right)k^2\eta||\nabla\hat{\mathbf{v}}^j||^2_{L^2} + k(\bar{\mathbf{h}}(\mathbf{m}^j), \hat{\mathbf{v}}^j)$$

$$+ \theta k^2(\bar{\mathbf{h}}_e, \hat{\mathbf{v}}^j) - \frac{1}{2}\int_\Omega (\bar{\mathbf{h}}(\mathbf{m}^{j+1}) + \bar{\mathbf{h}}(\mathbf{m}^j)) \cdot (\mathbf{m}^{j+1} - \mathbf{m}^j). \tag{4.65}$$

by (4.23) from section 4.4.2. For $0 \le \theta < \frac{1}{2}$, the second term on the right has an upper bound

$$\left(\theta - \frac{1}{2}\right)k^2\eta \left\|\nabla\hat{\mathbf{v}}^j\right\|^2_{L^2(\Omega)} \le k^2\eta \left\|\nabla\hat{\mathbf{v}}^j\right\|^2_{L^2(\Omega)} \le C_7 k\eta\frac{k}{h^2} \left\|\hat{\mathbf{v}}^j\right\|^2_{L^2(\Omega)} \le C_7 C_0 \eta k \left\|\hat{\mathbf{v}}^j\right\|^2_{L^2(\Omega)} \tag{4.66}$$

and by choosing $C_0 \leq \frac{1}{2} \frac{\alpha}{1+\alpha^2} \frac{C_1}{C_6} \frac{1}{C_7 \eta}$, this term and the first term on the right hand side of (4.65) can be combined to be less than equal to

$$-\frac{k}{2} \left(\frac{\alpha}{1+\alpha^2} \right) \frac{C_1}{C_6} ||\hat{\mathbf{v}}^j||^2_{L^2(\Omega)} \tag{4.67}$$

The second term on the right of equation(4.65) can be disregarded for $\frac{1}{2} \leq \theta \leq 1$. We will derive the upper bound for the rest of the terms of right hand side of (4.65).

The third and the last terms on the right can be combined to be written as

$$\left| k(\bar{\mathbf{h}}(\mathbf{m}^j), \hat{\mathbf{v}}^j) - \frac{1}{2} \int_\Omega (\bar{\mathbf{h}}(\mathbf{m}^{j+1}) + \bar{\mathbf{h}}(\mathbf{m}^j)) \cdot (\mathbf{m}^{j+1} - \mathbf{m}^j) \right|. \tag{4.68}$$

and has an upper bound

$$\left| \int_\Omega \bar{\mathbf{h}}(\mathbf{m}^j) \cdot (\mathbf{m}^{j+1} - \mathbf{m}^j - k\hat{\mathbf{v}}^j) \right| + \left| \frac{1}{2} \int_\Omega (\bar{\mathbf{h}}(\mathbf{m}^{j+1}) - \bar{\mathbf{h}}(\mathbf{m}^j)) \cdot (\mathbf{m}^{j+1} - \mathbf{m}^j) \right|. \tag{4.69}$$

The first term of (4.69) is bounded by

$$C_{24} k^2 \left(\left\| \hat{\mathbf{v}}^j \right\|_{L^2(\Omega)} \left\| \hat{\mathbf{v}}^j \right\|_{L^4(\Omega)} \right) \leq C_{24} \frac{k^2}{2} \left(\left\| \hat{\mathbf{v}}^j \right\|^2_{L^2(\Omega)} + \left\| \hat{\mathbf{v}}^j \right\|^2_{L^4(\Omega)} \right) \tag{4.70}$$

for some constant $C_{24} > 0$, by (4.33), and (4.19). The second term of (4.69) is bounded by $C_{25} k^2 \left\| \hat{\mathbf{v}}^j \right\|^2_{L^2(\Omega)}$ for some constant $C_{25} > 0$, by (4.29) and (4.19).

The fourth term on the right has the upper bound $|\theta k^2 (\bar{\mathbf{h}}_e, \hat{\mathbf{v}}^j)| \leq C_{26} k^2 \left\| \hat{\mathbf{v}}^j \right\|_{L^2(\Omega)}$ for some constant $C_{26} > 0$. Then (4.65) has an upper bound

$$\begin{aligned} E(\mathbf{m}^{j+1}) - E(\mathbf{m}^j) + \frac{k}{2} \left(\frac{\alpha}{1+\alpha^2} \right) \frac{C_1}{C_6} ||\hat{\mathbf{v}}^j||^2_{L^2(\Omega)} &\leq C_{27} k^2 \left(\left\| \hat{\mathbf{v}}^j \right\|^2_{L^4(\Omega)} + \left\| \hat{\mathbf{v}}^j \right\|^2_{L^2(\Omega)} \right) \\ &\leq C_{28} k^2 \left(\left\| \nabla \hat{\mathbf{v}}^j \right\|^2_{L^2(\Omega)} + \left\| \hat{\mathbf{v}}^j \right\|^2_{L^2(\Omega)} \right) \end{aligned} \tag{4.71}$$

for some constants $C_{27}, C_{28} > 0$, by using Sobolev embedding theorem [4], $\left\| \hat{\mathbf{v}}^j \right\|_{L^4(\Omega)} \leq C_{29} \left\| \nabla \hat{\mathbf{v}}^j \right\|_{L^2(\Omega)}$ for some constant $C_{29} > 0$. Summing from $j = 0, \ldots, J-1$, we get

$$\begin{aligned} E(\mathbf{m}^J) - E(\mathbf{m}^0) + \frac{1}{2} \left(\frac{\alpha}{1+\alpha^2} \right) \frac{C_1}{C_6} \int_{\Omega_T} |\hat{\mathbf{v}}^{h,k}|^2 \\ \leq C_{28} k \left(\left\| \nabla \hat{\mathbf{v}}^{h,k} \right\|^2_{L^2(\Omega_T)} + \left\| \hat{\mathbf{v}}^{h,k} \right\|^2_{L^2(\Omega_T)} \right) \end{aligned} \tag{4.72}$$

Therefore, taking $h, k \to 0$, we get the energy inequality (4.2).

4.4.6 Magnitude of m

By the same argument in [7], we have $|\mathbf{m}(x,t)| = 1$ *a.e.* for $(x,t) \in \Omega_T$ (See equation (28) and (29) on page 1347 of [7]). In this section, we will prove that the magnitude of $\mathbf{m}$, which is the limit of the sequence $\{\mathbf{m}^{h,k}\}$, is 1 almost everywhere in Ω_T. We follow the same argument from [5], and first state the following fact from [5]:

For any $\mathbf{q} \in F^h$, we have

$$||\mathbf{q}(x)| - |\mathbf{q}(x_i)||^2 \leq C_{30}h^2|\nabla\mathbf{q}(x)|^2 \tag{4.73}$$

for $x \in E$, x_i a vertex of E and $L \in \mathcal{T}_h$, which is a triangle or tetrahedron, and for some constant $C_{30} > 0$.

Taking $\mathbf{q}$ as $\mathbf{m}^{h,k}$, we have

$$\int_{\Omega_T} \left||\mathbf{m}^{h,k}(x,t)| - 1\right|^2 \leq Ch^2 \left\|\nabla\mathbf{m}^{h,k}\right\|_{L^2(\Omega_T)}^2. \tag{4.74}$$

Since $\left\|\nabla\mathbf{m}^{h,k}\right\|_{L^2(\Omega_T)}$ is bounded by the energy estimates (4.27) for $0 \leq \theta \leq \frac{1}{2}$, and (4.27) for $\frac{1}{2} \leq \theta \leq 1$, we have

$$\int_{\Omega_T} |\,|\mathbf{m}(x,t)| - 1|^2 \leq 0, \tag{4.75}$$

by taking $h, k \to 0$. Therefore, $\mathbf{m}$ satisfies $|\mathbf{m}(x,t)| = 1$ *a.e.* for $(x,t) \in \Omega_T$.

Chapter 5

Conclusion

A number of unique features of the Landau-Lifshitz equation in micromagnetics impose interesting challenges in the development and analysis in numerical methods for the Landau-Lifshitz equation. The Landau-Lifshitz equation is highly nonlinear, has a non-convex constraint, has several equivalent forms and involves solving an auxiliary problem in the infinite domain. In this thesis, we presented numerical methods for the Landau-Lifshitz equation in micromagnetics, that preserve the properties of the underlying PDE : the mimetic finite difference method and the mass-lumped finite element method.

We developed the mimetic finite difference method for the Landau-Lifshitz equation that works on general polytopal meshes on general geometries. In Chapter 2, we presented low order mimetic finite difference method for the Landau-Lifshitz equation that works on general unstructured meshes on general geometries, preserves non-convex constraint, is energy (exchange) decreasing, requires only a linear solver at each time step and is easily applicable to the limiting cases. We tested the method on various meshes. We performed a numerical simulation for NIST's micromag standard problem #4, which is to simulate the magnetization dynamics in a permalloy thin film with applied fields. In Chapter 3, we presented high order mimetic finite difference method for the Landau-Lifshitz equation which is third order in space and second order in time. In fact, it is arbitrarily high order in space. We compared the efficiencies of high order mimetic finite difference method to low order mimetic finite difference method using a simulation of the static skyrmion in chiral magnet. It showed that the high order method is more efficient than the low order method for already coarse meshes.

In Chapter 4, we presented a mass-lumped finite element method for the Landau-Lifshitz equation that deals with weak solution. The scheme is practical in that it deals with a weak solution. The scheme preserves non-convex constraint, requires only a linear solver at each time step and is easily applicable to the limiting cases. We showed that the numerical solution of our method has a subsequence that converges weakly to a weak solution of the Landau-Lifshitz-Gilbert equation. Numerical tests show that the method is second order accurate in space and first order accurate in time when the underlying solution is smooth. A second-order in time variant was also presented and tested numerically, but not analyzed

rigorously in the present work.

Bibliography

[1]   Claas Abert et al. "A fast finite-difference method for micromagnetics using the magnetic scalar potential". In: *IEEE Transactions on Magnetics* 48.3 (2012), pp. 1105–1109.

[2]   Claas Abert et al. "Numerical methods for the stray-field calculation: A comparison of recently developed algorithms". In: *Journal of Magnetism and Magnetic Materials* 326 (2013), pp. 176–185.

[3]   Mehmet Acet. "Magnetic shape memory: Magnetoelastic sponges". In: *Nature Materials* 8.11 (2009), pp. 854–855.

[4]   Robert A Adams and John JF Fournier. *Sobolev spaces.* Vol. 140. Academic press, 2003.

[5]   François Alouges. "A new finite element scheme for Landau-Lifchitz equations". In: *Discrete Contin. Dyn. Syst. Ser. S* 1.2 (2008), pp. 187–196.

[6]   François Alouges and Pascal Jaisson. "Convergence of a finite element discretization for the Landau–Lifshitz equations in micromagnetism". In: *Mathematical Models and Methods in Applied Sciences* 16.02 (2006), pp. 299–316.

[7]   François Alouges, Evaggelos Kritsikis, and Jean-Christophe Toussaint. "A convergent finite element approximation for Landau–Lifschitz–Gilbert equation". In: *Physica B: Condensed Matter* 407.9 (2012), pp. 1345–1349.

[8]   François Alouges and Alain Soyeur. "On global weak solutions for Landau-Lifshitz equations: existence and nonuniqueness". In: *Nonlinear Analysis: Theory, Methods & Applications* 18.11 (1992), pp. 1071–1084.

[9]   François Alouges et al. "A convergent and precise finite element scheme for Landau–Lifschitz–Gilbert equation". In: *Numerische Mathematik* 128.3 (2014), pp. 407–430.

[10]   François Alouges et al. "Energetics and switching of quasi-uniform states in small ferromagnetic particles". In: *ESAIM: Mathematical Modelling and Numerical Analysis-Modélisation Mathématique et Analyse Numérique* 38.2 (2004), pp. 235–248.

[11]   Jayasimha Atulasimha and Alison B Flatau. "A review of magnetostrictive iron–gallium alloys". In: *Smart Materials and Structures* 20.4 (2011), p. 043001.

[12] Sören Bartels. "Stability and convergence of finite-element approximation schemes for harmonic maps". In: *SIAM Journal on Numerical Analysis* 43.1 (2005), pp. 220–238.

[13] Sören Bartels and Andreas Prohl. "Convergence of an implicit finite element method for the Landau-Lifshitz-Gilbert equation". In: *SIAM Journal on Numerical Analysis* 44.4 (2006), pp. 1405–1419.

[14] Abraham Berman and Robert J Plemmons. *Nonnegative matrices in the mathematical sciences*. SIAM, 1994.

[15] Giorgio Bertotti, Claudio Serpico, and Isaak D Mayergoyz. "Nonlinear magnetization dynamics under circularly polarized field". In: *Physical Review Letters* 86.4 (2001), p. 724.

[16] P Bhargava and DB Bogy. "Numerical simulation of operational-shock in small form factor hard disk drives". In: *Journal of Tribology* 129.1 (2007), pp. 153–160.

[17] James L Blue and MR Scheinfein. "Using multipoles decreases computation time for magnetostatic self-energy". In: *IEEE Transactions on Magnetics* 27.6 (1991), pp. 4778–4780.

[18] DB Bogy. "A Numerical Simulation of the Head-Disk Assembly in Magnetic Hard Disk Files: Part 1 – Component Models". In: *Journal of Tribology* 112 (1990), p. 593.

[19] Olivier Boulle et al. "Room-temperature chiral magnetic skyrmions in ultrathin magnetic nanostructures". In: *Nature Nanotechnology* 11.5 (2016), pp. 449–454.

[20] Dietrich Braess. *Finite elements: Theory, fast solvers, and applications in solid mechanics*. Cambridge University Press, 2007.

[21] Franco Brezzi, Konstantin Lipnikov, and Valeria Simoncini. "A family of mimetic finite difference methods on polygonal and polyhedral meshes". In: *Mathematical Models and Methods in Applied Sciences* 15.10 (2005), pp. 1533–1551.

[22] Xavier Brunotte, Gérard Meunier, and Jean-François Imhoff. "Finite element modeling of unbounded problems using transformations: a rigorous, powerful and easy solution". In: *IEEE Transactions on Magnetics* 28.2 (1992), pp. 1663–1666.

[23] Gilles Carbou and Pierre Fabrie. "Regular solutions for Landau-Lifschitz equation in $\mathbb{R}^3$". In: *Communications in Applied Analysis* 5.1 (2001), pp. 17–30.

[24] Gilles Carbou, Pierre Fabrie, et al. "Regular solutions for Landau-Lifschitz equation in a bounded domain". In: *Differential and Integral Equations* 14.2 (2001), pp. 213–229.

[25] Maria M Cerimele, Francesca Pistella, and V Valente. "Numerical study of an evolutive model for magnetostrictive materials". In: *Mathematics and Computers in Simulation* 77.1 (2008), pp. 22–33.

[26] Yung-Kan Chen, Jih-Ping Peng, and David B Bogy. "Experimental and simulation study of thermal protrusion-induced head-disk contact instabilities in hard disk drives". In: *IEEE Transactions on Magnetics* 50.11 (2014), pp. 1–5.

[27] Markus Chmielus et al. "Magnetic-field-induced recovery strain in polycrystalline Ni–Mn–Ga foam". In: *Journal of Applied Physics* 108.12 (2010), p. 123526.

[28] Snorre H Christiansen. "A div-curl lemma for edge elements". In: *SIAM Journal on Numerical Analysis* 43.1 (2005), pp. 116–126.

[29] Ivan Cimrák. "A survey on the numerics and computations for the Landau-Lifshitz equation of micromagnetism". In: *Archives of Computational Methods in Engineering* 15.3 (2007), pp. 1–37.

[30] Ivan Cimrák. "Convergence result for the constraint preserving mid-point scheme for micromagnetism". In: *Journal of Computational and Applied Mathematics* 228.1 (2009), pp. 238–246.

[31] Ivan Cimrák. "Error estimates for a semi-implicit numerical scheme solving the Landau–Lifshitz equation with an exchange field". In: *IMA Journal of Numerical Analysis* 25.3 (2005), pp. 611–634.

[32] Massimiliano d'Aquino, Claudio Serpico, and Giovanni Miano. "Geometrical integration of Landau–Lifshitz–Gilbert equation based on the mid-point rule". In: *Journal of Computational Physics* 209.2 (2005), pp. 730–753.

[33] A Yu Dobin and HJ Richter. "Domain wall assisted magnetic recording". In: *Applied Physics Letters* 89.6 (2006), p. 062512.

[34] Lukas Exl et al. "Fast stray field computation on tensor grids". In: *Journal of Computational Physics* 231.7 (2012), pp. 2840–2850.

[35] R Fischer and H Kronmüller. "Importance of ideal grain boundaries of high remanent composite permanent magnets". In: *Journal of Applied Physics* 83.6 (1998), pp. 3271–3275.

[36] R Fischer et al. "Grain-size dependence of remanence and coercive field of isotropic nanocrystalline composite permanent magnets". In: *Journal of Magnetism and Magnetic Materials* 153.1 (1996), pp. 35–49.

[37] DR Fredkin and TR Koehler. "Hybrid method for computing demagnetizing fields". In: *IEEE Transactions on Magnetics* 26.2 (1990), pp. 415–417.

[38] Atsushi Fuwa, Tetsuya Ishiwata, and Masayoshi Tsutsumi. "Finite difference scheme for the Landau–Lifshitz equation". In: *Japan Journal of Industrial and Applied Mathematics* 29.1 (2012), pp. 83–110.

[39] Carlos J García-Cervera and W E. "Improved Gauss-Seidel projection method for micromagnetics simulations". In: *IEEE Transactions on Magnetics* 39.3 (2003), pp. 1766–1770.

[40] Carlos J García-Cervera. "Numerical micromagnetics: A review". In: *Bol. Soc. Esp. Mat. Apl.* 39 (2007), pp. 103–135.

[41]   Carlos J García-Cervera, Zydrunas Gimbutas, and W E. "Accurate numerical methods for micromagnetics simulations with general geometries". In: *Journal of Computational Physics* 184.1 (2003), pp. 37–52.

[42]   Carlos J García-Cervera and Alexandre M Roma. "Adaptive mesh refinement for micromagnetics simulations". In: *IEEE Transactions on Magnetics* 42.6 (2006), pp. 1648–1654.

[43]   TL Gilbert. "A Lagrangian formulation of the gyromagnetic equation of the magnetization field". In: *Phys. Rev.* 100 (1955), pp. 1243–1255.

[44]   David J Griffiths. *Introduction to electrodynamics*. Pearson, 2013.

[45]   Boling Guo and Min-Chun Hong. "The Landau-Lifshitz equation of the ferromagnetic spin chain and harmonic maps". In: *Calculus of Variations and Partial Differential Equations* 1.3 (1993), pp. 311–334.

[46]   Stephen Gustafson, Kenji Nakanishi, and Tai-Peng Tsai. "Asymptotic Stability, Concentration, and Oscillation in Harmonic Map Heat-Flow, Landau-Lifshitz, and Schrödinger Maps on $\mathbb{R}^2$". In: *Communications in Mathematical Physics* 300.1 (2010), pp. 205–242.

[47]   Vitaliy Gyrya, Konstantin Lipnikov, and Gianmarco Manzini. "The arbitrary order mixed mimetic finite difference method for the diffusion equation". In: *ESAIM: Mathematical Modelling and Numerical Analysis* 50.3 (2016), pp. 851–877.

[48]   Richard D James and Manfred Wuttig. "Magnetostriction of martensite". In: *Philosophical Magazine A* 77.5 (1998), pp. 1273–1299.

[49]   J Samuel Jiang, Hans G Kaper, and Gary K Leaf. "Hysteresis in layered spring magnets". In: *Discrete and Continuous Dynamical Systems Series B* 1 (2001), pp. 219–323.

[50]   Stavros Komineas and Nikos Papanicolaou. "Skyrmion dynamics in chiral ferromagnets". In: *Physical Review B* 92.6 (2015), p. 064412.

[51]   Perinkulam S Krishnaprasad and Xiaobo Tan. "Cayley transforms in micromagnetics". In: *Physica B: Condensed Matter* 306.1 (2001), pp. 195–199.

[52]   Evaggelos Kritsikis et al. "Beyond first-order finite element schemes in micromagnetics". In: *Journal of Computational Physics* 256 (2014), pp. 357–366.

[53]   Jehyun Lee et al. "Magnetic characteristics of ferromagnetic nanotube". In: *Journal of Magnetism and Magnetic Materials* 310.2 (2007), pp. 2445–2447.

[54]   Debra Lewis and Nilima Nigam. "Geometric integration on spheres and some interesting applications". In: *Journal of Computational and Applied Mathematics* 151.1 (2003), pp. 141–170.

[55]   Liping Li and David B Bogy. "Numerical analysis of head disk interface response during operational shock with disk-ramp contact". In: *IEEE Transactions on Magnetics* 50.4 (2014), pp. 1–6.

[56] Shi-Zeng Lin, Charles Reichhardt, and Avadh Saxena. "Manipulation of skyrmions in nanodisks with a current pulse and skyrmion rectifier". In: *Applied Physics Letters* 102.22 (2013), p. 222405.

[57] Shi-Zeng Lin et al. "Dynamics of skyrmions in chiral magnets: Dynamic phase transitions and equation of motion". In: *Journal of Applied Physics* 115.17 (2014), p. 17D109.

[58] K. Lipnikov, G. Manzini, and M. Shashkov. "Mimetic finite difference method". In: *J. Comp. Phys.* 257 (2014), pp. 1163–1227.

[59] Konstantin Lipnikov, Gianmarco Manzini, and Daniil Svyatskiy. "Analysis of the monotonicity conditions in the mimetic finite difference method for elliptic problems". In: *Journal of Computational Physics* 230.7 (2011), pp. 2620–2642.

[60] Boris Livshitz et al. "Nonuniform grid algorithm for fast calculation of magnetostatic interactions in micromagnetics". In: *Journal of Applied Physics* 105.7 (2009), p. 07D541.

[61] HH Long et al. "Fast Fourier transform on multipoles for rapid calculation of magnetostatic fields". In: *IEEE Transactions on Magnetics* 42.2 (2006), pp. 295–300.

[62] *μMAG Micromagnetic Modeling Activity Group.* `http://www.ctcms.nist.gov/~rdm/mumag.org.html`.

[63] Jacques E Miltat and Michael J Donahue. "Numerical Micromagnetics: Finite difference methods". In: *Handbook of magnetism and advanced magnetic materials* (2007).

[64] R Mohr et al. "Initiation of shape-memory effect by inductive heating of magnetic nanoparticles in thermoplastic polymers". In: *Proceedings of the National Academy of Sciences of the United States of America* 103.10 (2006), pp. 3540–3545.

[65] S Mühlbauer et al. "Skyrmion lattice in a chiral magnet". In: *Science* 323.5916 (2009), pp. 915–919.

[66] Naoto Nagaosa and Yoshinori Tokura. "Topological properties and dynamics of magnetic skyrmions". In: *Nature Nanotechnology* 8.12 (2013), pp. 899–911.

[67] T Oikawa et al. "Large-scale micromagnetic simulation of Nd-Fe-B sintered magnets with Dy-rich shell structures". In: *AIP Advances* 6.5 (2016), p. 056006.

[68] Per-Olof Persson and Gilbert Strang. "A simple mesh generator in MATLAB". In: *SIAM review* 46.2 (2004), pp. 329–345.

[69] Martin L Plumer, Johannes Van Ek, and Dieter Weller. *The physics of ultra-high-density magnetic recording.* Vol. 41. Springer Science & Business Media, 2012.

[70] N Popović and Dirk Praetorius. "Applications of $\mathcal{H}$-Matrix Techniques in Micromagnetics". In: *Computing* 74.3 (2005), pp. 177–204.

[71] Narayan Poudyal and J Ping Liu. "Advances in nanostructured permanent magnets research". In: *Journal of Physics D: Applied Physics* 46.4 (2012), p. 043001.

[72] Andreas Prohl. *Computational Micromagnetism*. Advances in Numerical Mathematics. Teubner, Stuttgar, 2001.

[73] JC Rife et al. "Design and performance of GMR sensors for the detection of magnetic microbeads in biosensors". In: *Sensors and Actuators A: Physical* 107.3 (2003), pp. 209–218.

[74] Caroline A Ross. "Patterned magnetic recording media". In: *Annual Review of Materials Research* 31.1 (2001), pp. 203–235.

[75] OJ Ruiz and DB Bogy. "A numerical simulation of the head-disk assembly in magnetic hard disk files: Part II – solution of the coupled system". In: *Journal of Tribology* 112.4 (1990), pp. 603–613.

[76] Piotr Rybka and Mitchell Luskin. "Existence of energy minimizers for magnetostrictive materials". In: *SIAM journal on mathematical analysis* 36.6 (2005), pp. 2004–2019.

[77] NM Saiden et al. "Micromagnetic finite element simulation of nanocrystalline α-Fe/Nd$_2$Fe$_{14}$B/Fe$_3$B magnets". In: *Journal of Magnetism and Magnetic Materials* 365 (2014), pp. 45–50.

[78] Manfred E Schabes. "Micromagnetic theory of non-uniform magnetization processes in magnetic recording particles". In: *Journal of Magnetism and Magnetic Materials* 95.3 (1991), pp. 249–288.

[79] Thomas Schrefl et al. "First order reversal curve studies of permanent magnets". In: *Journal of Applied Physics* 111.7 (2012), 07A728.

[80] Klaus Szielasko et al. "Minimalistic devices and sensors for micromagnetic materials characterization". In: *IEEE Transactions on Magnetics* 49.1 (2013), pp. 101–104.

[81] Kenichi Takano. "Micromagnetic-FEM models of a perpendicular writer and reader". In: *IEEE Transactions on Magnetics* 41.2 (2005), pp. 696–701.

[82] Luc Tartar. *The general theory of homogenization: a personalized introduction*. Vol. 7. Springer Science & Business Media, 2009.

[83] Gen Tatara, Hiroshi Kohno, and Junya Shibata. "Microscopic approach to current-driven domain wall dynamics". In: *Physics Reports* 468.6 (2008), pp. 213–301.

[84] Igor Tsukerman, Alexander Plaks, and H Neal Bertram. "Multigrid methods for computation of magnetostatic fields in magnetic recording problems". In: *Journal of Applied Physics* 83.11 (1998), pp. 6344–6346.

[85] HAM Van den Berg et al. *Magnetic multilayers and giant magnetoresistance: fundamentals and industrial applications*. Vol. 37. Springer Science & Business Media, 2013.

[86] Reiner Vanselow. "About Delaunay triangulations and discrete maximum principles for the linear conforming FEM applied to the Poisson equation". In: *Applications of Mathematics* 46.1 (2001), pp. 13–28.

[87] Xiao-Ping Wang and W E. "Numerical Methods for the Landau–Lifshitz Equation". In: *SIAM Journal on Numerical Analysis* 38.5 (2000), pp. 1647–1665.

[88] Xiao-Ping Wang, Carlos J García-Cervera, and W E. "A Gauss–Seidel projection method for micromagnetics simulations". In: *Journal of Computational Physics* 171.1 (2001), pp. 357–372.

[89] Xiao-Ping Wang, Ke Wang, and W E. "Simulations of 3-D domain wall structures in thin films". In: *Discrete and Continuous Dynamical Systems Series B* 6.2 (2006), p. 373.

[90] Cassie Witherspoon et al. "Texture and training of magnetic shape memory foam". In: *Acta Materialia* 61.6 (2013), pp. 2113–2120.

[91] C Witherspoon et al. "Effect of porosity on the magneto-mechanical behavior of polycrystalline magnetic shape-memory Ni–Mn–Ga foams". In: *Acta Materialia* 92 (2015), pp. 64–71.

[92] Lin Wu and DB Bogy. "Numerical simulation of the slider air bearing problem of hard disk drives by two multidimensional upwind residual distribution schemes over unstructured triangular meshes". In: *Journal of Computational Physics* 172.2 (2001), pp. 640–657.

[93] Shaomin Xiong et al. "A two-stage heating scheme for heat assisted magnetic recording". In: *Journal of Applied Physics* 115.17 (2014), 17B702.

[94] XZ Yu et al. "Near room-temperature formation of a skyrmion crystal in thin-films of the helimagnet FeGe". In: *Nature Materials* 10.2 (2011), pp. 106–109.

[95] XZ Yu et al. "Real-space observation of a two-dimensional skyrmion crystal". In: *Nature* 465.7300 (2010), pp. 901–904.

[96] Samuel W Yuan and H Neal Bertram. "Fast adaptive algorithms for micromagnetics". In: *IEEE Transactions on Magnetics* 28.5 (1992), pp. 2031–2036.

[97] QH Zeng and DB Bogy. "Numerical simulation of shock response of disk-suspension-slider air bearing systems in hard disk drives". In: *Microsystem Technologies* 8.4 (2002), pp. 289–296.